The efficiency of earth berms in supporting retaining walls

Tom Gilbertovitch Monteiro Tavares

Thesis to obtain the Master of Science Degree in

Civil Engineering

Supervisor: Prof. Peter John Bourne-Webb

Examination Committee

Chairperson: Profª Maria Rafaela Pinheiro Cardoso

Supervisor: Prof. Peter John Bourne-Webb

Member of Committee: Prof. Alexandre da Luz Pinto

October 2017

Acknowledgements

In this part of the thesis, I would like to thank everybody who somehow helped and supported me on this journey of becoming an engineer and something more than just that. I would like to thank my parents Natalia and Gilberto and my family who supported me both spiritually and financially. I would like to thank my friends especially Andre who always helped and supported me in every endeavor ever since I came to Portugal, whom I can verily call my brother even without some sanguine relation and who accepted me as part of his family.

I would like to thank every member of the IST community which offered me the opportunity to achieve a higher degree of knowledge and personal qualities. I would like to thank the members of committee – Profª Rafaela Cardoso, Prof. Alexandre Pinto and Prof. Peter Bourne Webb for their assistance as well as an offer of the opportunity to present this thesis. I wanted to offer my special gratitude to Professor Peter Bourne-Webb whose doors were always open for any type of support and guidance ever since the very first lecture of his lessons. Who was always there to offer help and encouragements even through some of the most adverse times of my life.

I would like to offer my obeisance and gratitude to my teacher Amrita Dhuni who brought me peace and life meaning. And I would like to thank the Lord SÍva who is always within my heart. Om tat sat!

Resumé PT

As banquetas são frequentemente usadas para promover um suporte temporário em estruturas de contenção como alternativa (ou em conjunto com) as estacas/ancoragens. Há varias maneiras de contabilizar o efeito estabilizante das banquetas no dimensionamento. Os métodos mais comuns são Equivalent Surcharge Method (ESM), Raised Effective Formation (REF) and Multiple Coulomb's Wedge (MCW) method. O MCW (efetivamente analise equilíbrio limite) é um dos métodos mais populares, no entanto é sabido que os valores da resistência passiva obtidos a partir das superfícies do deslizamento planar aplicadas nesse método não são sempre conservativos, especialmente quando os valores de resistência ao corte e o angulo de atrito entre o solo e a parede são elevados. O método dos elementos finito (FEA) é o outro método muito comum utilizado na avaliação dos efeitos promovidos pelas banquetas, esse analise também possibilita efetuar a análise com diferentes parâmetros relacionados com as propriedades do solo ou estrutura de contenção. Foram efectuados os análises para geometrias diferentes utilizando o MCW e o FEA. Os resultados obtidos foram comparados entre si e com os outros métodos. Os resultados demonstraram uma grande discrepância em termos de distribuição das tensões ao longo da estrutura de contenção entre o MCW e FEA como também uma distribuição pouco realista ao longo da parede obtida através do método MCW. Também foi demonstrado que a variação dos valores dos parâmetros que representam as tensões horizontais iniciais, a rigidez do solo e a rigidez da parede têm o efeito muito reduzido sobre a distribuição das tensões ao longo da estrutura de contenção.

Summary EN

Earth berms are often used to provide temporary support for embedded retaining walls as an alternative (or in conjunction with) props/anchors. There are several means by which the stabilizing effect of an earth berm can be accounted for in the design. The most common methods are Equivalent Surcharge Method (ESM), Raised Effective Formation (REF) and Multiple Coulomb Wedge (MCW) method. The use of MCW method (effectively a limit equilibrium analysis) is one of the more popular however it is well known that the passive resistance derived by a linear slip surface using this approach is not always conservative, especially when the soil angle of shearing resistance and/or the wall interface friction is high. The Finite Element Analysis (FEA) is another common method for the evaluation of the support provided by berms, which allows performing the analysis with different parameters for the soil and wall properties. Analysis of a different set of geometry layouts was carried out using the aforementioned MCW and FEA methods. The obtained results were compared with each other and with other methods. The results showed a great discrepancy in terms of stress distribution along the wall between the two methods as well as some unrealistic stress distribution along the wall in MCW method, also it was found that variation of parameters that affect the initial horizontal stresses, soil and wall stiffness do not affect greatly the stress distribution inside the berm.

KEYWORDS: embedded retaining wall, berm, drained stability analysis, finite elements

Contents

List of Tables:

List of Figures:

1. INTRODUCTION

1.1. Overview

Earth berms are often used to provide temporary support for embedded retaining walls as an alternative (or in conjunction with) props/anchors. There are several means by which the stabilizing effect of an earth berm can be accounted for in the design. The most common methods are Equivalent Surcharge Method (ESM), Raised Effective Formation (REF) and Multiple Coulomb's Wedge (MCW) method. The use of MCW method (effectively a limit equilibrium analysis) is one of the more popular however it is well known that the passive resistance derived by a linear slip surface using this approach is not always conservative, especially when the soil angle of shearing resistance and/or the wall interface friction is high (wall inclination also has an effect but vertical embedded walls are considered here). The main advantage of the MCW method over the other two methods is the possibility to obtain the earth pressure distribution instead of just the resultant impulse, furthermore in the case of the ESM method it is assumed that the contribution of the berm to the overall resistance is the contribution of the surcharge associated with the weight of the berm providing no direct lateral resistance at all. In the REF method the later resistance partially simulated as the raise in the ground level, however, this assumption is only empirical and it is common to obtain over-conservative results when using this method. The MCW method for drained analysis has been assessed. An automatic spreadsheet was developed (with use of the internal solver algorithms for the problem solving). Even though the MCW method seems to deliver more information than the other methods it is still considerably limited due to the fact that it is a limit-equilibrium method so the pressure distribution obtained by this method is associated with the ultimate limit state which is close to failure. It is known that for the full mobilisation of the passive earth pressures greater displacements are needed then for the mobilisation of the active pressures and as one of the main concerns during the wall retained constructions is the control of the displacements due to possible existence of the nearby structures and the quality control, it makes this method less feasible for that intent. The other parameters that are not being accounted by this method are the material properties like soil stiffness, wall stiffness or initial horizontal stresses. Taking this into account the Finite Element Analysis (FEA) was carried out with variations of these parameters in order to evidence the change in the output provided by them. The finite element software PLAXIS was used to perform this evaluation.

1.2. Objectives

The objective of this project is to examine existing methods for the evaluation of the support provided by earth berms in terms of accounting for the passive restraint offered by the berm, particularly in the drained conditions. The main focus was set on two particular methods, namely the Multiple Coulomb Wedge method and Finite Element Analysis. The application and the comparison of the obtained results as well as the advantages and limitations of two methods as well as comparison with some other methods are the aims of this study.

1.3. Structure of thesis

The thesis presented here has the following layout:

1) Literature review – overview and description of the existing methods and the general evaluation of state of art. As well as some life applications, conditions and underlying assumptions.

2) Analysis utilizing the Multiple Coulomb Wedge (MCW) method – the brief description of the method. Validation against and comparison with the results obtained in Smethurst & Powrie (2008). Analysis of two different geometry layouts.

3) Finite element analysis utilizing Plaxis software – General approach and conditions. Analysis of two geometries used in MCW method.

4) Comparison and the discussion of the results.

5) Conclusions and future recommendations.

6) Appendix: Manual for the automated MCW spreadsheet.

2. LITERATURE REVIEW

2.1. Excavation support - general

The use of embedded retaining walls is a routine approach in the construction of the basement excavations or road tunnels/cuttings. The objective of the retaining wall is to secure the excavated working area from possible soil movements, by offering resistance to the active impulses that are occurring on the back of the wall. The retaining structures may be a temporary or a permanent measure depending on the type of construction and the objectives. The retaining structures also differ by their stiffness which is the global stiffness resulting from the relative stiffness of the wall, support and ground. This aspect plays an important role, especially when the construction is very sensitive with regard to displacements.

Often these types of retaining structures need some form of support in order to respect all of the safety and serviceability demands. Those demands are usually moment equilibrium about some rotation point, force equilibrium, and displacements (vertical and horizontal). There are different ways that this support may be provided the most common are anchors, horizontal or raked props, and earth berms.

Anchor systems are widely used in the support of embedded walls; there are numerous reasons for this, such as the fact that they don't occupy any working space when compared to props or berms, they don't need another wall or construction element in order to offer resistance as in the case of props. However, there are some drawbacks usually with regard to the cost of renting of the equipment for their installation and providing access for this equipment in the working site. Another drawback is the constant revision of the tension in the anchors when they are prestressed.

Props, on the other hand, are usually easy to implement and it is a very inexpensive measure to provide the support. However, some other structural element is necessary inside the excavating area for the prop to be installed against which the prop is supported, which is not always possible or convenient. The overall resistance and displacement control provided by horizontal props is very adequate and the solution itself is inexpensive and easy to implement with the only issue being the type of excavation that allows those props to be installed which is dependent on the distance between the two opposite or adjacent elements. Raked props, on the other hand, allow implementation at any point of the construction but the resistance offered by them is reduced when compared to the horizontal props due to the fact that they rely on the friction provided by the support that is driven into the soil.

Another type of the support that may be used is earth berms that are made in-situ. The most obvious advantage of this solution is the economic and temporal aspect of the solution. The berm is formed by leaving the in situ material in place when forming the excavation, hence reducing the cost of the support system. The downside of earth berm supports is the space occupied by the structure which is the very crucial factor in the constructions inside the urban areas. Another downside would be the evaluation of

the resistance and displacement control offered by the structure. The evaluation of the resistance offered by the structure is the main objective of the following study.

2.2. Berm examples/case studies

There are several examples of the application of the berms in the construction site as the means for providing temporary support. One of them is the A4/A46 Batheaston-Swainswick Bypass which is discussed in Easton & Darley (1999).

Diaphragm type walls were constructed in conjunction with earth berms that provided temporary support. Two-dimensional finite element analysis (FEA) was carried out for the berm supported structure and the proposed supporting structure and was compared with the results obtained by in-situ measurements. Figure 1 compares the predicted lateral movements of the wall when using a) berms only and b) raked props. The results for the berm support are also compared with the range of movements observed at the top of the wall (c. 7 to 13 mm), the predictions were close but slightly on the conservative side due to the inability of the plane strain analysis to simulate the procedure of the berm removal in sections. That procedure may be simulated in advanced finite element analysis software. And it has special importance for the Berlin type walls (often used in urban areas) that use the berms as the temporary support that is removed in sections.

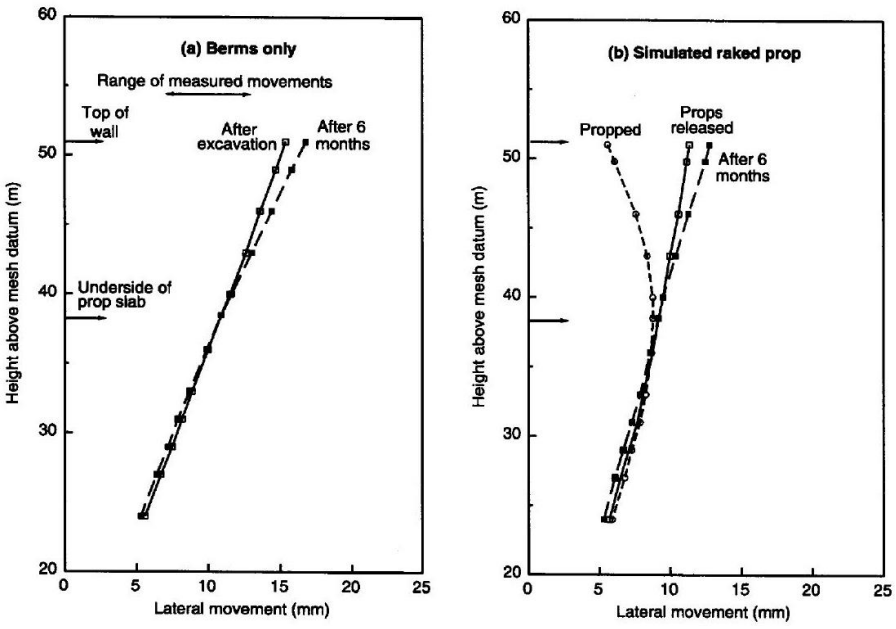

Figure 1 - Lateral moviments of the wall obtained by the FEA for the berm supported excavation and the proped excavation, Easton & Darley (1999).

This situation underlines the importance of three-dimensional (3D) effects in the evaluation of the berms influence on the structure. During the process of removal of the berms, they are not removed all at once but in sections. This problem is addressed in Gournevec & Powrie (2000) where the aforementioned case

study was used for validation of their 3D FEA analyses. The main focus of their study was a number of generic berm supported excavations with the different spacing between the excavated sections. One of the results that were obtained is illustrated in Figure 2. The β parameter was introduced as the ratio between the length of the excavated section B over the sum of the excavated section B and unexcavated section B'.

$$\beta = \frac{B}{B + B'}$$

For a given wall-berm geometry, ground conditions, and time period, there is a critical degree of discontinuity β that is independent of the length of the unsupported section B, such that if the degree of discontinuity β of a berm supported wall is less than critical value β_{crit}, displacements increase in proportion to the length of the unsupported sections; and if β exceeds its critical value, then displacements become a function not only of the length of the unsupported section but also of the degree of discontinuity which is the function of both of the B and B'. As β is increased above its critical value displacements increase more rapidly with continued increase in β.

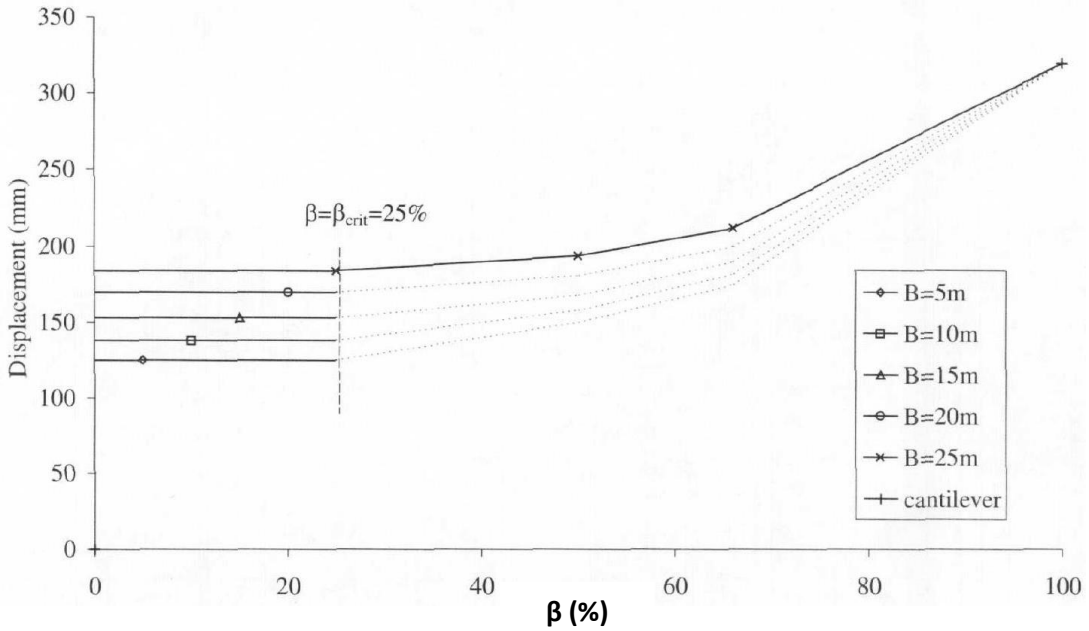

Figure 2 -Relationship between β and wall displacements, Gourvenec & Powrie (2000)

2.3. Analysis of berm effect

2.3.1. Underlying assumptions

2.3.1.1. Drained versus undrained

One of the main assumptions regarding the evaluation of the effects caused by the earth berms is the assessment of the soil conditions as drained or undrained. This assessment is highly influenced by the material permeability which will contribute to the rate at which the pore water pressures are being dissipated. Other important factors are surrounding groundwater conditions and soil stratification, for example, the presence of sandy layers in a clay material may contribute to accelerated drainage and therefore more rapid transition towards drained conditions. Time is a very relevant factor as well, taking into consideration that earth berms are often used as a means to provide temporary support, it is important to know both the necessary time that the berm should provide the support and the rate at which drainage and respective transition to the drained behavior occurs Gaba et al. (2003). The analysis presented in this study is performed based on drained conditions as it was the main purpose of the study.

2.3.1.2. Pore water pressures and suctions in berm

Regarding the pore water pressure distribution, the drained analysis was performed in order to compare the results with the drained approach of the Multiple Coulomb Wedge Method. As suggested in Gaba et al. (2003) for the drained conditions: "The designer should evaluate the water pressure over the whole of the wall assuming steady-state conditions at relevant stages of construction and over the lifetime of the wall."

For that, the method indicated in Padfield & Mair (1984) was adopted, wherein the long-term, steady-state linear seepage develops when there is a difference in water levels behind and in front of the wall, as illustrated in the flow-net given in Figure 3. The same approach was used in Smethurst & Powrie (2008) and more detailed explanation of the approach may be found in Appendix A.
On various occasions the suctions are assumed in the berm. The main two reasons for the suctions to occur are 1) the rapid undrained unloading during the excavation or 2) long-term suctions in materials due to the capillary effect.

Smethurst & Powrie (2008), assumed suctions remained in the berm while carrying out a drained analysis based on the assumption that measures were taken to impermeabilize the berm and to prevent swelling. To estimate the suctions in the berm, Smethurst & Powrie (2008) assumed they could be evaluated by extrapolating the pore water pressure gradient established from the linear seepage assumption through the berm. This assumption does not seem very realistic due to the fact that even with all of the aforementioned measures applied it is not really possible to maintain this suction profile. As it will be

shown further in the study this suction profile may result in the negative total stress and unrealistic effective pressure increase (spike) in the top of the berm.

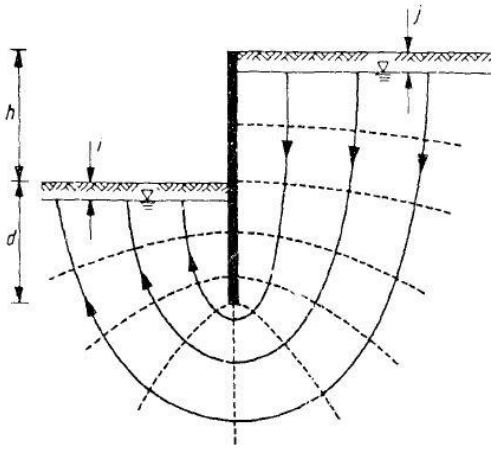

Figure 3 - Flow net, Padfield & Mair (1984)

2.3.2 Evaluating the stabilizing effect provided by berms

Most methods of representing the effect of the earth berms utilize the limit equilibrium approach and are semi-empirical. The most common methods are Equivalent Surcharge Method (ESM), Raised Effective Formation (REF) method and Multiple Coulomb Wedge (MCW) method. There is also Culmann's graphical method for determining the passive resistance of earth, NAVFAC 7.02 (1986). Another approach is used in the program WALLAP which has some similarities with the MCW approach. The effect may also be calculated using finite element analysis (FEA). Another approach that may be of interest is that which evaluates the resistance of the retaining walls with a backfill that has a negative inclination, e.g. Lam (1991) and Shiau et al. (2008).

It is important to note that for the aforementioned methods (except for FEA) the stability of the berm face, as well as the general stability of the whole soil-wall system, must be assured in a separate evaluation.

2.3.2.1. Equivalent Surcharge Method (ESM)

In the ESM, the weight of the berm is calculated and is applied as a surcharge over a distance defined by the intersection with the excavation level of the line emanating from the toe of the wall at an angle of (45° - ϕ'/2) to the horizontal. The lateral resistance offered by the berm is not taken into consideration, thus making this approach conservative when compared with other methods. A schematic representation of the method is presented in Figure 4.

The analysis carried out in Smethurst & Powrie (2008) for effective stresses and Daly & Powrie (2001) for undrained cases confirm that this method is conservative Simpson & Powrie (2001).

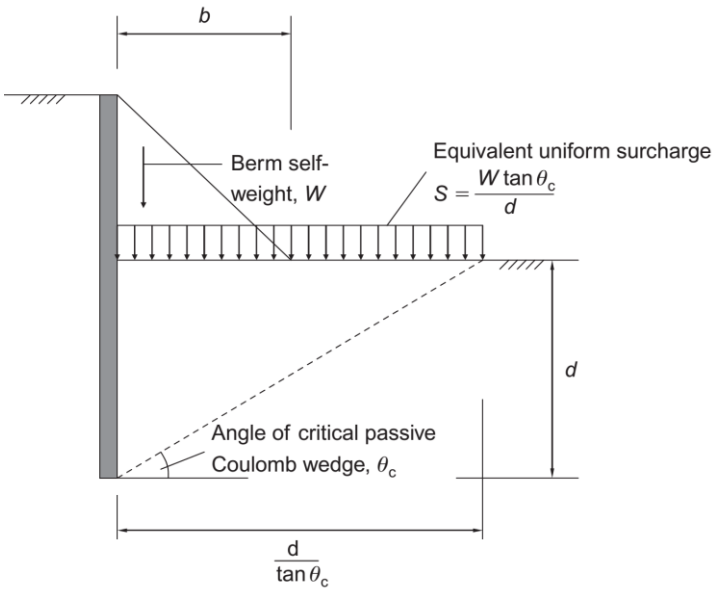

Figure 4 - Schematic representation of the ESM method, Smethurst & Powrie (2008)

2.3.2.2. Raised Effective Formation Method (REF)

Another limit equilibrium method which is highly empirical is the Raised Effective Formation method (REF), Fleming et al. (2009). The raised effective formation approach defines a design berm geometry that has the same base width b as the actual berm but has a slope of 1:3, the maximum height of the design berm then becomes b/3. The design berm is modeled in the analysis by raising the formation level by half the design berm height, i.e. b/6. Any of the actual berm extending above the design berm geometry (the area shown shaded in Figure 5 can then be applied as a surcharge to the new dredge level using the equivalent surcharge approach. The lateral pressure exerted by the berm is partly modeled by this approach.

The main differences between this method and the ESM is that the lateral resistance of the berm is partially modelled, so the effect of the berm is not only due to its weight but also in the alteration of the point of the application of the resulting earth impulse, which in this method is applied at a higher level hence increasing the leverage in relation to the rotating point near the base of the wall, resulting in a greater stabilizing moment.

The results of this methods tend to be un-conservative for both drained and undrained analysis, as shown in Smethurst & Powrie (2008) and Daly & Powrie (2001) respectively.

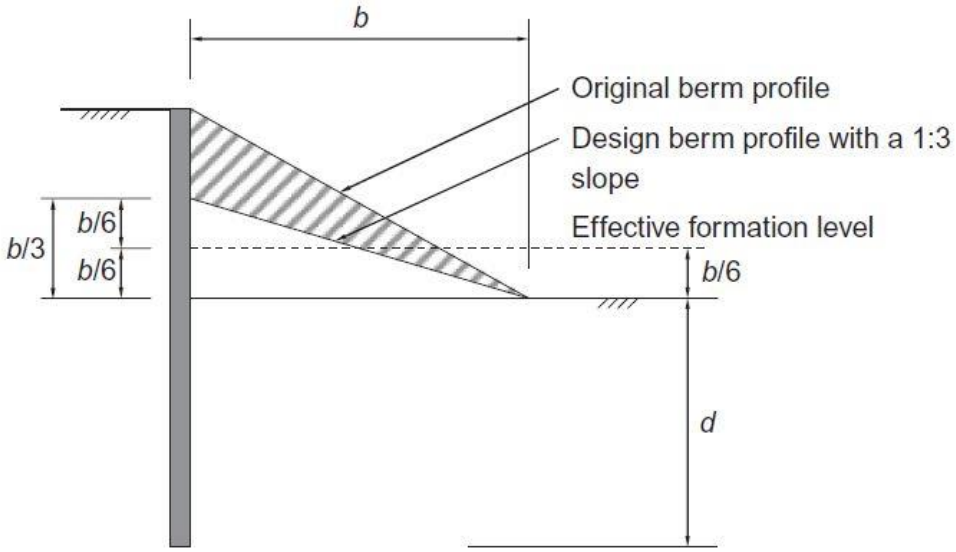

Figure 5 - Schematic representation of the REF method, Smethurst & Powrie (2008)

2.3.2.4. Multiple Coulomb Wedge Approach (MCW)

The MCW approach uses a series of Coulomb wedges spaced at regular intervals along the wall to calculate the lateral pressure distribution from the berm. Daly & Powrie (2001) present a limit equilibrium stress analysis for berm-stabilized walls that, as well as providing an estimate of the lateral pressure exerted by the berm, enables the factor of safety on soil strength to be calculated for any given combination of berm and wall geometry and undrained soil strength properties. This analysis may be modified to use effective stress soil parameters (the frictional soil strength ϕ', effective cohesion c' and pore water pressure, u) Smethurst & Powrie (2008).

This approach will be explained and demonstrated in more detail in Chapter 3 and in Appendix A.

2.3.2.5. WALLAP Approach

The program Wallap uses an approach that has some similarities with the MCW method. The calculation of the pressure is made by the following steps (WALLAP, 2012):

Step 1: The limiting passive resistance at each elevation within or below a berm is taken as the least of the following values:

1) The resistance calculated as if the ground level were horizontal at the top of the berm.
2) Sliding resistance along a horizontal plane within the berm.
3) Sliding resistance on an inclined plane passing through the toe of the berm.
4) Sliding on a horizontal plane below the toe of the berm in conjunction with a passive wedge beyond the toe of the berm as shown in Figure 6

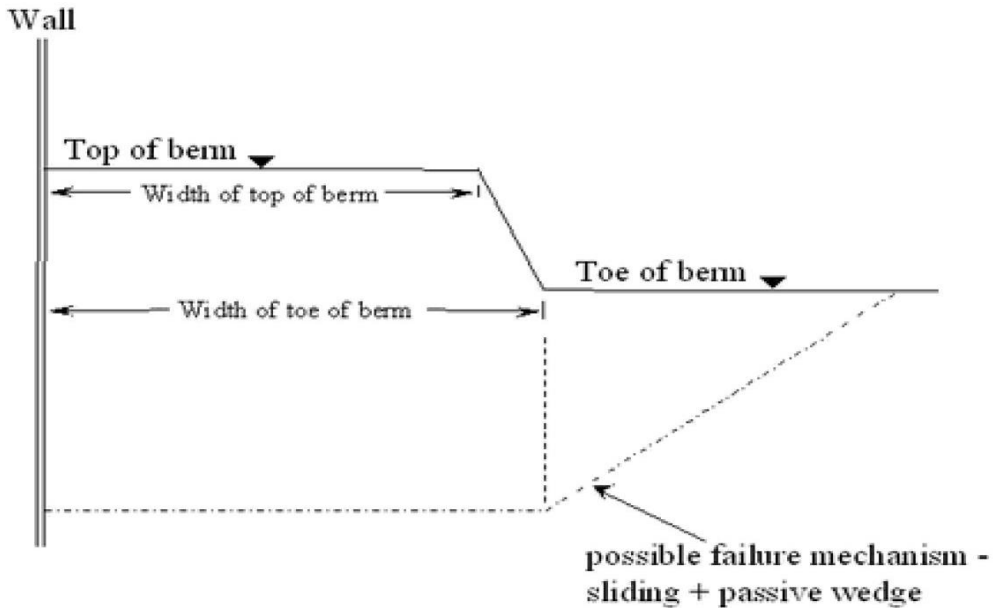

Figure 6 - Failure mechanism for WALLAP Step 1, Part 4) mechanism.

Step 2: The above calculation produces a profile of available (passive) force at each elevation. In normal circumstances (increasing strength with depth) the available passive resistance increases steadily with depth. In special cases however e.g. a buried soft layer, there may be a sudden drop off in total resistance at the soft layer. In order to avoid that, the force profile is adjusted so that available force at higher elevations is never greater than that at lower elevations.

Step 3: The profile of available force is now differentiated with respect to depth to produce a profile of available passive pressures.

Considering this approach especially during Step 1, it seems like there might be some benefits in implementing the MCW approach into the calculations so the wedges in between the toe of the berm and the top of the berm would be taken into consideration, as sometimes those slip surfaces are more critical as will be shown in the next sections.

2.3.2.6. Finite Element Analysis (FEA)

Another tool at hand is the Finite Element Analysis that can be carried out by using software such as Plaxis or CRISP. The FEA that is presented in this thesis was performed using Plaxis. There are numerous advantages of using FEA; one of the advantages that was already mentioned was the possibility to carry out 3D analysis, allowing the possibility to simulate partial excavations of the berm, this is especially important for construction sites that require support over an extended length such as road embankments. However, there are many other advantages such as the possibility to evaluate the displacements which are important for the SLS.

2.3.2.7. Earth pressures with sloping ground

Another possible way to address the passive resistance provided by the berm is to utilize the approaches like charts that give the horizontal pressure coefficient for the retaining walls with negatively inclined backfill. Lam (1991) carried out a series of calculation using the MJSM program, which is based on the simplified method of slices, in order to estimate the passive resistance coefficient for different angles of shearing resistance, wall friction, and ground inclinations. The results were compared with the results of the Caquot & Kerisel (with log spiral surfaces) and the ones obtained utilizing the K_p coefficient of the Coulomb's theory for walls with soil- friction and sloping ground.

The comparison of the results indicates that they are close for negatively inclined backfills (that can be compared to berm geometry) even with an increasing value of the wall friction which indicates that in those cases a planar slip surface is an adequate assumption. For the horizontal or positively inclined backfills, the Coulomb method tends to overestimate the passive resistance. The results for the shearing angle of 30 ° are presented in Figure 7, it is important to note that negative value of β/ϕ represents the backfill sloping downwards and "0" value represents horizontal backfill. The discrepancy also tends to increase with the angle of shearing resistance, which also may be due to the fact that the wall friction is not given an absolute value but is calculated as the direct proportion to the value of the angle of the shearing resistance of the soil. The resulting values of the coefficients of the horizontal soil pressure will be compared with the values obtained by the MCW approach for similar configurations.

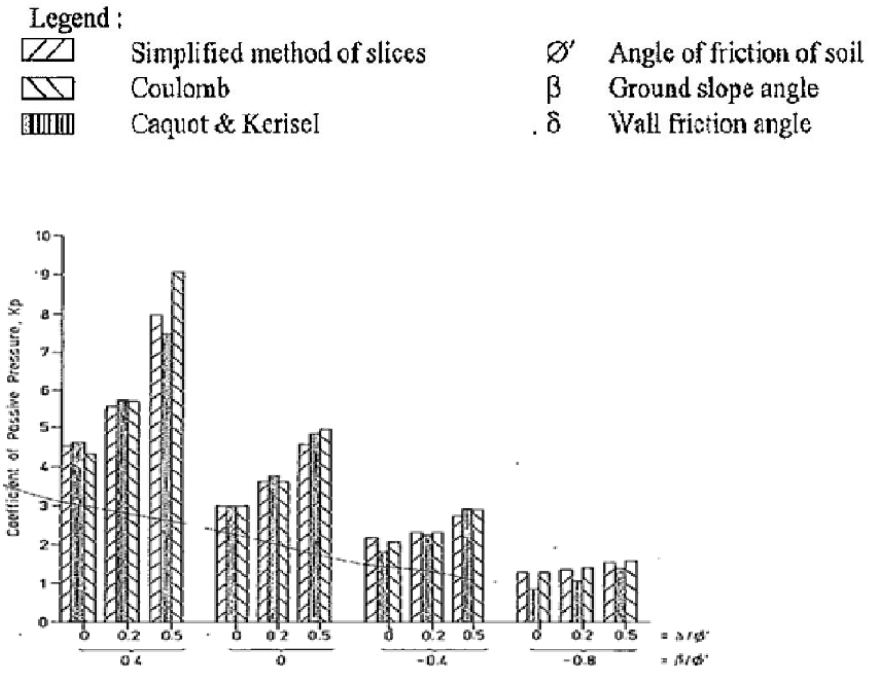

Figure 7 - Comparison of passive pressure coefficients for a cohesionless material with a friction angle of 30°, Lam (1991).

A similar observation was made in Shiau et al. (2008) from their analysis based on finite element formulations of the bound theorems of limit analysis and non-linear programming techniques. The analysis was carried out for different values of the soil-wall friction, wall inclination, and backfill surface configuration. Figure 8 presents contours of the velocity fields obtained in this analysis for horizontal and negatively inclined backfill, which also indicates that the linear slip surface is an adequate approximation for the failure mechanism.

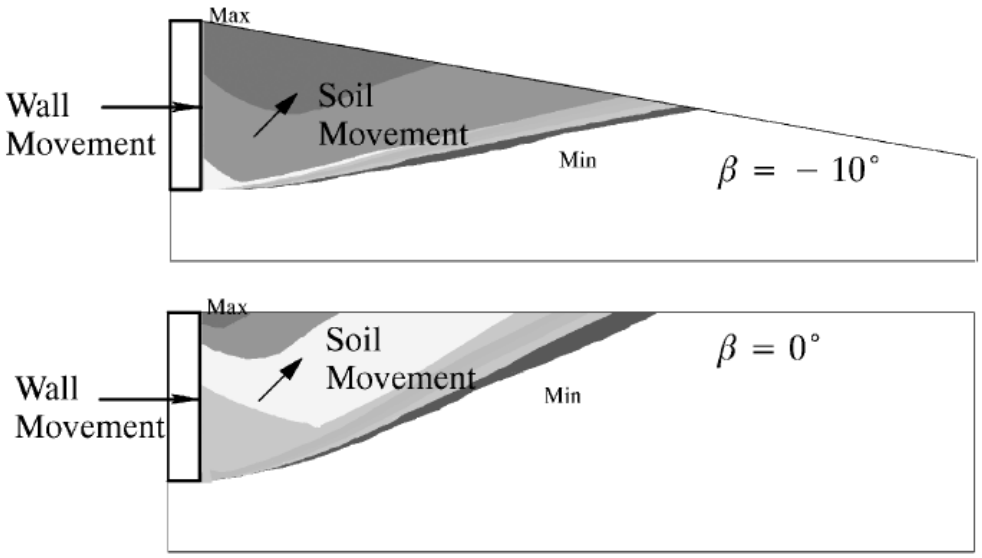

Figure 8 - Contours of velocity fields for various backfill inclinations, Shiau et al. (2008)

Considering the analysis and the conclusions drawn by Lam (1991) and Shiau et al. (2008) it seems that for negatively sloping ground like in the case of the berms, the MCW approach should provide an adequate estimation of the passive pressures even considering that the slip surfaces for the passive wedges are better represented with the spiral logarithmic curves, however, those methods do not consider a slope with finite dimensions such as a berm which may lead to a different results.

3. MULTIPLE COULOMB WEDGE (MCW) METHOD

3.1 Implementation & validation

3.1.1. General description.

The Multiple Coulomb Wedge method (MCW) is a limit equilibrium method that can be used to evaluate the lateral stress distribution acting on berm-stabilized retaining walls, by dividing the wall by equally spaced nodes that will correspond to the different wedges. The critical slip surface associated with the minimal impulse in the case of the passive wedge and the maximum impulse in the case of the active wedge is calculated for each node. The pressure is obtained by dividing the maximum/minimum impulse by the distance between the nodes. As represented in Figure 9.

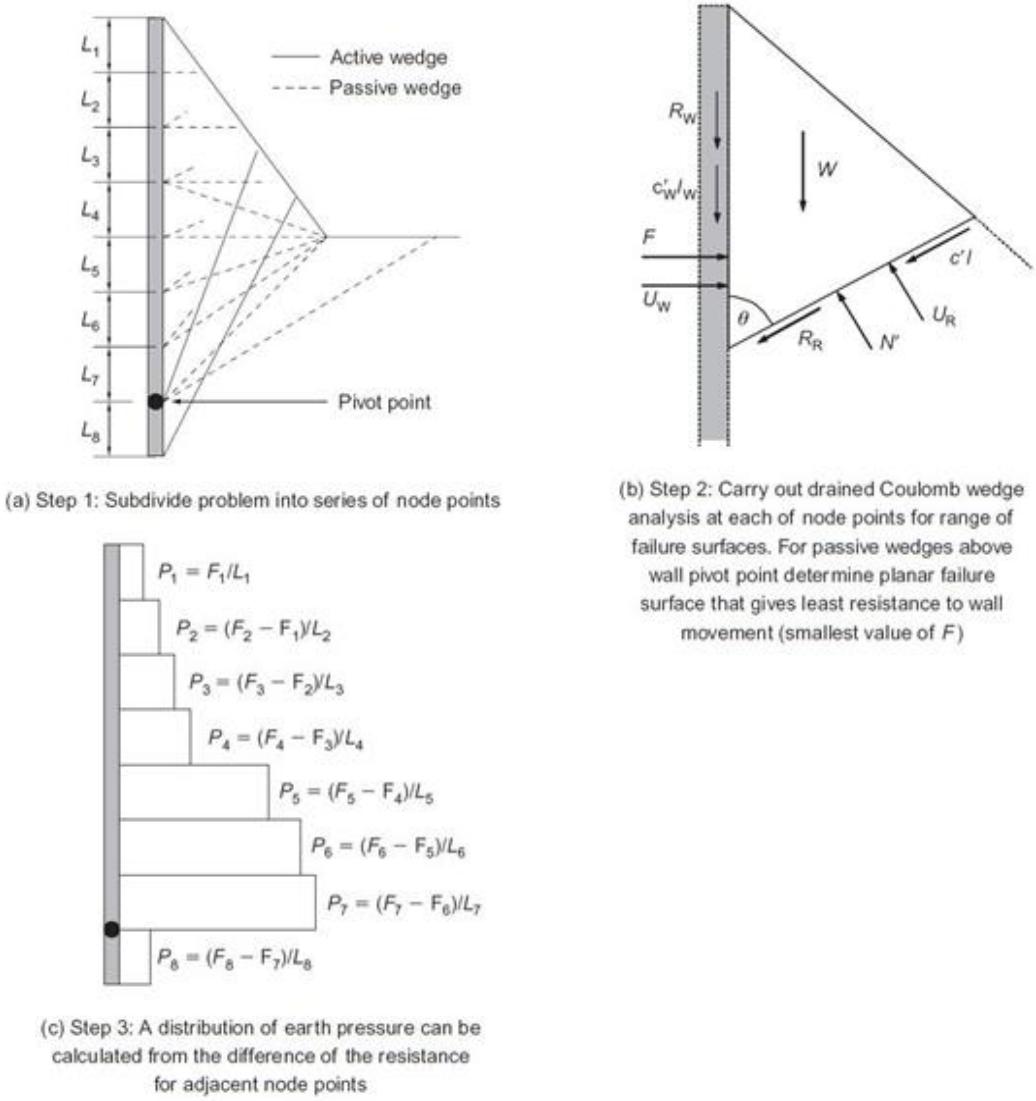

Figure 9 - MCW application steps, Smethurst & Powrie (2008).

The determination of the critical angle of the slip surface is crucial, due to the fact that it's associated with the critical wedge and earth impulse. As was previously explained, the pressure distribution is

approximated as the value obtained by dividing the difference in the critical passive/active forces of the adjacent nodes by the distance between them, which suggests that for a certain extent a larger amount of nodes is associated with more accurate pressure distribution. In order to optimize the determination of the critical slip surfaces and the respective earth impulses, an automated Excel spreadsheet was developed. It allows the MCW calculations to be executed with different possible configurations such as water level, geometry, node quantity and material characteristics (including cohesion, wall friction, soil-wall adhesion and others). The spreadsheet was optimized by using automatic calculations built into the Microsoft Excel Solver, in particular, GRG-nonlinear and Evolutionary methods in conjunction with Excel's VBA macros which allow the aforementioned methods to be executed repeatedly, by writing a program. The MCW spreadsheet is explained in detail in Appendix A.

3.1.2 Verification of the MCW method

One of the ways to validate aforementioned spreadsheet was by recreating the results presented by Smethurst & Powrie (2008), using the geometry and conditions. The geometry used in Smethurst & Powrie (2008) was based on a 7 m deep excavation with a 21 m deep diaphragm wall. The water level was at the ground level on the active side of the wall and at the excavated level on the passive side of the wall. Pore-water pressures acting on the wall were evaluated using a linear steady state seepage approximation. Suctions were assumed above the excavated level, i.e. in the berm with the same gradient as the pore water pressures below the water table.

Regarding the materials, the soil-wall adhesion and cohesion, as well as the wall friction on the passive side, were set to zero. An angle of shearing resistance of 26° was assumed for the soil. The unsaturated and saturated unit weight was set to 20 kN/m^3. The unit weight of water was set to 9.81 kN/m^3.

On the wall, and based on the results presented by Smethurst & Powrie (2008), the rotational pivot point was located at a depth of 20.19 m and a factor of safety of 1.27 was applied to the shear strength, which results in a mobilized angle of shearing resistance of approximately 21°.

In Smethurst & Powrie (2008) a spacing of 1 m between nodes was utilized, however for increased precision, a nodal spacing of 0.175 m was used for the current analysis.

In the following, charts representing the effective stresses, pore water pressures, and the total stresses are presented. The results of the current analysis are plotted on top of the results obtained (J.A. Smethurst, 2007), with the same scale for the better perception and easier comparison. The first chart illustrated in Figure 10 shows the effective active and passive stresses along the wall.

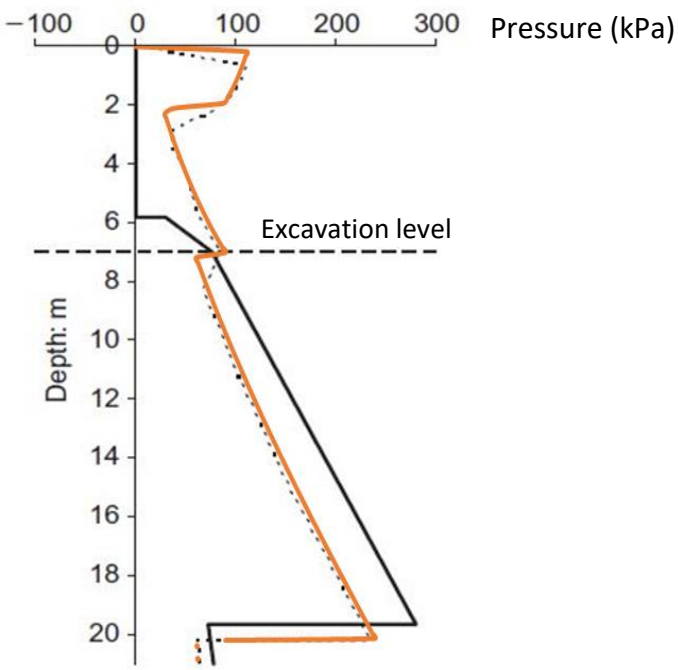

Figure 10 - Comparison of effective earth pressure distributions using MCW method.
MCW earth pressures from Smethurst & Powrie, 2007 are dashed black line; REF, solid black lines; orange lines, this work.

The results are similar but due to the fact that in the current analysis the distance between the nodes is smaller, there are three zones where the results differ from those in Smethurst & Powrie (2008).

The first is at the very top of the berm, where it can be noted that in Smethurst & Powrie (2008) the line is extrapolated from ground level to the first node 1 m below ground level, whereas in the current analysis five nodes are located within the same interval. This higher density of nodal points results in the pressures remaining higher closer to the ground surface.

A similar situation occurs between 2 and 3 m, and 7 and 8 m depth; in both cases due to the lack of intermediate nodes in these intervals, the pressure changes at a slower rate in the results from Smethurst & Powrie (2008) than the current analysis. The sharp change in the stress distribution at these level will be discussed later.

Regarding the pore water pressures illustrated in Figure 11, the distribution is identical in the two analyses which confirm the methodology used in the MCW spreadsheet and suggests that any differences between the analyses cannot be attributed to the pore water pressure distribution.

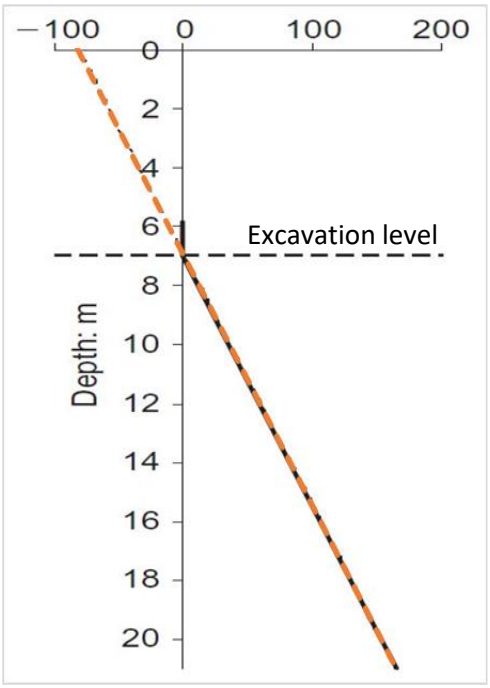

Figure 11 - Comparison of pore water pressure distributions from MCW method.

MCW earth pressures from Smethurst & Powrie, 2007 are black line; orange line, this work.

In terms of total stresses, Figure 12 the same discrepancies as for the effective earth pressures may be observed as the PWP distributions were identical. The great negative value of the total stresses in the top of the berm is due to the great value of suctions in this area. There is an inconsistency in the Smethurst & Powrie (2008) results; at ground level, the effective stresses are zero and the pore water pressures are -86 kPa (suction) and therefore the total stress should be non-zero as indicated in the current analysis.

Overall the results obtained by the MCW spreadsheet are identical to those obtained by Smethurst & Powrie (2008) but is more precise due to the increased number of nodes, which is more practical when the calculation model is automated.

Figure 13 represents some of the critical slip surfaces along the whole wall obtained using the MCW method and based on the above conditions. It is interesting to observe that due to the suctions in the berm, at the top, there are few critical slip surfaces that have an upward inclination. Afterwards, as the node depth increases the critical slip surface inclination alters, moving to almost horizontal, below horizontal and ultimately all of them slope down towards the toe of the berm.

Another important observation is that due to the presence of the berm the critical slip surfaces below the excavated level have a flatter inclination compared to the theoretical solution for the mobilized passive wedge in the cantilever wall with no berm which would result in:

$$\theta_{crit} = 45° - \frac{\varphi}{2} = 34.5°$$

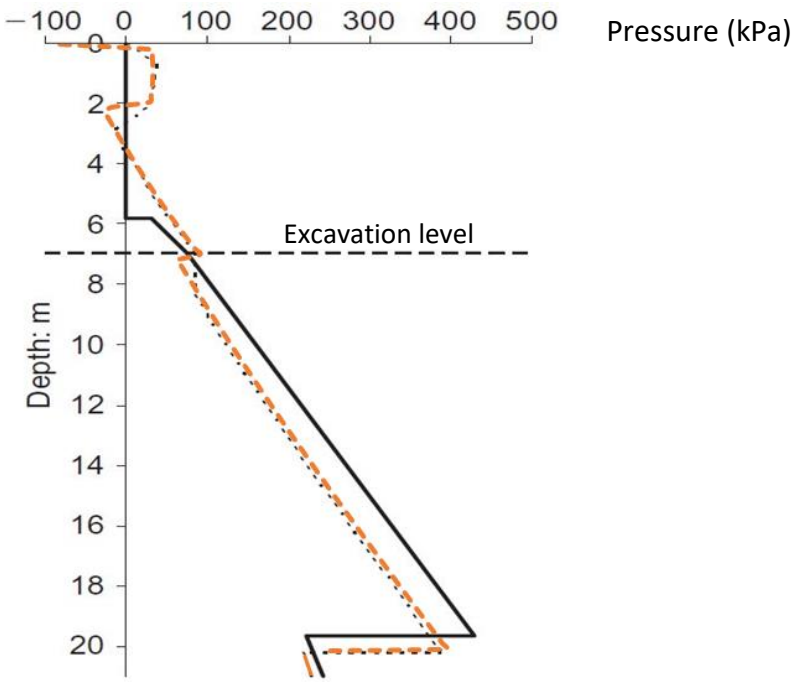

Figure 12 - Comparison of total earth pressure distributions from MCW method.
MCW earth pressures from Smethurst & Powrie, 2007 are dashed black line; REF, solid black lines; orange lines, this work.

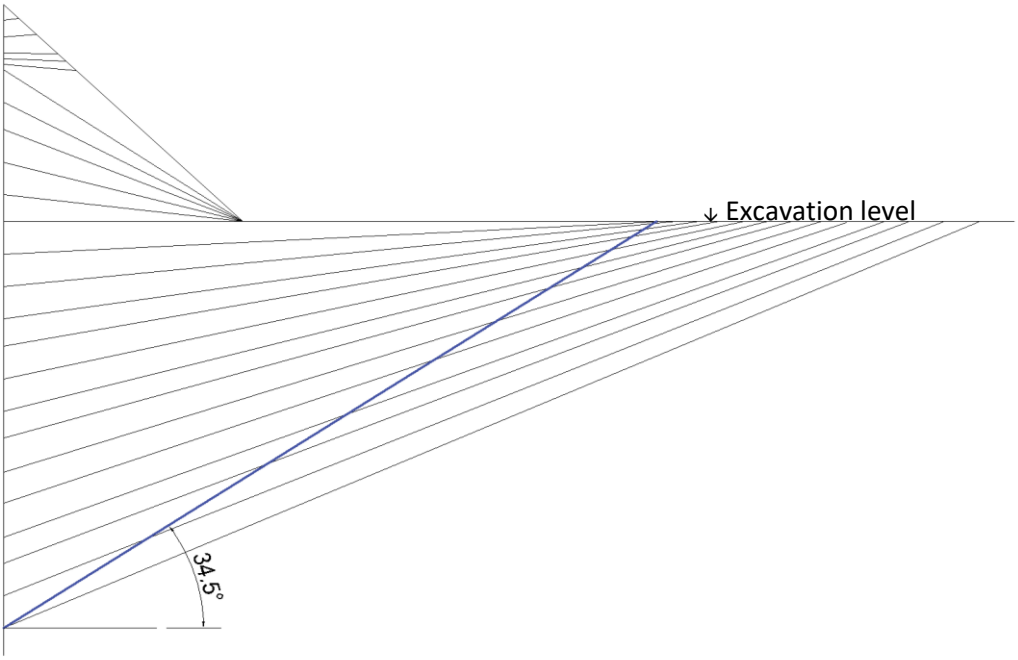

Figure 13 - Critical slip surface locations from MCW method, with Coulomb slip surface (blue line) for horizontal excavation level and friction-less wall for comparison

3.1.3 Comments on the S&P Results and assumptions

a) Suctions

The whole analysis that was developed by Smethurst & Powrie (2008) relies on the suctions developed in the 1H:1V berm, but even for this assumption the face stability of the berm was not achieved.

Overall, the Smethurst & Powrie (2008) approach seems unrealistic especially taking into consideration that the analysis was made for the drained condition in which the suctions dissipate at a high rate even when some of the techniques described in the paper are applied. Hence this approach may not be preferred for the long-term stability evaluation of the berm but more as some kind of transitory phase between the undrained and drained behavior.

b) Spike in the effective earth pressures

As was noticed before there is an earth pressure spike at the top of the berm. In Smethurst & Powrie (2008) this is explained by the suction and the berm geometry. Smethurst & Powrie (2008) indicate that this spike disappears for trapezoidal type berms with a 2 m bench at the top. However, the same analysis was carried out for the berm with the top bench of 2 m with the rest of the conditions and geometry unaltered and Figure 14 presents the distribution of the effective earth pressures obtained.

The pressure spike occurs between 0 m and approximately 0,875 m depth, below which the values of effective stresses drop back and most remained unnoticed due to the 1 m nodal interval used by Smethurst & Powrie (2008).

An analysis was also made for a berm with a flatter inclination of 2H:1V (Horizontal: Vertical), the results of which are represented in Figure 15. It can be observed that the maximum value of the spike extends over a greater depth than in the case of a 1:1 slope and the maximum value of the effective earth pressures was increased as well.

Further, the 2H:1V geometry with no suctions was analyzed in order to evaluate the possible effect of suctions. The resulting effective pressures are illustrated in Figure 16. Note that a 1H:1V berm without suctions is not represented due to the fact that it is unstable. In this analysis, the spike disappeared, however, the offset that occurs in the transition between the berm and ground below are now more pronounced.

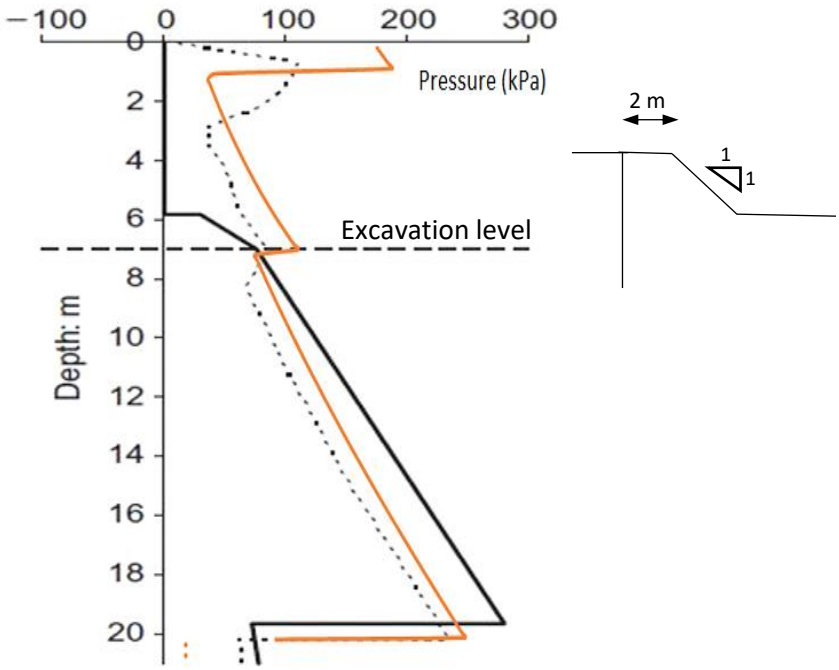

Figure 14 - Earth pressure distributions for 1H:1V berm with 2 m wide top bench with suctions.
MCW earth pressures from Smethurst & Powrie, 2007 are dashed black line; REF, solid black lines; orange lines, this work.

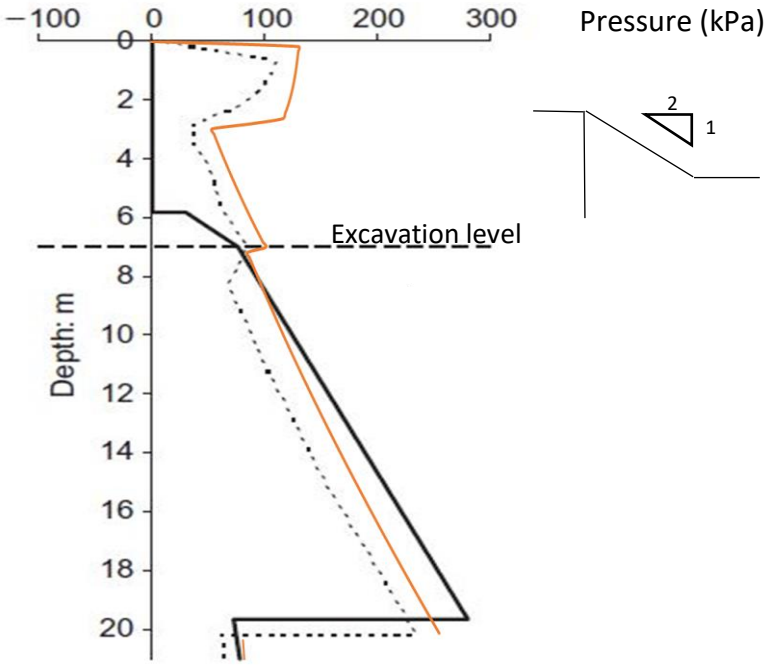

Figure 15 - Effective earth pressure distributions for 2H:1V berm with no top bench with suctions.
MCW earth pressures from Smethurst & Powrie, 2007 are dashed black line; REF, solid black lines; orange lines, this work.

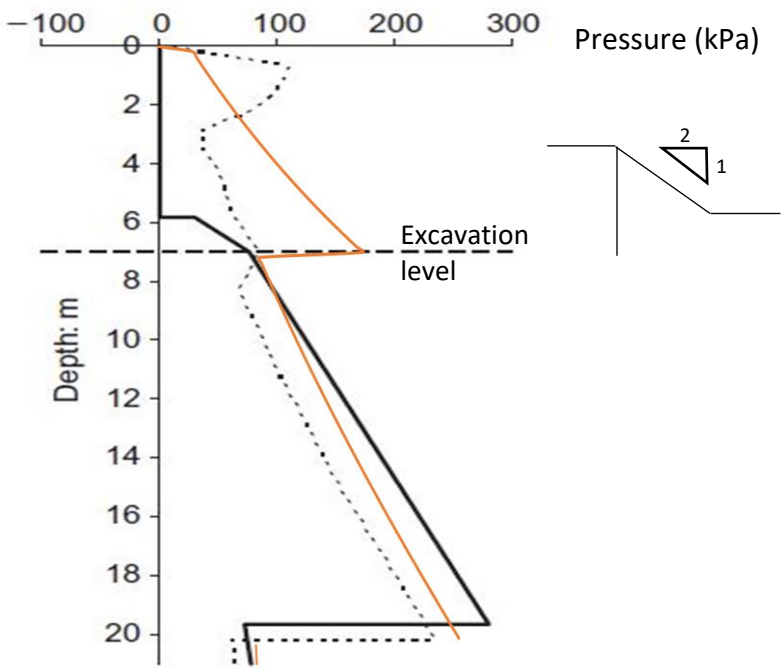

Figure 16 - Effective earth pressure distributions for 2H:1V berm with no suctions.
MCW earth pressures from Smethurst & Powrie, 2007 are dashed black line; REF, solid black lines; orange lines, this work.

In Figure 17, the slip surfaces inside the berm are illustrated for the aforementioned berm configurations.

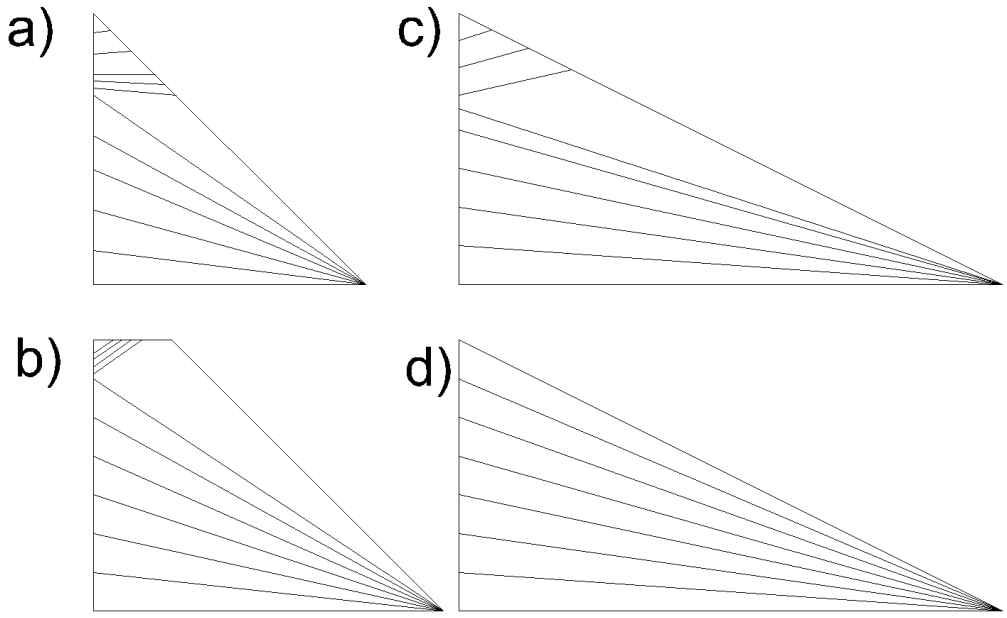

Figure 17 - Critical slip surfaces for differing berm configurations.

a) 1H:1V triangular berm with suctions b) 1H:1V trapezoidal berm (2 m wide bench) with suctions c) 2H:1V triangular berm with suctions d) 2H:1V triangular berm without suctions.

From observing Figure 17, it can be noticed that in (a) the slip surfaces have a gradual transition from slightly upward inclination to the lines that are sloping to the toe of the berm while in the trapezoidal

shape berm (b), there is a sudden change in the direction of upward inclination to the toe of the berm, even with the nodal spacing as small as 0,175 m. In Figure 17(c) a sudden change in the direction of the critical slip surface occurs as well but in (d) which is identical to the (c) case but has no suctions in the berm, the slip surfaces always slope towards the toe of the berm.

3.2 Application

In this section the MCW method will be applied to 2H:1V and 3H:1V trapezoidal berms. The intention is to compare the results regarding the effective earth pressures obtained from the MCW method to the results obtained in the same berm configurations using the finite element program Plaxis.

For that purpose, some assumptions regarding the model geometry were made. It is necessary first to establish the angle of shearing resistance for each of the geometries for which the berm is stable. After the berm stability is assured, the required wall embedment below the excavated level was determined assuming as a final condition that the wall is supported by a single prop at the top of the wall after removal of the berm. The objective is to determine the wall depth below the excavated level for which the ratio of stabilizing to destabilizing moment is close to unity in order to get as close to collapse in the whole soil-wall-berm system as possible in the FEA for the maximum mobilization of the passive earth pressures while ensuring the berm remains stable or only fails as one with the wall system.

Two berm geometries were considered, one with a face inclination of 2H:1V and one with 3H:1V, the top of the berms is at ground level and is 2 m wide. The height of the berm was maintained at 7 m and therefore the width of the base of the berms was 16 m and 23 m respectively, Figure 18.

In order to ensure that berm stability did not have an impact on the FEA calculations, suitable resistance parameters had to be defined. The version of PLAXIS used for this study does not allow the use of suctions and so they were not considered as a stabilizing effect in these calculations. The angle of shearing resistance was then defined as the minimum value for which the berm remains stable in the FEA. Thus, angles of shearing resistance of 28° and 20° were defined for the 2H:1V and 3H:1V berms respectively.

The final configuration of the excavation is with an embedded retaining wall supported by a single prop located at the ground level which is installed before the berm is removed. The required wall length is defined by this condition and was 12 m and 16 m for the 2H:1V and 3H:1V berm geometries respectively. It should be noted that for the 3H:1V berm the value of the angle of shearing angle is lower due to the fact that the berm is more stable, but at the same time due to the reduction of the shearing angle the total impulse is reduced so in order to confine the overall stability the wall length is greater.

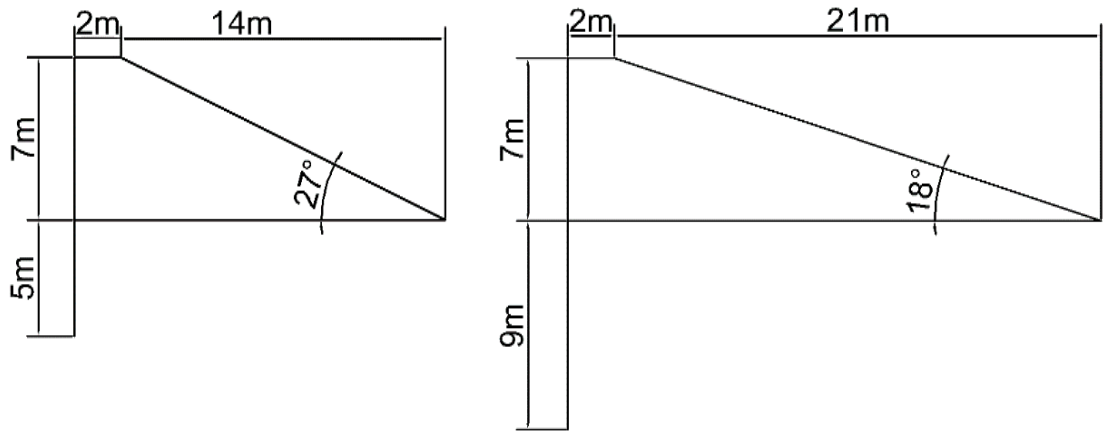

Figure 18 - Berm configuration.

Unlike the validation problem, wall friction was taken into account in these calculations and was assumed to be 2/3 of the angle of shearing resistance both on the front and the back of the wall – this is probably a more realistic assumption and also avoided the problems associated with using low values of wall friction that occur in PLAXIS due to the factor also being applied to the stiffness in the interface formulation. The pore water pressure distribution is similar to the one used in the previous studies, using the linear steady-state seepage approach. A summary of these details for each berm configuration is provided in **Table 1.**

Table 1 Parameters for the analysis.

Definition	**Symbol**	**Unit**	**2H:1V**	**3H:1V**
Top bench width	b	m	2.0	2.0
Slope inclination	α	°	26.57	18.43
Height	h_{berm}	m	7.0	7.0
Wall geometry:				
Wall length above the ground level	f	m	7	7
Wall length below the ground level	d	m	5	9
Depth of the pivot point	Z_p	m	11.5	15.5
Node spacing	h*	m	0.25	0.25
Material characteristics				
Angle of shearing Resistance	ϕ'	°	28	20
Apparent cohesion	c'	kPa	0.00	0.00
Wall adhesion	c_w	kPa	0.00	0.00
Passive wall friction	δ_p/ϕ'	-	0.667	0.667
Active wall friction	δ_a/ϕ'	-	0.667	0.667
Unit weight of soil	γ	kN/m^3	20.00	20.00
Pore water pressure				
Unit weight of water	γ_w	kN/m^3	9.81	9.81
PWP at the bottom of the wall	u_f	kPa	69.25	113.01
PWP gradient in front of the wall	$u_{gr,f}$	kPa/m	13.85	12.56
PWP gradient behind the wall	$u_{gr,b}$	kPa/m	5.77	7.06

3.2.1 2H:1V Berm analysis

The results of the MCW analysis regarding the passive pressures are presented in Figure 19. It can be observed that due to the assumed soil-wall friction, the pressure spike at the top of the berm and the spike in the transition from the berm to the ground below the excavated level are greatly increased compared to the previous case where the wall friction was assumed to be zero. The spike at excavated level is decreased when suctions are assumed. Overall, due to the presence of the soil-wall friction and trapezoidal form of the berm, the resistance has considerably increased inside the berm when compared to the previously discussed 2H:1V triangular geometry with no suctions and no soil-wall friction but also with a slightly lower angle of shearing resistance of 26°.

Overall the pressure distribution does not seem very realistic, due to the exaggerated pressure spike. This might be explained by the fact that in evaluating the passive resistance especially when the soil-wall friction is taken into account the logarithmic spiral slip surfaces gives more adequate results when compared to the linear slip surfaces used in the MCW.

Another reason might be the fact that the slip surface at the excavated level is forced to slope towards the toe of the berm. The maximum value of the effective stresses is achieved inside the berm due to the big spike that was mentioned previously and due to the short extent of the wall below the excavated level. The critical slip surfaces of some of the wedges are represented in Figure 20. Over the first 2 m at the top of the wall, a node spacing of 0.25 m was used in order to better illustrate how the critical slip surfaces change their inclination inside the berm. Over the remainder of the wall, a node spacing of 1 m was used.

The slip surface lines are transitioning gradually from the upward inclination towards the toe of the berm. Below the excavated level, the slip surface lines have very slight inclination that might be explained by the presence of the soil-wall friction. The assumption of the soil-wall friction may also explain the upward sloping of slip surfaces in the top of the berm as well as other slip surfaces that do not slope directly to the toe of the berm.

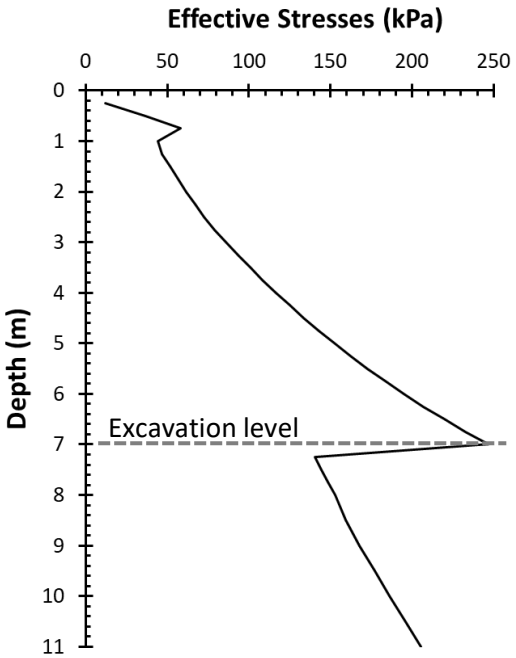

Figure - 19 Effective earth pressure distributions for 2H:1V berm.

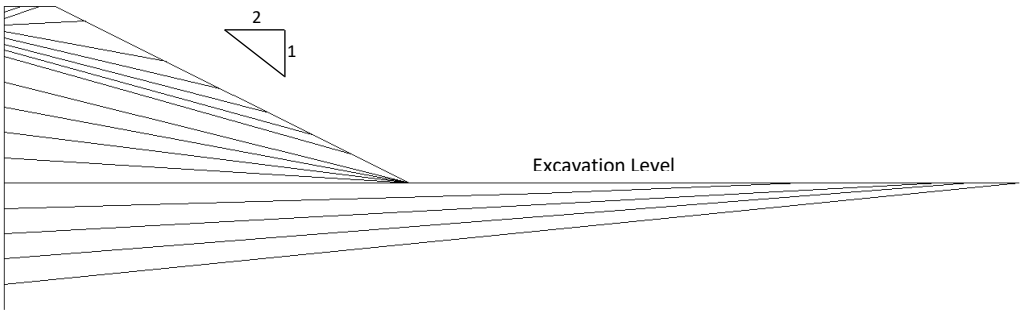

Figure 20 - Critical slip surfaces for 2H:1V berm.

3.2.2 3H:1V Berm analysis

In Figure 21, the results of the MCW analysis regarding the passive pressures are represented. Overall the stress distribution is very similar to the one obtained in the 2H:1V case with pressure spikes in the effective stress profile. But in this distribution, the maximum value is achieved below the excavated level due to the greater extension of the wall and reduced value of the shearing resistance of the soil.

The critical slip surfaces are illustrated in Figure 22, the distribution of slip surfaces is close to the one obtained in the previous analysis, with the gradual transition from the upward inclination towards the toe of the berm.

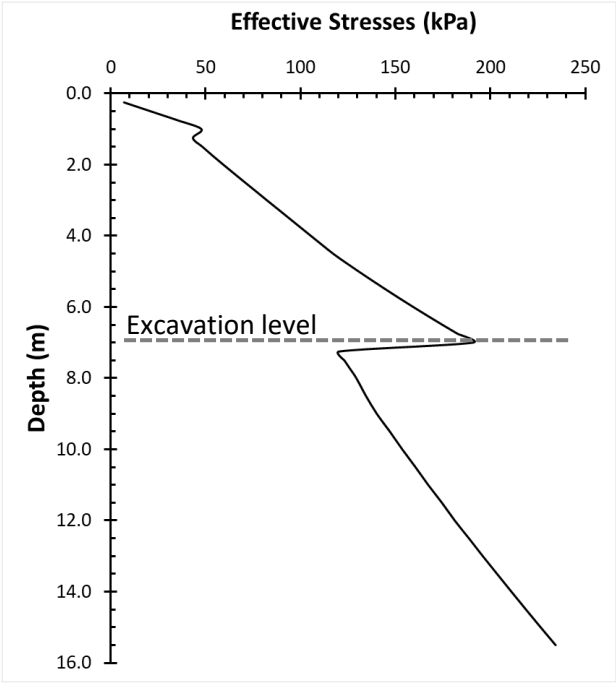

Figure 21 - Effective earth pressure distributions for 3H:1V berm.

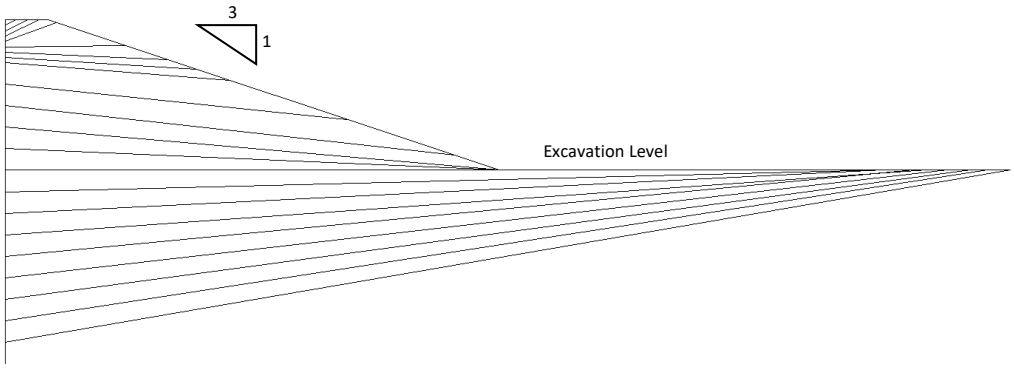

Figure 22 - Critical slip surfaces for 3H:1V berm.

4. FINITE ELEMENT ANALYSIS

4.1 Basis for the analysis

4.1.1 General approach for the wall depth and angle of shearing resistance definition

a) General approach for the wall depth and angle of shearing resistance definition

In order to have conditions that are close to the one used in the MCW, it is necessary to first establish the angle of shearing resistance for each of the geometries for which the berm is stable. After berm stability has been assured, the wall depth below the excavated level was determined by using a simple prop model, with the prop at the top of the wall. This is assumed to be the final configuration after the berm is removed. For this model, the objective is to determine the wall depth below the excavated level for which the ratio of stabilizing to destabilizing moment is close to unity. This has been done in order to ensure that the soil-wall-berm system collapses as one.

Using the wall depth and soil angle of shearing resistance determined by the above methodology, the model is implemented in PLAXIS and compared with the MCW method. PLAXIS analysis takes into consideration another group of factors that are not taken into consideration in MCW methods, i.e. soil stiffness, wall bending stiffness, initial horizontal stresses and overall soil-wall interaction mechanics. The analysis of the effect of these parameters is of interest, as it should alter the mobilized forces, displacements and stresses in the model.

b) General geometry settings

In generating the finite element model, plane strain conditions were assumed and 15 node elements were used to construct the finite element mesh.

The overall dimension of the finite element model was 120 m x 50 m with the wall located in the middle. The elevation at ground level is 50 m, Figure 23. The final excavation level is 7 m below the ground level (at 43 m elevation). Two berm geometries have been considered one with a face inclination of 2H:1V (Horizontal: Vertical) and one, 3H:1V, the top of the berms is at ground level and is 2 m wide. The width of the base of the berm is 16 m and 23 m respectively.

The final configuration of the excavation is with an embedded retaining wall supported by a single prop located at ground level. The required wall length is defined by this condition and was 12 m and 16 m for the 2H:1V and 3H:1V berm geometries respectively.

The base of the finite element model was fixed against movement in the vertical and horizontal and the sides of the model were fixed against horizontal movement, i.e. they were free to move vertically. Figure 23 illustrates the model with approximate dimension proportions when compared to the excavation

depth, H. The adequate distance from the berm towards the borders of the model shall be assured in order to allow the complete development of the displacements and failure surfaces and to disperse the effect caused by the boundary conditions close to borders.

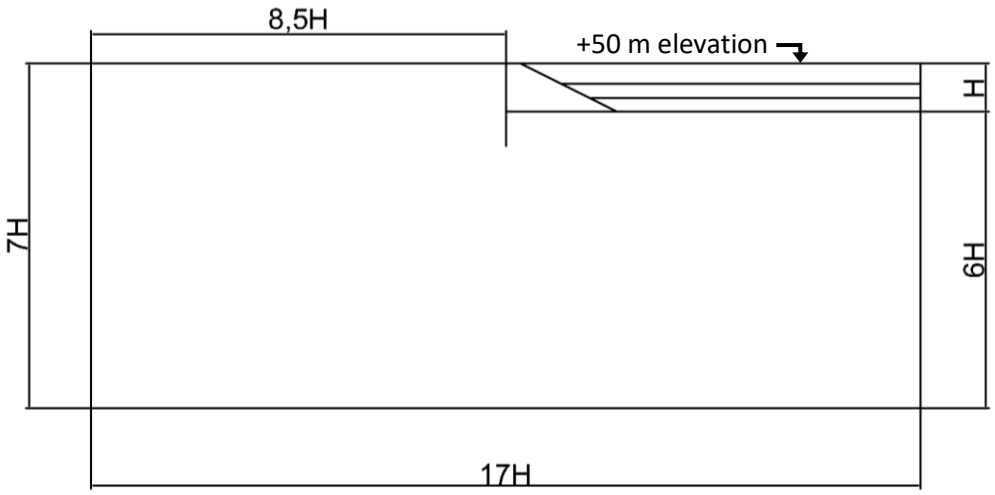

Figure 23 - Overall geometry used for developing finite element mesh.

c) Mesh

For the given geometry a "fine" finite element mesh was used as it seems to have an adequate number of elements for the given geometry. The mesh was refined along the plate in order to conceive higher level of precision by reducing the local element factor to 0.5 in that area and make the more gradual transition between the soil and wall.

4.1.2 Soil and wall properties

a) Soil

For the soil modeling, linear elasticity was assumed and yield was described by the Mohr-Coulomb model. For all of the analyses presented in this thesis, the following soil properties were used, except where otherwise indicated in the text, Table 2.

Regarding the angle of shearing resistance was set to 28° and 20° for the 2H:1V and 3H:1V geometry setup respectively. The base value of the soil stiffness was set to 50 GPa as a default and 100 GPa and 150 GPa as alternative input characteristics. The coefficient of the initial horizontal stresses K_o was set to 0.5 for the base configuration and to 1, 1.5 and 2 as the variation values. Those values have the main objective the evaluation of the numerical effect of the parameters and not the modeling of real material properties.

Table 2 Summary of soil parameters.

Parameter	Symbol	Units	Base value	Variations
Unsaturated unit weight	γ_{unsat}	kN/m³	20	
Saturated unit weight	γ_{sat}	kN/m³	20	
At-rest earth pressure coefficient	K_0	-	0.5	1, 1.5, 2
Horizontal permeability	k_x	m/day	0.1	
Vertical permeability	k_y	m/day	0.1	
Base soil stiffness	E_{ref}	MN/m²	50	100, 150
Poisson Ratio	ν		0.2	
Cohesion	c'	kN/m²	0.1	
Angle of shearing resistance	φ'	°	2H:1V: 28 3H:1V: 20	
Angle of dilatancy	ψ	°	0.0	
Increase in soil stiffness with the depth	E_{inc}	kN/m²/m	5000	
Cohesion increment	$c_{increment}$	kN/m²/m	0.00	
Soil-wall friction coefficient	$R_{inter.}$	-	0.667	

b) Plate and interface elements

The baseline setup for the wall was taken to be a steel combi wall comprising reinforced concrete filled 1600 mm diameter steel tubes with a wall thickness of 19.2 mm, at a center-to-center spacing of 2.86 m. The parameters for this model are summarised in Table 3.

Table 3 Wall parameters

No.	Identification	EA [kN/m]	EI [kNm²/m]	W [kN/m/m]	ν [-]
1	1600d_tubes	2,27E7	4,59E6	0,00	0,20

As the variation of the initial input characteristics, wall bending stiffness EI were increased and reduced by x100 and x10000 times compared to the default setup, it is important to note that those modifications of values are used mainly to evaluate the numerical effect and not to model real material properties. So the analysis with values of 4,59E8 and 4,59E10 for the wall stiffness EI was performed.

Interface elements were defined along the wall in order to model the interaction between the wall and the soil and were extended slightly below the wall in order to avoid stress oscillations. The shearing resistance and stiffness if the interface elements are derived from the equivalent soil parameters using the factor R_{int}.

4.1.3 Initial PWP and boundary conditions

The main objective regarding the pore water pressure (pwp) boundary conditions and analysis is to get the pressure distribution as close to the one used for the MCW method as possible, so that the possible difference in the results between the two methods may not be addressed to the difference in the PWP distribution.

The following initial pwp boundary conditions were applied:

1) Constant head level of 50 m along the left border to model the undisturbed water hydrostatic conditions and along the ground level assuming the constant level of the water table (on the left side of the wall).

2) A closed-flow boundary condition was applied to the bottom border of the model.

3) A closed-flow boundary condition was applied to the right border of the model due to the symmetry of the excavation.

These were maintained throughout the analysis.

PWP boundary condition changes made during the analysis:

4) Constant head level corresponding to the respective stage of the construction is set along the excavated level for each phase (see a solid dark blue line at excavation level in Figure 24).

5) In order to match the MCW calculation assumptions, it was necessary to maintain the berm in a dry state (PWP = 0). A number of options were considered starting with the application of the "cluster dry" option but in this option, the designated cluster was not maintained as "dry" and the seepage flows pushed water up into the berm (actually this is probably a more realistic result however the idea was to match the MCW calculation procedure as closely as possible). Next, the "user defined pore pressure distribution" option was used in the berm with all of the parameters set to zero however the same problem persisted.

   Finally, drain elements were instead located within the berm at intermediate and final excavated levels as shown in Figure24. The drain elements were used to prescribe the lines inside the model where active pore pressures are set to zero when the drain is active. The drains are activated for each of the construction stages at the current excavated level and ensured that the berm elements (light grey elements above active line) remained dry. The other base configurations were tested but the presence of the water levels inside the berm made those options not feasible.

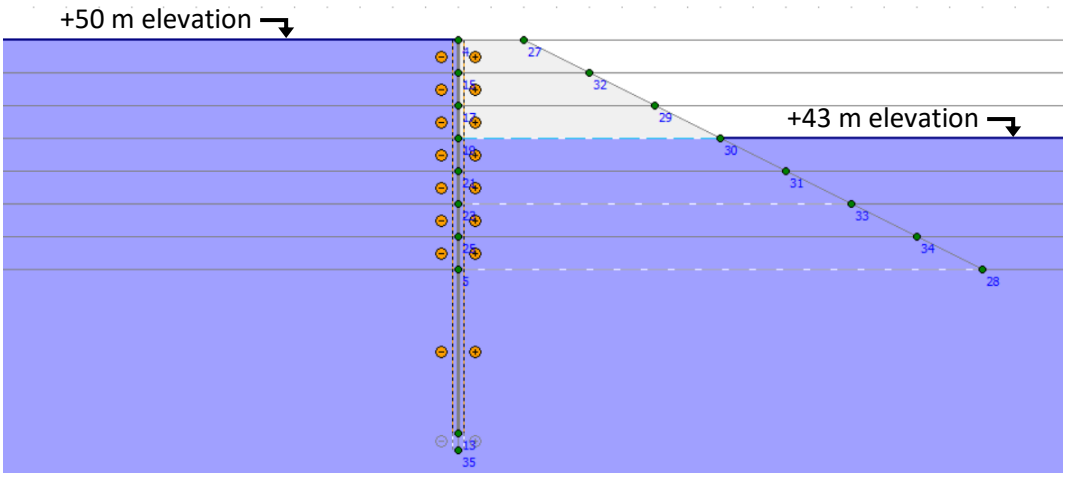

Figure 24 – Stage 1 of FEA - insertion of drains to maintain dry berm assumption (blue dash line - active; white dash - inactive).

4.1.4 Initial stresses

As the default setup, the initial horizontal effective stresses in all of the soil layers are defined as 50% of the vertical effective stresses, by setting the at-rest earth pressure coefficient, K_0 to 0.5. However, for each of the geometry, the values of 1; 1.5; 2 were used as well in order to evaluate the effect of the initial horizontal stress on the mobilized passive resistance.

4.1.5 Construction/Modelling Sequence

In the following Table 4 are represented the construction sequence with the respective actions/alterations that were made at each stage.

Table 4 Construction stages.

Stage	Activities	Changes in FE model
0	Initialization	Set general phreatic level Generate the initial stresses
1	Excavate to 47 m	Activate wall; Set constant head level of 50 m along the left border and at the ground level; Adjust PWP to the current excavated level of 47 m; Activate the Drain corresponding to the current excavated level
2	Excavate to 45 m	Adjust PWP to the current excavated level of 45 m; Activate the Drain corresponding to the current excavated level
3	Excavate to 43 m	Adjust PWP to the current excavated level of 43 m; Activate the Drain corresponding to the current excavated level

Assuming the conditions for the FE analysis described above for each of the geometry setups different input characteristics were introduced and analyzed in order to evaluate the possible differences in the outcomes. Those characteristics are 1) Soil stiffness “E” 2) Bending stiffness of the wall “EI” 3) Coefficient of the initial horizontal stresses “K_0”.

4.2 2H:1V Berm Geometry

4.2.1 Base configuration analysis

Following are the results that are obtained for the base configuration of the 2H:1V geometry represented schematically in Figure 25.

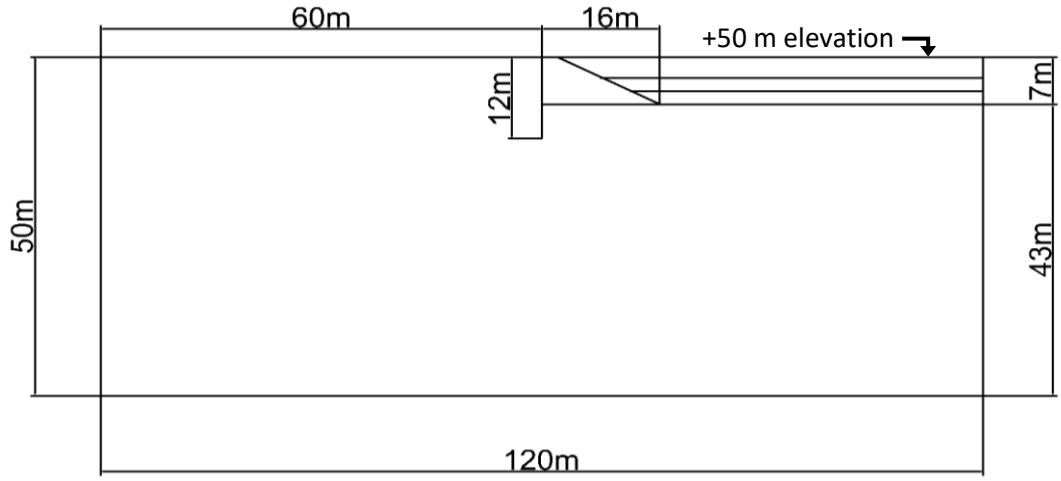

Figure 25 - Dimensions of 2H:1V berm model.

a) Effective earth pressures

Figure 26 presents the active and the passive effective earth pressures for each of the three construction phases. With the Coulomb's calculated active earth pressures represented on the active side of the wall, giving results close to those obtained by the FE analysis, which suggests as expected that the Coulomb's method is an adequate approximation. It can be observed that the active earth pressures do not vary much from phase to phase as opposed to the passive earth pressures which are known to require greater displacements for the full mobilization, which have occurred towards the end of the third phase.

The other thing to note is that the passive earth pressures for each of the phases have two angular points at which the line representing the earth pressures changes its inclination, being first one at the very top of the berm this section has the inclination that is quite close to that of the line that represents the Coulomb's calculated passive earth pressures and the second one at the excavated level after which the inclination is smaller.

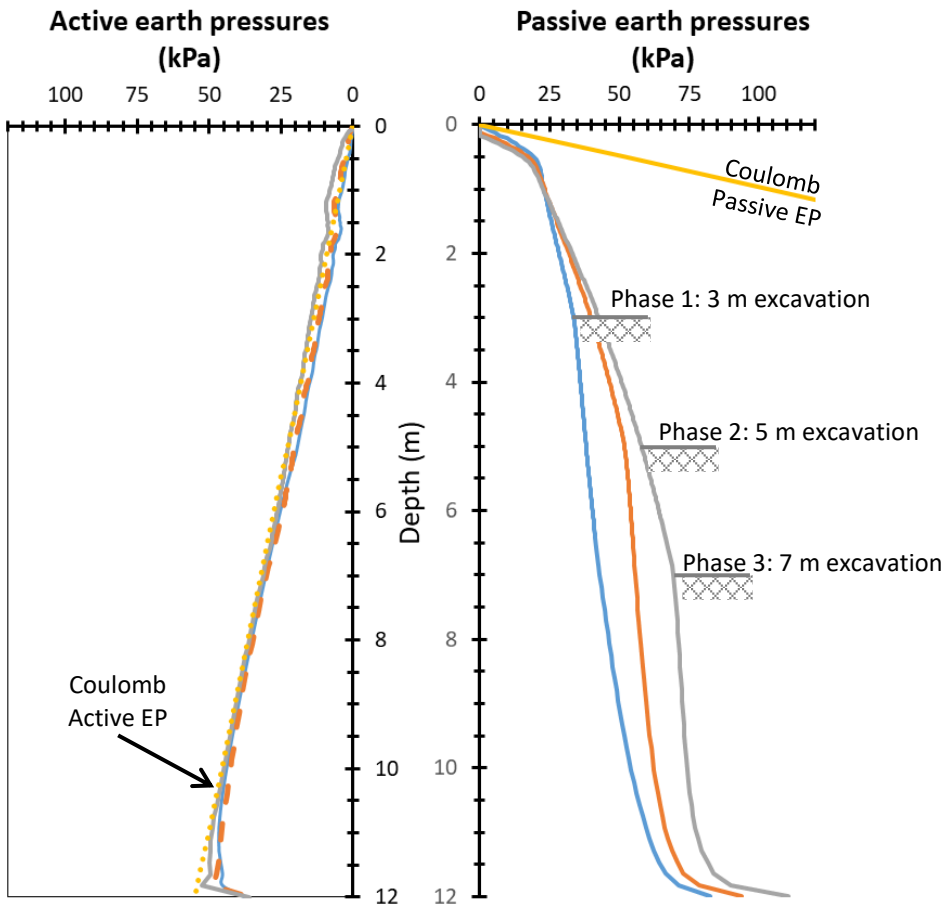

Figure 26 - Base analysis – Development of earth pressures during berm formation

b) Pore water pressures

Regarding the pore water pressures, the steady state seepage solution from the FEA is consistent with the linear steady-state flow approximation used in the MCW method. Figure 27 illustrates the equipotential lines obtained for the final stage of analysis, these are consistent with the applied hydraulic boundary conditions. Note also how the hydraulic boundary condition at excavation level is enforced along the base of the berm by the inclusion of the drain element and the berm remains dry.

The resulting pore water pressures from the FEA, for each stage of the excavation, are presented in Figure 28. Also shown, for comparison with the final Phase 3 profile is the pore water pressure profile obtained from the linear seepage assumption used in the MCW method (dashed line). PWP profiles suggest that the linear steady-state approximation reasonable for the passive side but underestimate the pore water pressures on the active side of the wall which may be unconservative.

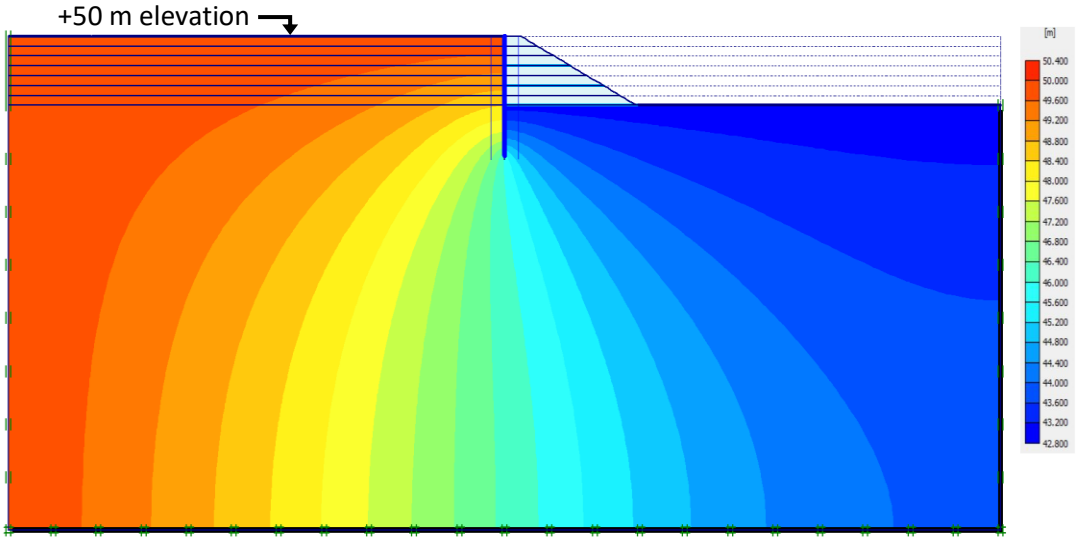

Figure 27 - Pore water pressure contours.

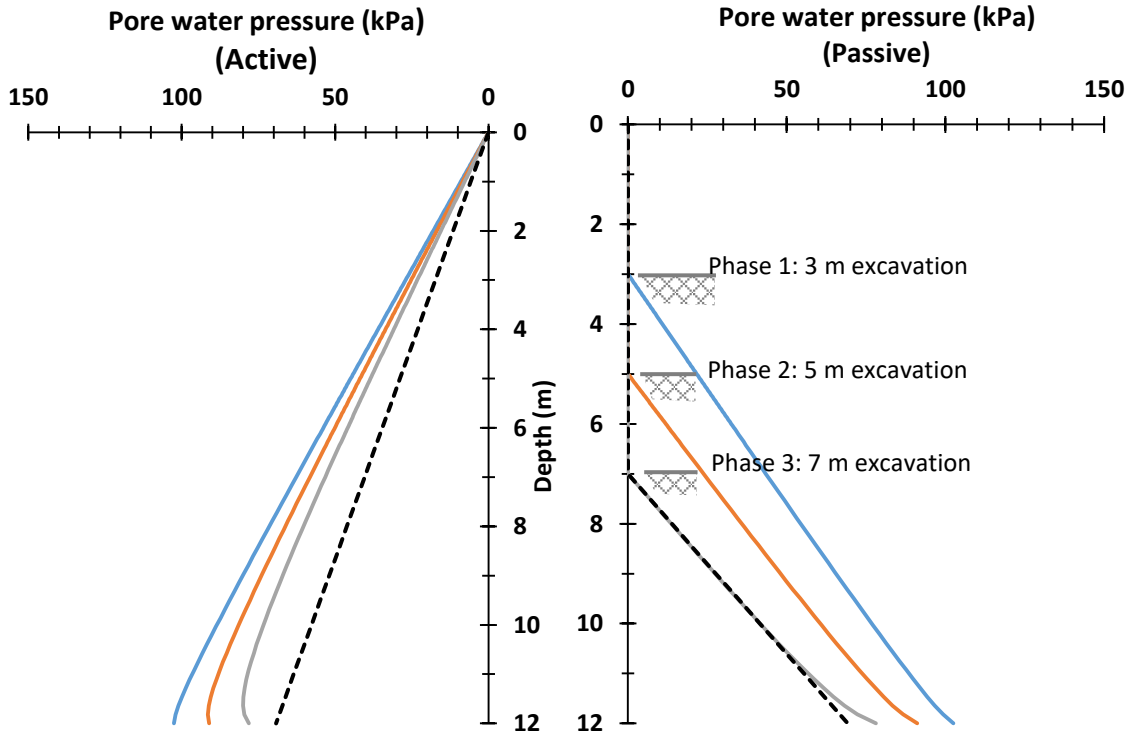

Figure 28 - Pore water pressures.

c) Wall internal forces and displacements

Figure 29 presents the wall forces that result from the interactions described above. Regarding the bending moment, as the excavation proceeds resulting passive earth pressure impulse is increasing and the point of the application of it is moving downwards resulting in a higher bending moment with the maximum value occurring at the deeper level. Even though the wall stiffness is high for this configuration

it is still possible to observe the general tendency of bending in the wall which is congruent with the occurred bending moments. That is a slight bending in the wall towards the active side, as illustrated in Figure 30.

The shear forces are congruent with earth pressure distribution and bending moments, having zero value at the points where the moment is maximum for each phase and having that value at the deeper level for the final stage of the excavation.

Relative shear stresses represented in Figure 31 indicate the mobilized shearing resistance for the respective regions of the wall interface, so that regions, where the full shearing resistance is being mobilized, are easily detected. It's calculated as the ratio of the mobilized shear stress over the maximum available shear stress for the given region in the wall interface.

$$\tau_{max} = R_{inter}\sigma_n \tan(\varphi_i) + R_{inter} \times c_i$$

Where R_{inter} is the soil wall interface parameter that was set to 0.667.

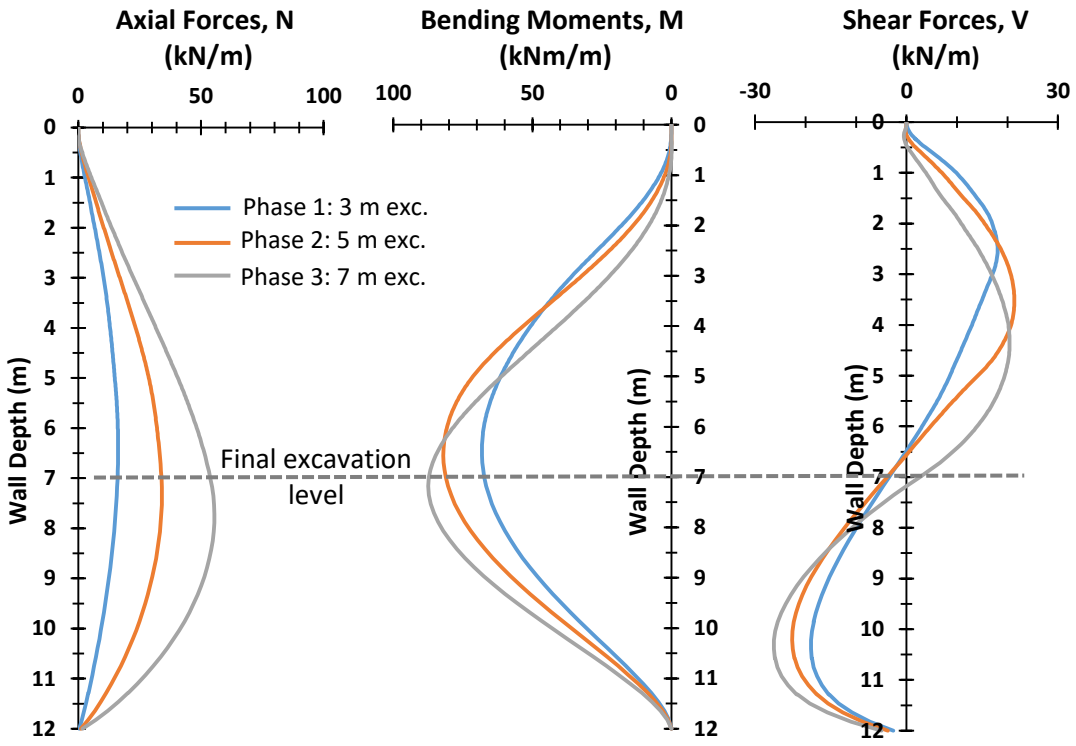

Figure 29 - Force distribution in the wall.

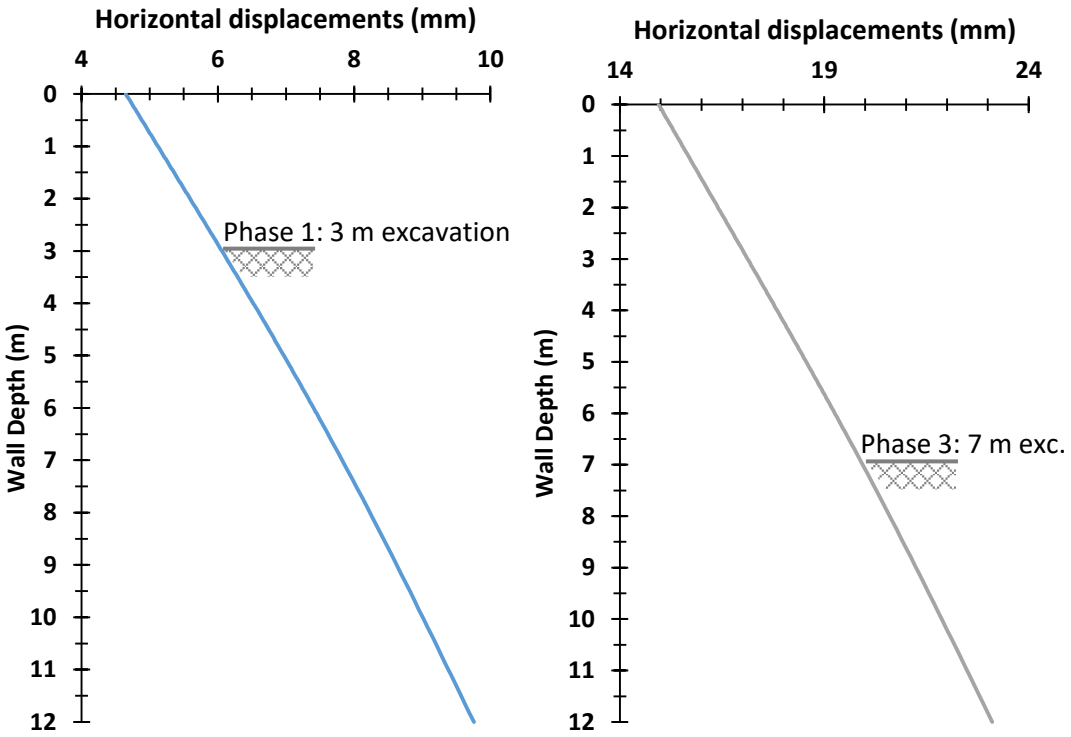

Figure 30 - Horizontal displacements of the wall for the 1st and 3rd excavation phases.

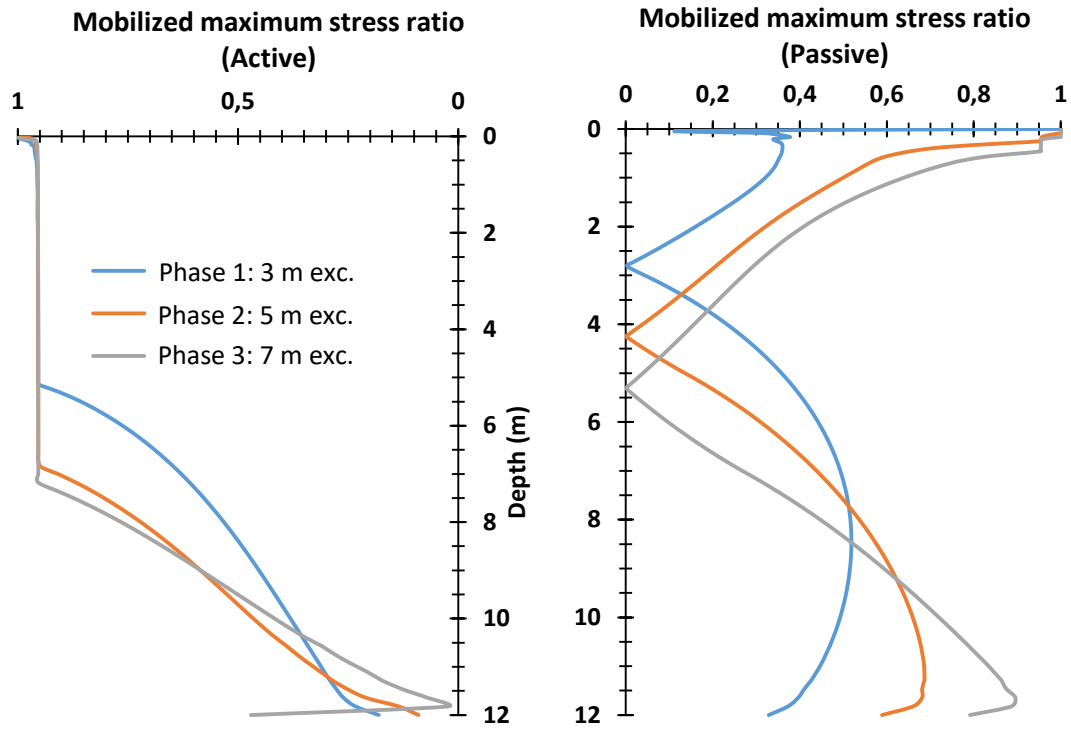

Figure 31 - Relative shear stresses on wall-soil interfaces.

By observing aforementioned charts it's possible to recognize that full active pressure is being mobilized from the top until down the excavated level. On the passive side, however, the full shearing resistance is mobilized at the top where the berm is less stable and then it decreases to zero until approximately or slightly above the excavated level, increasing immediately afterward down towards the end of the wall. Which indicates that the passive pressure that is being mobilized is far from its fullest capacity which might result in a considerable difference when compared to the MCW method later on.

Analyzing the e horizontal incremental displacements of the wall for each excavation phase shown in Figure 32, it is evident that in the initial phases the horizontal movement occurs mostly at the bottom of the wall. The general total displacement field is presented in Figure 33 (phase1) and Figure 34 (phase3) which shows the mobilized mechanism and the horizontal deformations obtained in Figure 32.

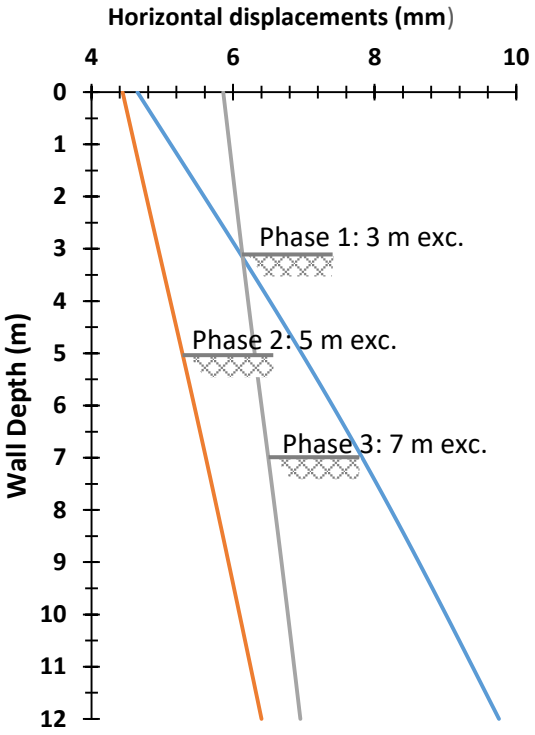

Figure 32 - Incremental horizontal displacements.

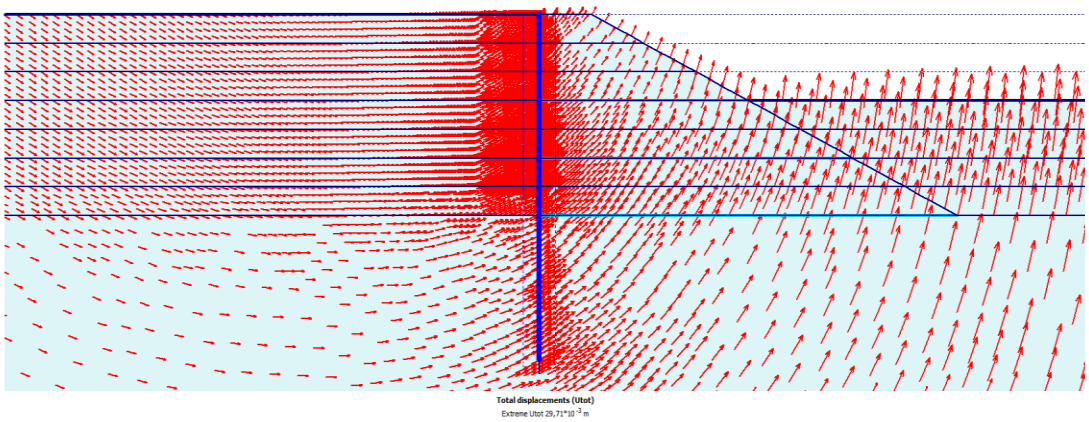

Figure 33 - Total displacement field for the 1st phase.

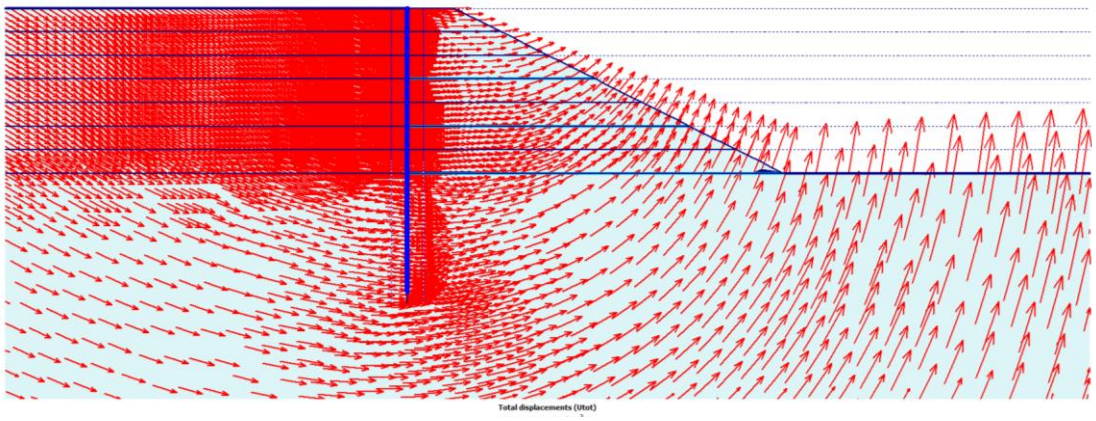

Figure 34 - Total displacement field for the 3rd phase.

4.2.2 Modified wall stiffness EI

After analyzing the base configuration a series of different configurations were analyzed as mentioned before. The results of this analysis regarding the final phase are represented in the following charts. The charts are separated into groups with different wall stiffnesses, different soil stiffnesses, and different initial horizontal stresses respectively.

In the first group, different values of the wall stiffness were applied. The base configuration with EI = 4.59×10^6 kNm^2/m and other configurations being this value modified by x100, x10000, /100 and /10000. Resulting in the following earth pressure distribution along the wall, Figure 35.

As can be observed the different values of the wall stiffnesses does not have any considerable effect on the active pressure mobilization. Slightly greater pressures at the top and at the very bottom can be observed for the configurations with lower values of wall stiffness. And no changes can be observed for the higher values of stiffness when compared with the base configuration. However, for the passive earth pressure distribution, the configuration is considerably different when compared to the base or stiffer

configurations of the wall. This effect is caused by the difference in the deformations of the wall and displacements resulting in the slightly different pressure mobilization pattern.

The wall stiffness for the base configuration is already elevated which might explain the reason for no apparent alterations when compared with stiffer configurations in which the wall behavior is almost rigid.

Regarding the respective forces in the wall, the axial forces are not varying much as can be observed in **Figure 36**, slightly greater values for the lower wall stiffness and slightly lower for higher values of wall stiffness.

As expected the bending moment is much smaller for the lower values of wall stiffness and only slightly higher for the greater values of stiffness. As with the stiffer wall displacements are smaller which will result in the greater values of forces. In the wall with lower stiffness, the work of the external forces is mostly accommodated by the wall deformations which result in much-reduced values of forces. As was mentioned before in the base configuration the wall stiffness is elevated and the behavior is already close to the rigid so that the stiffness increments don't alter much the output results.

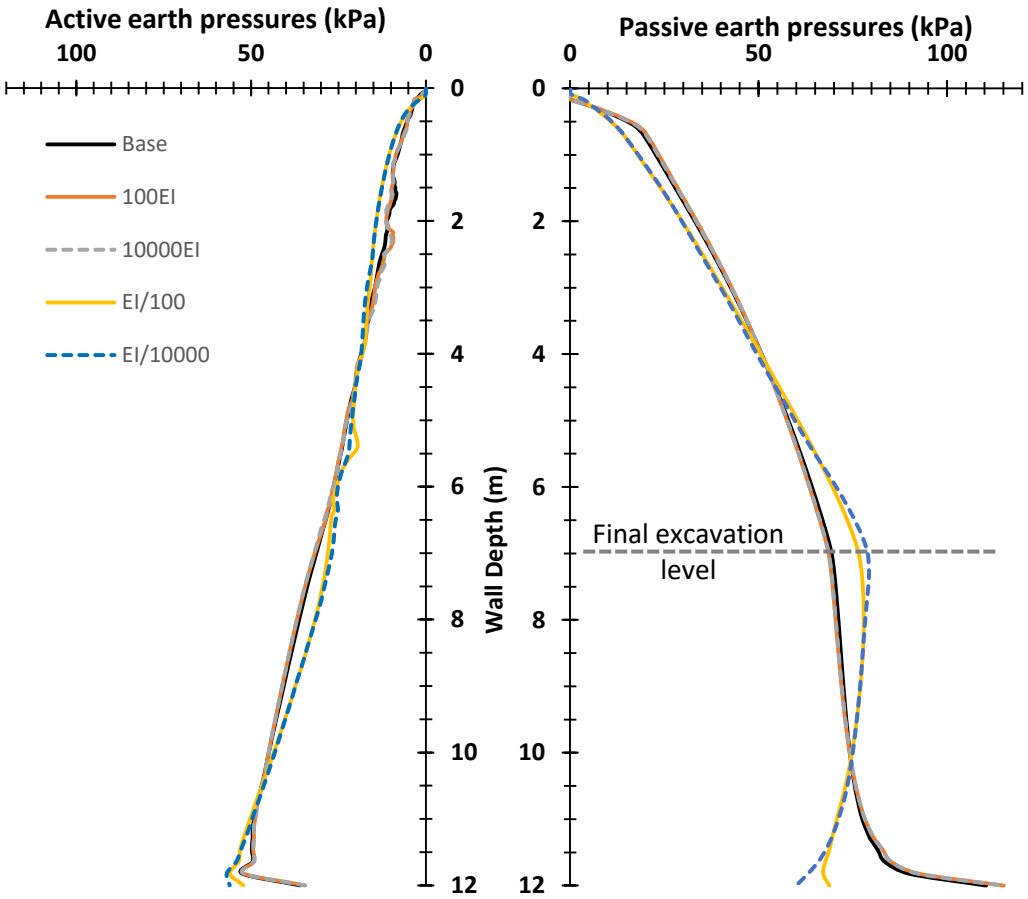

Figure 35 - Earth pressures for different values of wall stiffness (left side – active, right side – passive).

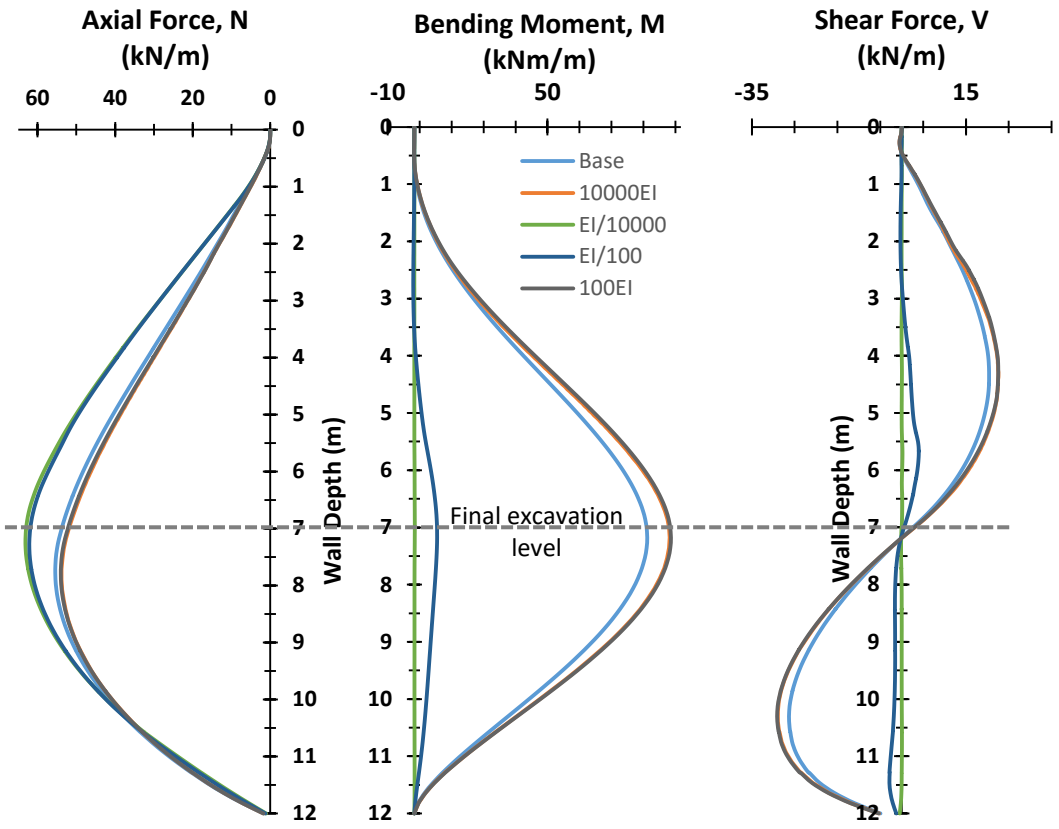

Figure 36 - Forces along the wall for different values of wall stiffness.

The effect of wall stiffness on the shear forces is similar to that observed in the bending moments – greater values for the higher stiffness and lower and almost none for the low wall stiffness.

Analyzing the horizontal displacements represented in Figure 37 in the configurations of the wall with reduced stiffness it is easier to perceive the wall behavior concerning deformation and displacements. The bottom of the wall is dislocated forward towards the excavation, following the general rotating motion as were described previously for the base case. The bending at the top occurs towards the unexcavated area. For the stiffer wall configurations, the mechanism is similar although not so obvious due to the scale. The stiffer configuration does not allow such a pronounciate bending which is compensated by the increased horizontal displacement at the bottom.

The vertical displacements can explain the axial forces inside the wall which are slightly affected by the wall stiffness variations.

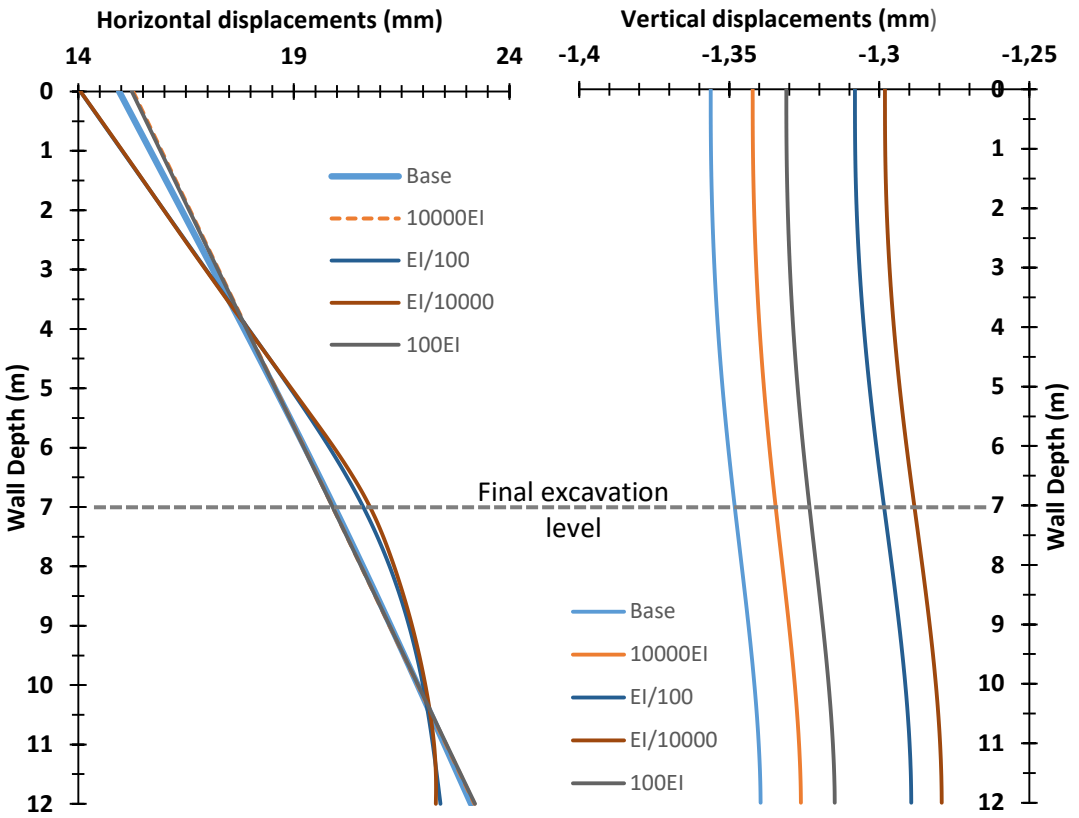

Figure 37 - Horizontal and vertical displacements for different wall stiffness values, at final excavation level and berm fully formed.

4.2.3 Modified soil stiffness E

The other analyzed group involved different values of soil stiffness. Three configurations were tested – the base configuration with E = 50 GPa, the second with E = 100 GPa and the third with E = 150 GPa. In all of the variations, the increase in stiffness with the depth is 5 GPa/m.

As can be observed in the following charts (see Figure 38) the variations of this parameter have a minor effect on the earth pressure distribution, when compared to the base scenario.

However, as can be demonstrated in Figure 39 even though the pressure distribution in the wall is almost identical the forces in the wall have some differences. As expected with the stiffer soils the bending moment and the shear stress are reduced.

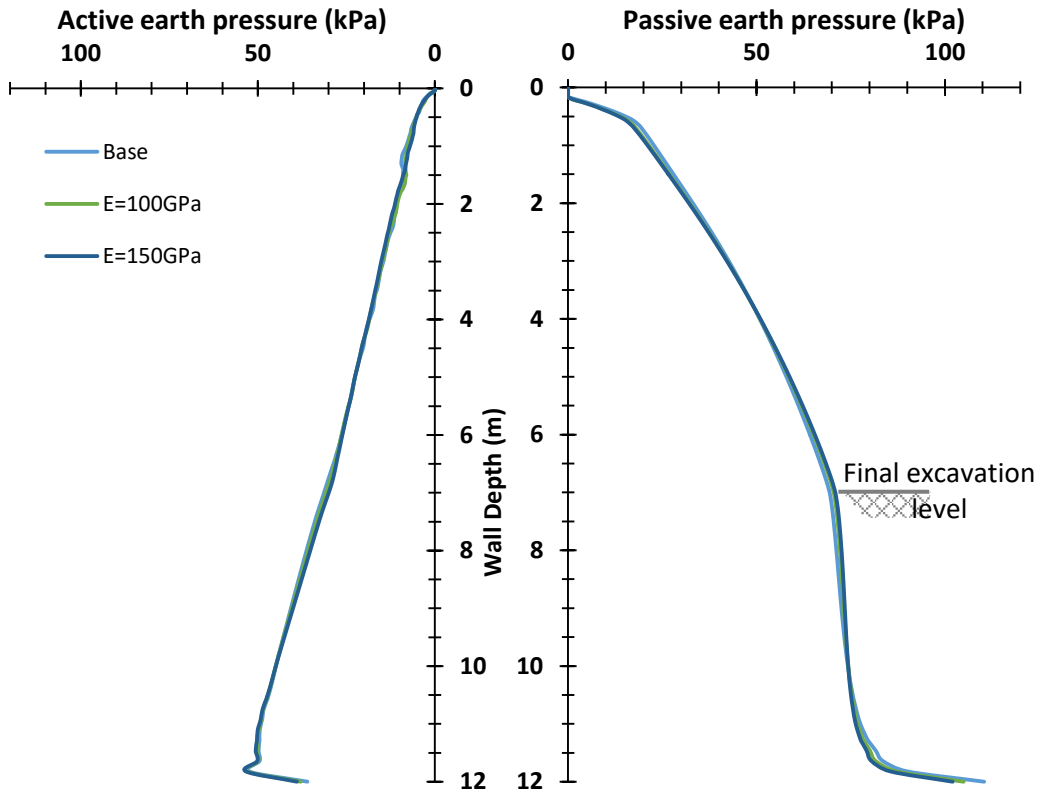

Figure 38 - Earth pressures for different values of soil stiffness

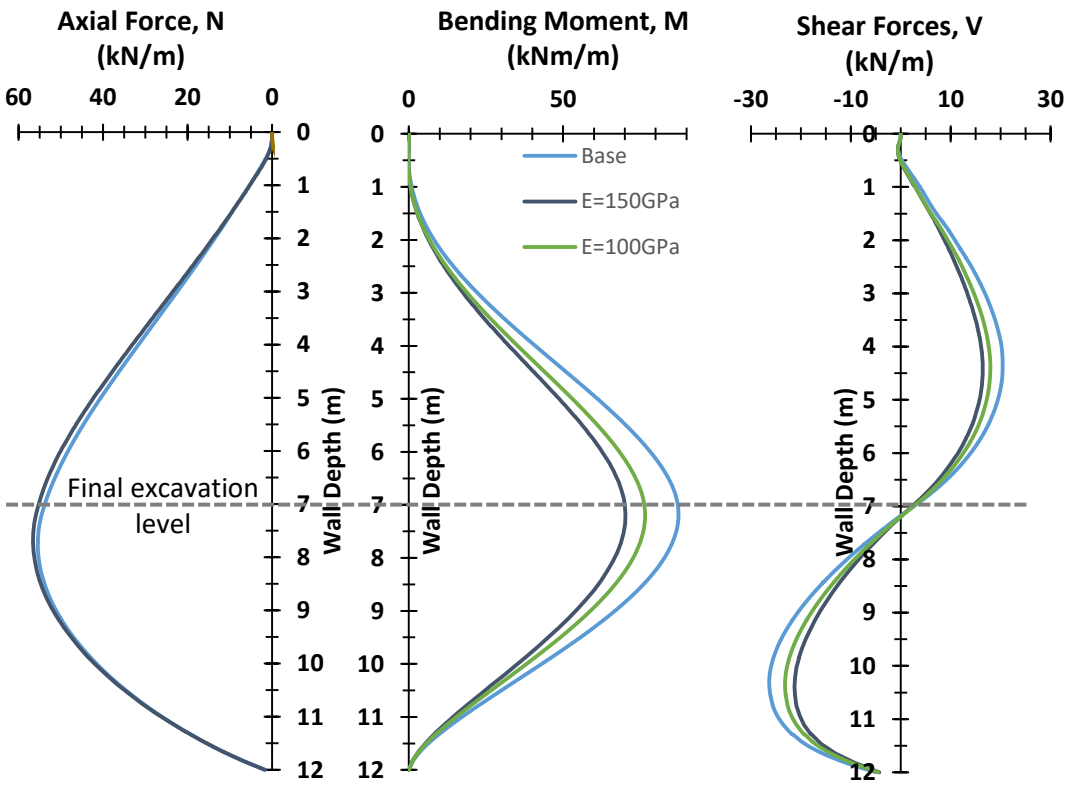

Figure 39 - Forces in the wall for different values of soil stiffness.

The displacements are consistent with the values of the soil stiffness, with higher displacements in the wall associated with the lower values of the soil stiffness, Figure 40.

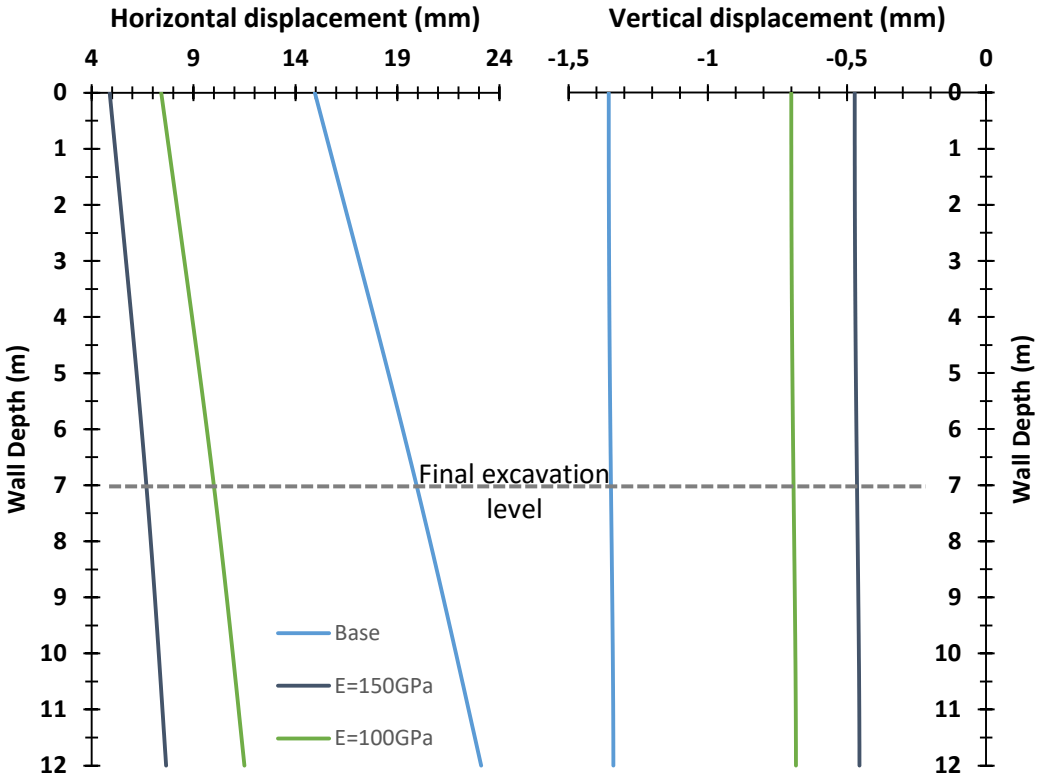

Figure 40 - Vertical and horizontal displacements for the different values of the soil stiffness.

4.2.4 Modified initial stresses

In the final variation, the initial horizontal stresses were changed. In the base configuration Ko=0.5. For the variations the values of Ko = 1, Ko = 1.5 and Ko = 2 were used. These coefficients represent the ratio between the horizontal and the vertical stresses for the initial conditions.

The effect of the initial horizontal stresses on the mobilized active pressure is minor at the top and of high magnitude from slightly above the excavated level down to the bottom, Figure 41**.** For the passive earth pressures, the situation is alike. And for both cases, the difference in the effective earth pressures are gradually increasing with the increase of the from Ko = 0.5 to Ko = 2.

In **Figure 42**, the moment distribution for the Ko = 2 configurations is considerably different when compared to the rest of the group with some negative values at the top and two curves in the opposite direction, which suggest that the wall is bending in two different directions. But as was already mentioned before the wall stiffness for the base case is high so for that reason it is hard to perceive the actual wall deformation for the Ko = 2 case. For that reason, the additional configuration was tested with Ko = 2 and

the wall stiffness EI decreased by 100 compared to the base scenario. In the next chart in Figure 41, the effective earth pressures are represented on the active and passive side of the wall respectively.

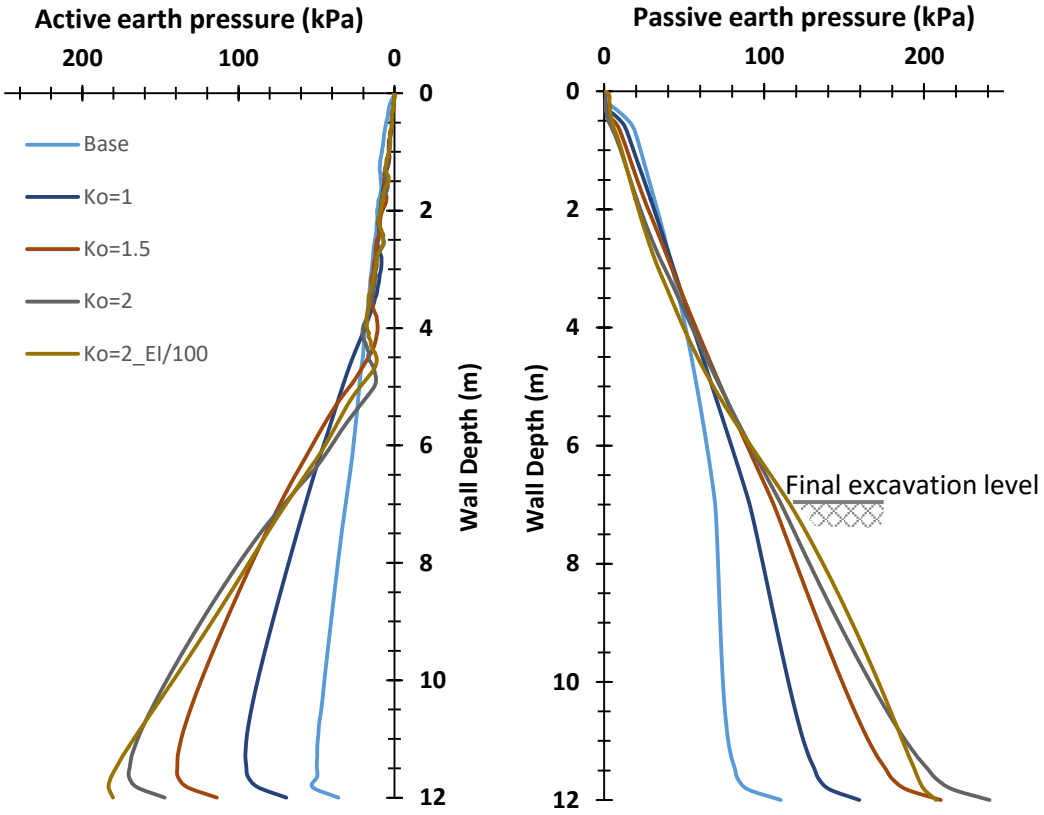

Figure 41 - The earth pressures for the different values of Ko

The effect of the initial horizontal stresses on the axial forces is a slight increase in a value due to the increased normal tension applied to the wall element.

Interesting is the effect of the initial horizontal stresses on the bending moment when comparing the Ko = 1 with the base configuration (Ko = 0.5), the moment generated has a higher maximum value and the maximum value is situated slightly below. However by further increasing the value of Ko to the value of 1.5 the maximum value of the moment is smaller and is situated at a deeper level. When the value of the Ko is increased to 2 the moment at the top is slightly negative with local maximum, which as was already mentioned before suggests that the wall is bending in two opposite directions which can be confirmed by the chart illustrated in Figure 44 for the configuration with Ko=2 and EI/100 as this configuration has the same pattern of the moment distribution as the one only with Ko=2 while at the same time being flexible enough to illustrate the bending behaviour of the wall element.

Figure 43 illustrates the magnitude of the horizontal displacements for the different configurations.

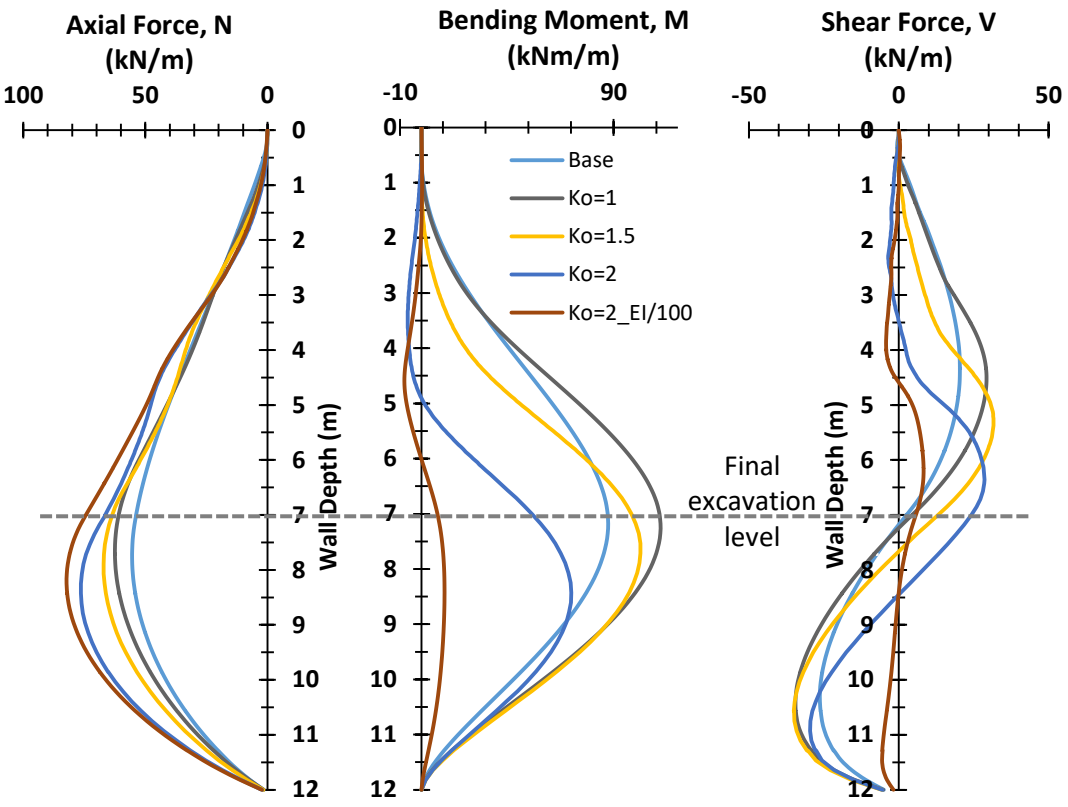

Figure 42 - Forces for the different values of Ko.

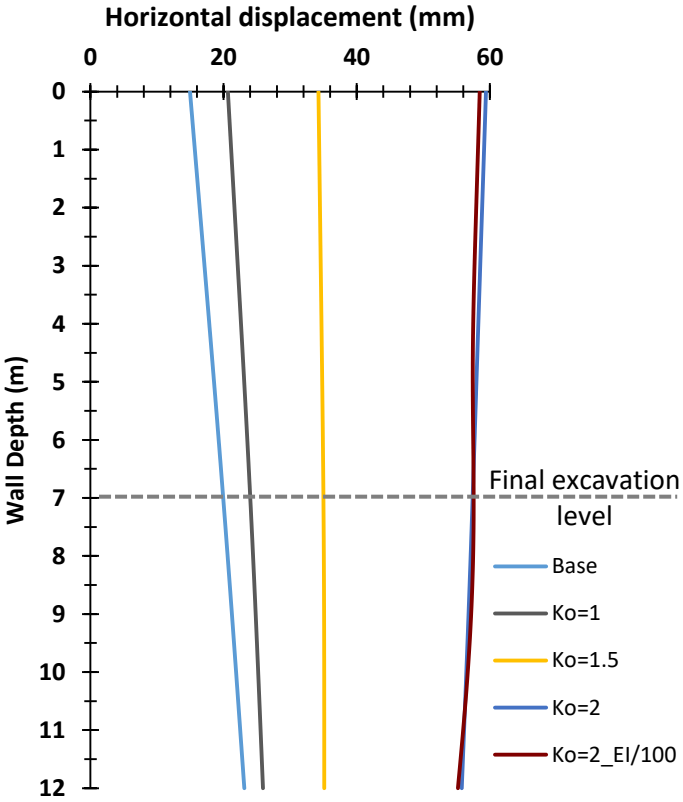

Figure 43 - Horizontal displacements for the different values of Ko.

To better illustrate the bending behavior of the walls for the different Ko values, the charts on Figure 44 are plotted with amplified scale.

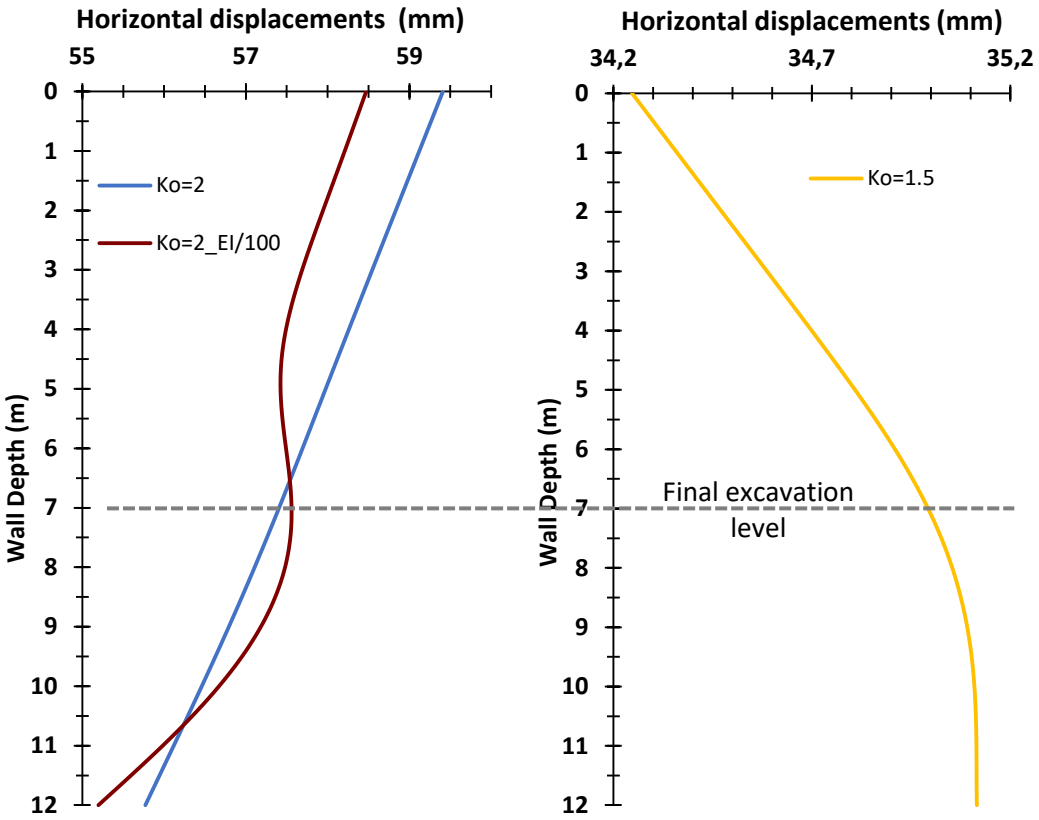

Figure 44 - Horizontal displacements for the different values of Ko with amplified scale.

As can be observed due to the elevated value of the wall stiffness and to the fact that the wall is bending in two opposite directions, which reduces the perception of the relative displacements occurring in the wall, it is complicated to evaluate the bending behavior of the configuration with Ko = 2. In the chart regarding Ko=2_EI/100, it is evident how the wall is bending.

Regarding the configuration with Ko = 1.5, it is evident that the wall bending pattern is similar to the base case, the same refers to the Ko = 1 configuration which is not represented. This suggests that the whole soil-wall interaction is altered for the different values of the initial horizontal stresses.

Regarding the vertical displacements occurring along the wall, as illustrated in Figure 45 for the higher values of the initial horizontal stresses the displacements are occurring in the opposite direction when compared to the base configuration, and for the higher values of the Ko, displacements are higher.

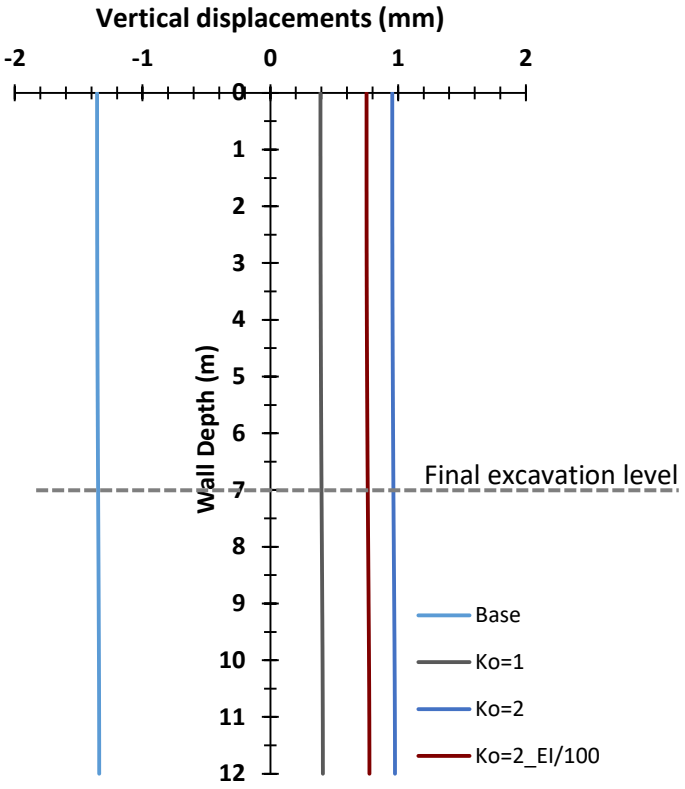

Figure 45 - Vertical displacements for the different values of the Ko.

4.3 3H:1V Berm Geometry

4.3.1 Base configuration analysis

The next analysis that was carried out was the analysis of the berm with the 3H:1V geometry. The schematic representation of the model is presented in Figure 46.

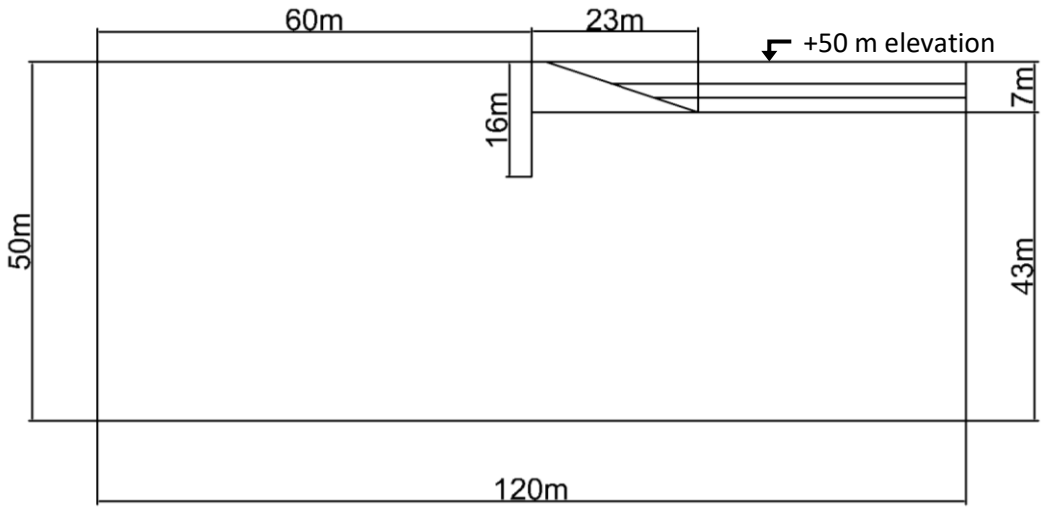

Figure 46 - Dimensions of the 3H:1V model.

Similarly to the results obtained in the 2H:1V geometry it can be observed in Figure 47 that the active earth pressure doesn't have a significant variation from phase to phase. On the other hand, the increase in the mobilization of the passive earth pressures is more evident from phase to phase as the passive earth pressure requires greater values of the displacements. In the current 3H:1V geometry the scale of magnitudes of the active and the passive pressures are close. Which suggests that in this configuration it was possible to obtain the equilibrium which is closer to the failure, which was one of the main goals for defining this geometry and material characteristics.

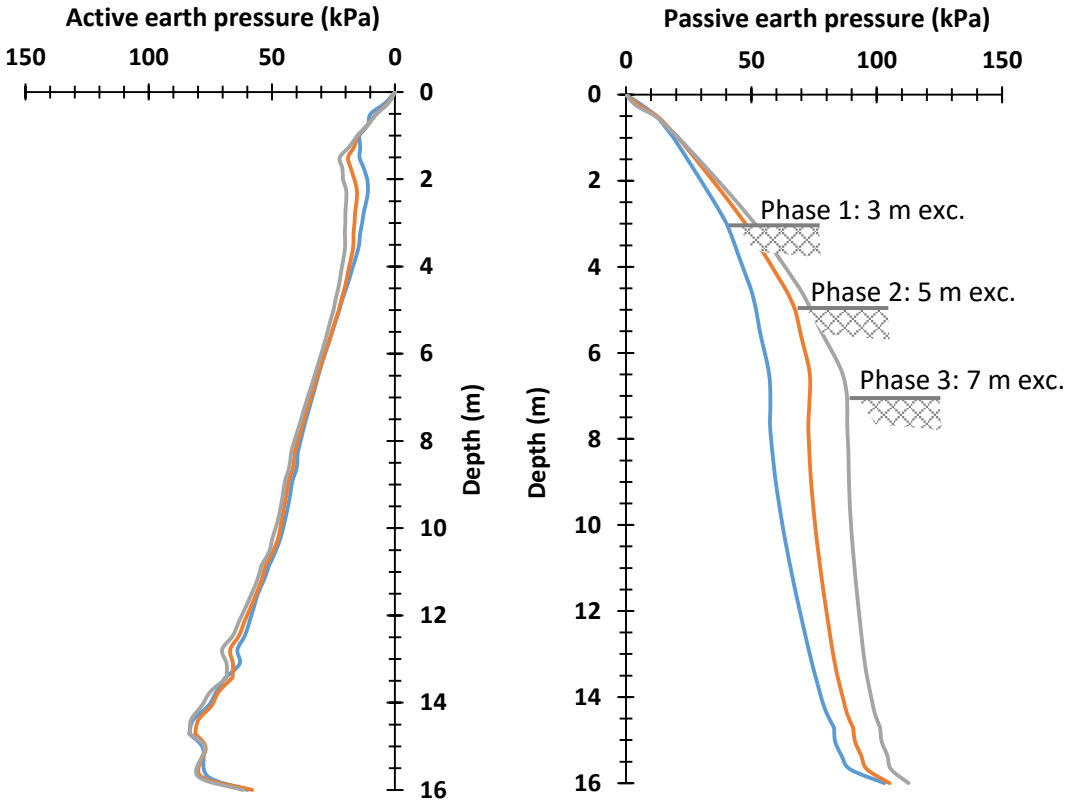

Figure 47 - Effective earth pressures for the three excavation phases of the base model

The resulting active and passive earth pressures distribution leads to the next force diagrams shown in Figure 48.

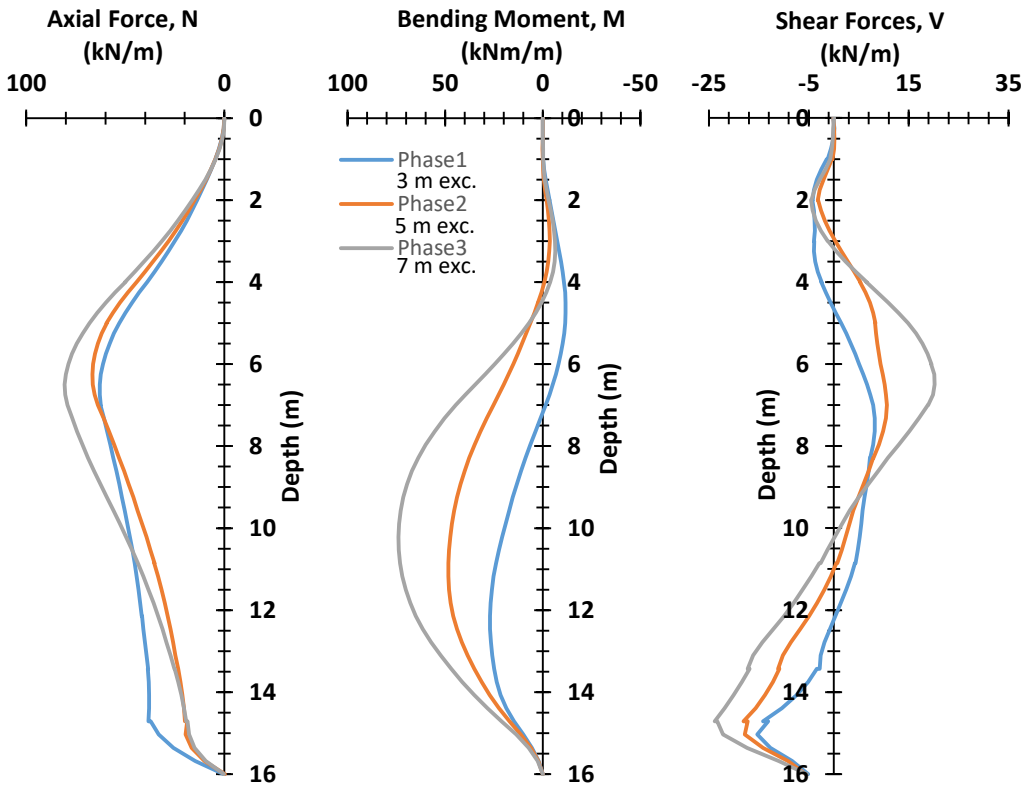

Figure 48 – Wall forces for three excavation phases of the base model

The axial forces have a slightly different distribution when compared with the 2H:1V geometry, this might be due to the fact that the wall length has been increased and due to the reduction of the angles of shearing resistance and of the soil-wall friction which leads to the drastically increased vertical displacements which are presented in Figure 49.

Regarding the bending moment when compared to the base configuration of the previous geometry, it can be noticed that there is two point of flexion which occurred due to the increased wall length with the increased earth pressures, which resulted in the wall bend. This effect also makes the value of the maximum bending moment to occur deeper in the ground.

Following in Figure 49 is presented the total phase horizontal and vertical displacements. As was already observed in the previous case the horizontal displacements are greater in the bottom and less at the top. Although not evident due to the scale and wall stiffness used in the base configuration there is a bending in the wall that corresponds to the zero value in the moment shown in the previous diagram.

As was already mentioned before the drastic increase in the vertical displacement took place resulting in the vertical displacement which is up to 60 times higher than the one obtained in the previous geometry. As the whole soil-wall system is situated closer to the failure. So only downward motion took place, unlike in the previous case where due to the soil swelling there was even some upward motion during the first phase.

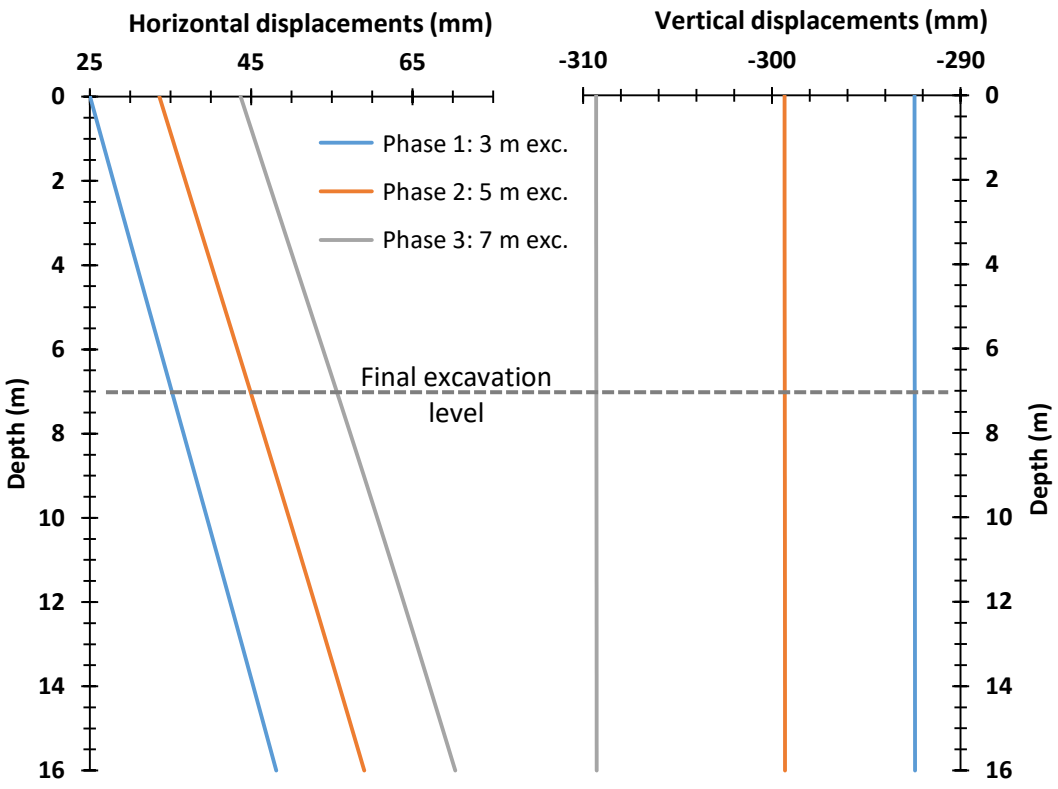

Figure 49 - Total displacements of the three excavation phases for the base model.

The next chart represented in Figure 50 shows the relative shear distribution. Makes it evident that in this geometry the full active pressure mobilization was obtained almost along the complete length of the wall which can also explain the higher values of the pressure in the previously presented active pressure diagram. The complete mobilization of the passive earth pressures along the most area of the wall also was obtained, which confirms the previously mentioned proposition for the more critical equilibrium state of the whole soil-wall system.

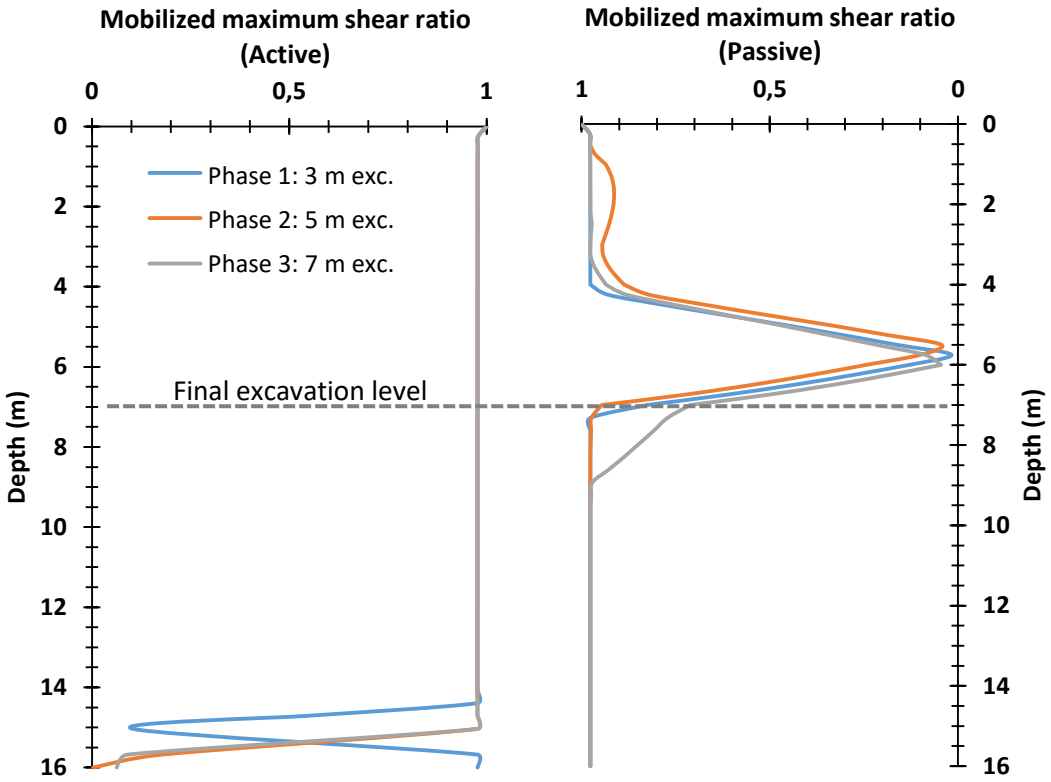

Figure 50 - Relative shear stresses for the three excavation phases of the base model

4.3.2 Analysis of the modified values of EI, E and K.

As was already observed in the previous geometry the increase in the wall stiffness EI over the base configuration does not give very representative results as the base configuration is already stiff. And the variation of the results for the different soil stiffness is also not evident. For that reason, only next modification of the parameters is represented, which are: EI/100, E=150Gpa, Ko=1, Ko=1.5 and Ko=2.

The results of these modifications were united and presented in the same charts. All of the variations are represented for the final third phase of the construction.

The first chart presented in Figure 51 shows the active and the passive earth pressures for the different parameters variations.

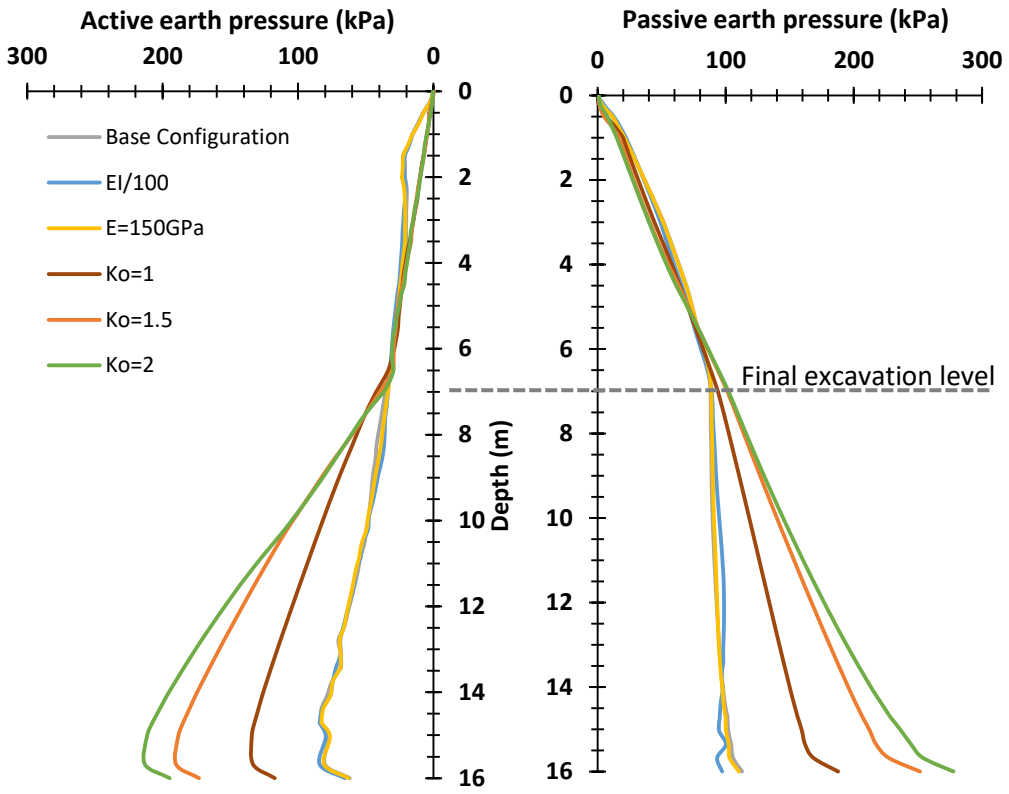

Figure 51 - Effective earth pressures for different values of Ko

Similarly to the previous geometry configuration, the wall stiffness, and the soil stiffness have a very slight effect on the earth pressure distribution and the initial horizontal stresses have a very pronounced effect. The overall pressure scale of magnitude between the passive and active pressures maintained close which indicates that the pre-failure state has been achieved.

The diagram of the forces that are presented in Figure 52 and Figure 53 was divided into two sets of charts in order for it to be more legible. The first set of charts is regarding the variation of the stiffness of the soil and wall stiffness.

The results are consistent with the observations made for the same variations for the 2H:1V geometry. The aforementioned modifications have a very slight effect on the axial forces. However, for the bending moment, the reduction of the wall stiffness has great reduction effect. And the slight reduction due to the increase in the soil stiffness. As was already explained for the previous geometry. The same great and slight reduction occurred in the absolute value of the shear forces.

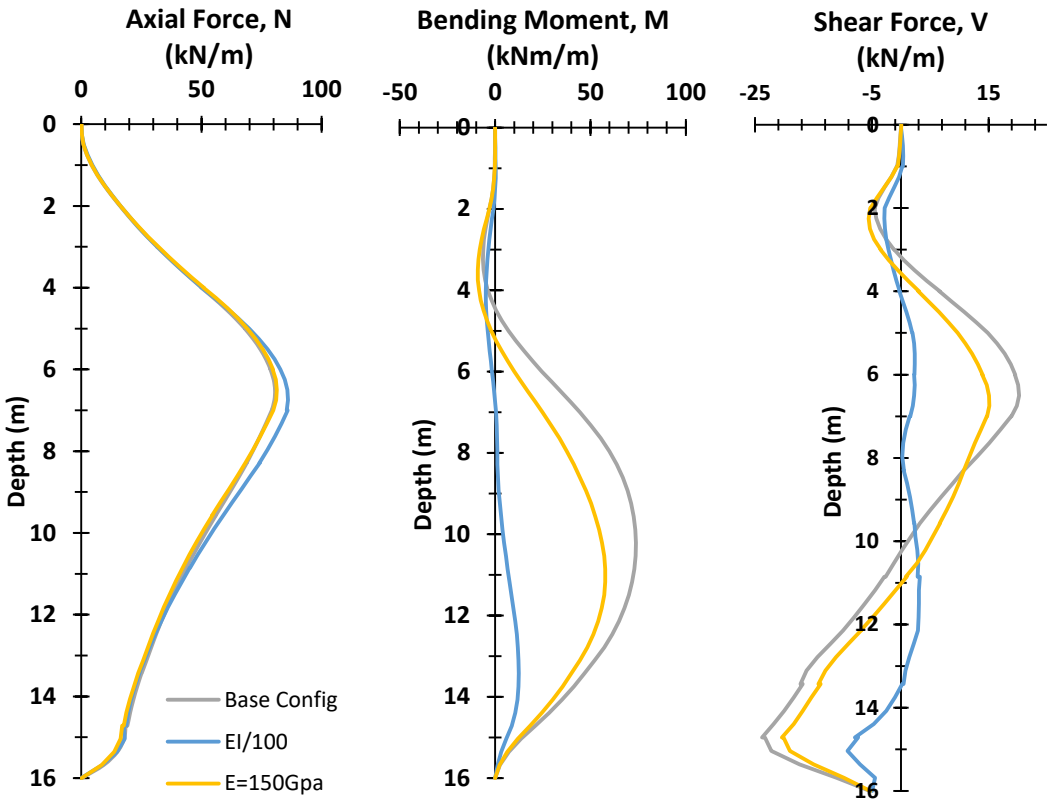

Figure 52 - Forces in the wall for different values of the soil stiffness and wall stiffness.

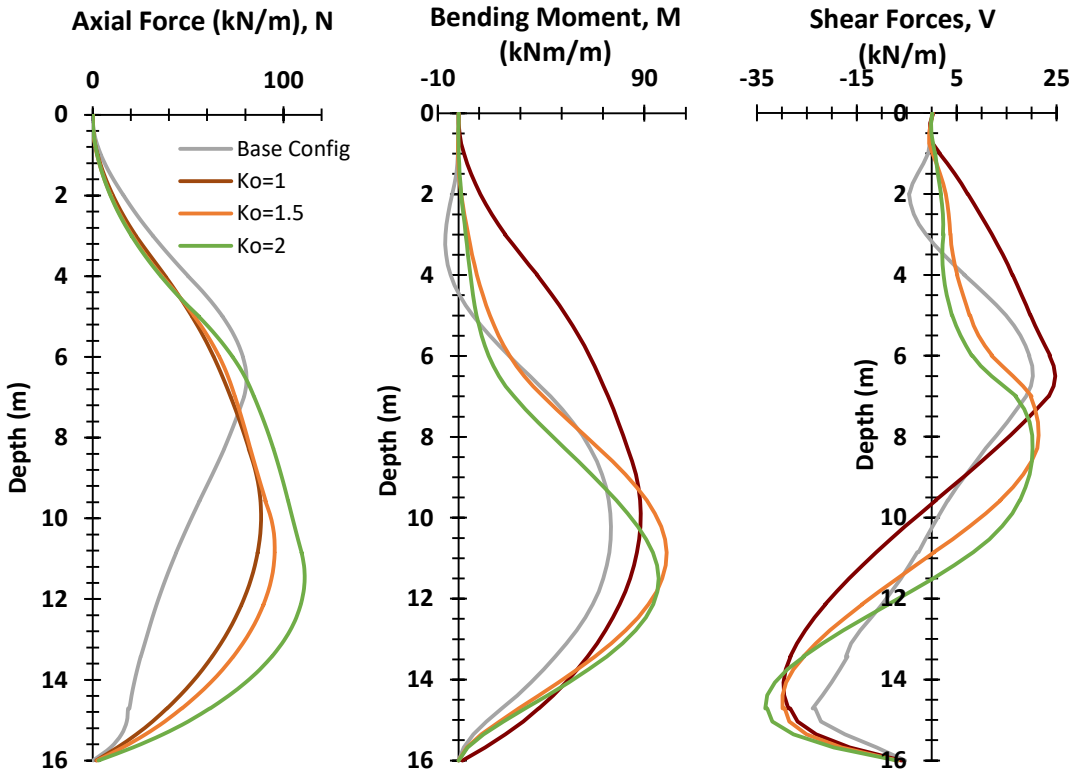

Figure 53 - Forces in the wall for different values of Ko.

For the variation of the initial horizontal stresses the axial forces distribution is affected due to the fact that the compared to the base configuration the vertical displacements are reduced and the forces perpendicular to the wall which contributes to the friction forces on the wall are greater.

The effect of the K on the bending moment is in an increase of the maximum value up to the value of K=1.5 after which there is a reduction of this value. Also, the maximum spike is occurring at the deeper level of the value of K greater than 1. The alteration of the position of the spike is coherent with the alteration of the distribution and zeros of the shear stress function.

In the next Figure 54 presenting the charts with the horizontal and vertical displacements, it can be observed that the increase in the initial horizontal stresses reduces the horizontal displacements and affect its distribution resulting in the more uniform horizontal displacement profile and less bending and more rigid-body type motion in the wall. In the vertical displacements chart, it can be observed that increase in the K in the displacements in opposite direction compared to the base configurations.

Regarding the soil stiffness, its effect is as expected is that it reduces the horizontal and vertical displacements of the wall as it is increased. The reduction of the wall stiffness, however, does not alter much the absolute values of the displacements but increases the bending in the wall.

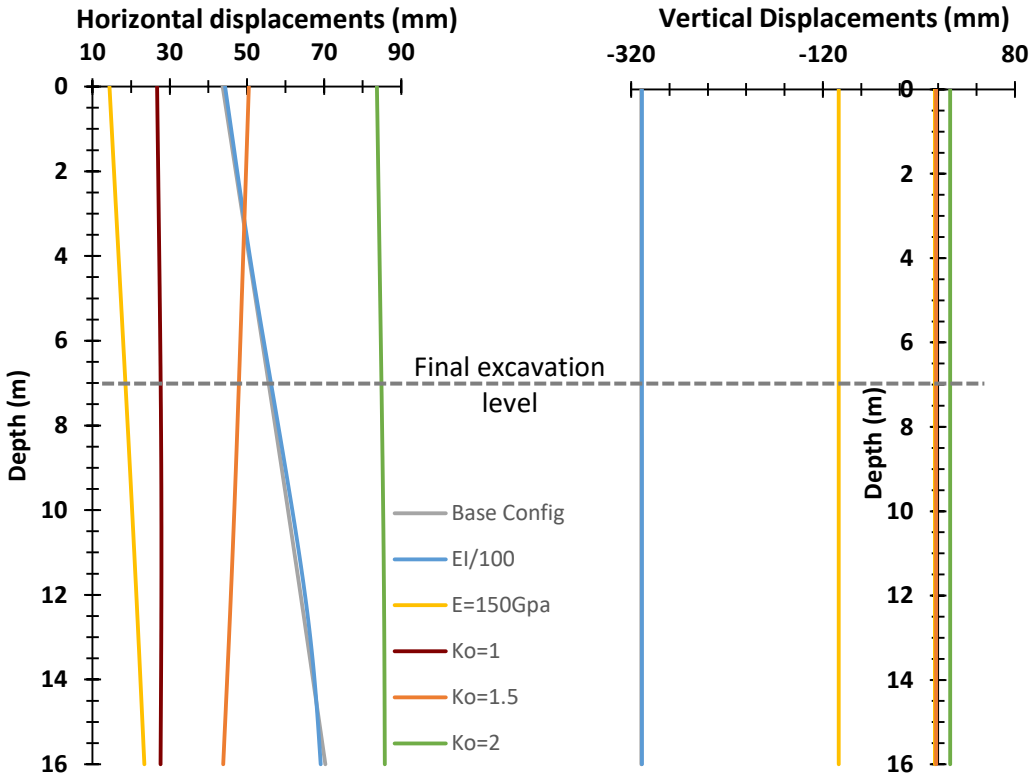

Figure 54 - Wall displacements for different configurations.

In Figure55 are represented relative shear stresses for the active and passive sides of the wall.

The variation in the wall stiffness EI or in the soil stiffness E has almost no effect on the mobilization of the shear stress as it is already almost fully mobilized in the base configuration. However, when the initial horizontal stresses are increased, the greater amount shearing is available as the consequence of the increase of the perpendicular to the wall pressures. Consequently, the reduction in the relative shear stress may be observed for the increased value of the K.

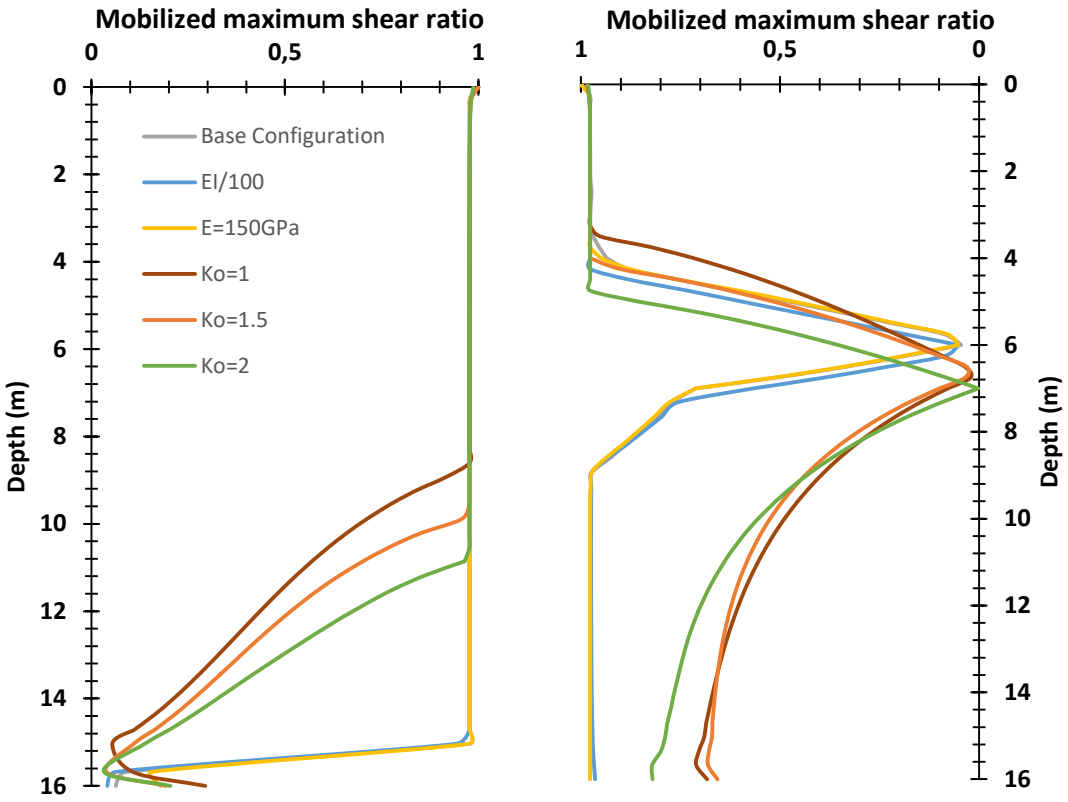

Figure 55 - Relative shear stresses for the different configurations.

5. COMPARISON AND DISCUSSION

The results obtained in the previous sections regarding the MCW analysis and FEA are presented in the following Figure 56 for the 2H_1V geometry and in Figure 57 for the 3H_1V geometry respectively. In those charts are also plotted the results obtained by utilizing the passive earth pressure coefficient indicated in the chart of NAVFAC 7.02 (1986) for the wall retained soils with inclined backfill. For the 2H_1V case was also plotted the result obtained by utilizing the earth pressure coefficient that is indicated in the aforementioned (Lam, 1991), that was obtained by utilizing the simplified method of slices (SMS) it was possible because of the similarity in the values of to the soil proprieties and the berm geometry.

By observing the aforementioned chart it can be noted that the pressure slope obtained by using the pressure coefficient of the NAVFAC chart is a close approximation of the slope at the top of the berm obtained by the MCW method. However, the overall pressure distribution obtained by this method are greatly superior when compared to the MCW method. The slope obtained by the SMS method utilized in the Lam (1991) does not represent well the pressure values at the top of the berm but on the other hand can serve as an adequate approximation of overall pressure diagram in the berm, having the overall area of the pressure close to the one obtained in the MCW method.

Another observation is regarding the comparison of the results obtained by the FEA and the MCW method which indicates the drastic difference in the pressure distribution. Even for the case where the coefficient of the initial horizontal stresses K_o=2, which mostly affects the values of the pressure below the excavated level but not inside the berm. The pressures in the berm are much greater for the MCW method. Those differences may be addressed to the fact that the MCW method gives the critical values of the pressure for each node by calculating the respective critical slip surface at each node, those values may not be achieved along the whole wall as that would suggest the simulations mobilisation of all of the available passive resistance along the whole wall. The FEA was carried out for the conditions close to failure so more passive resistance could be mobilized. Of all the parameters the initial horizontal pressures are the ones that have the greater effect on the pressure distribution. The difference in the soil stiffness and wall stiffness has a very slight effect on the pressure distribution along the wall. However as was already observed in the previous chapters the Force distribution inside the wall can be considerably affected by those parameters as well as wall displacements, which are crucial for the wall design and the SLS verification respectively.

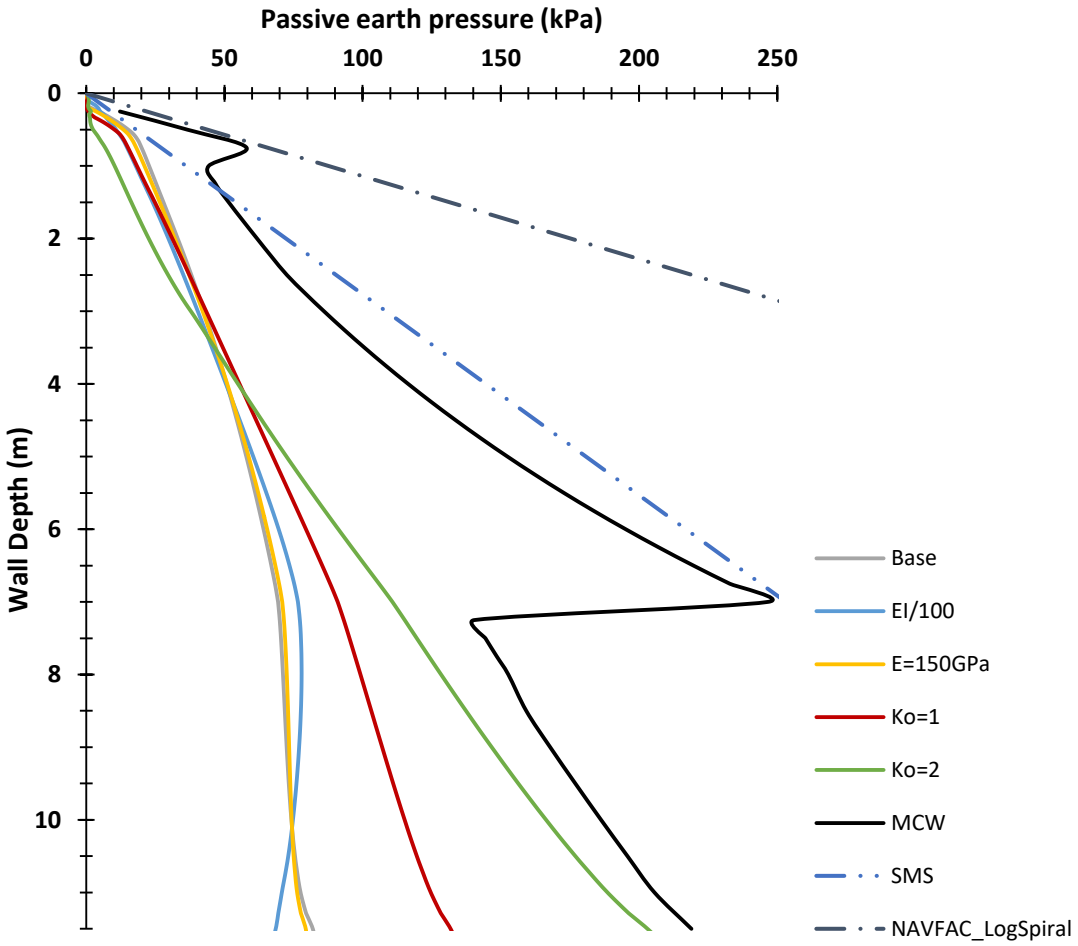

Figure 56 - Effective passive pressures of the 2H:1V geometry obtained by the different methods and configurations (FEA).

In the diagram regarding the 3H:1V geometry the difference between the results obtained by the FEA analysis and the MCW method is less noticeable, this difference may be explained by the fact that this configuration is closer to failure in the FEA analysis than the 2H:1V configuration. That was addressed in the previous chapter by demonstrating the shear forces diagram, wherein the 3H:1V much greater area had achieved the full mobilization. The same coincidence in the slope at the top of the berm is present when the MCW and NAVFAC results are compared.

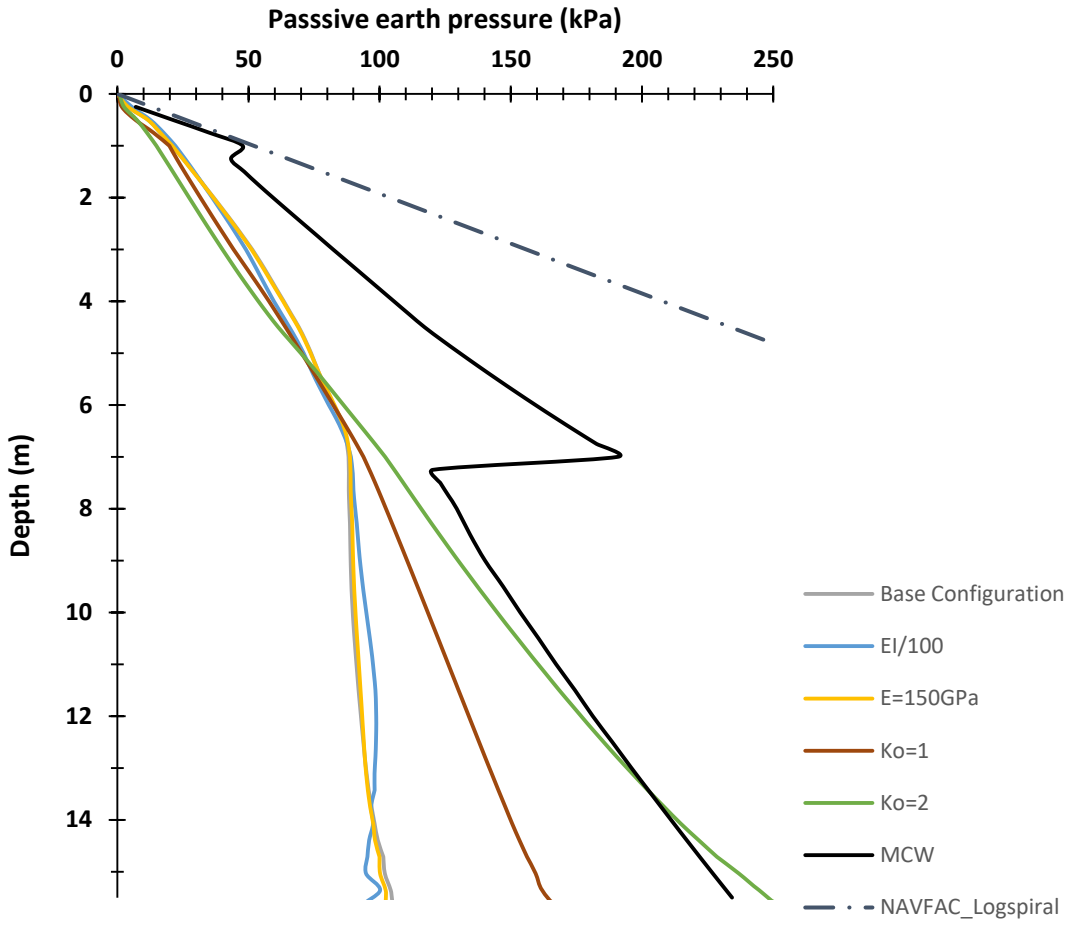

Figure 57 - Effective passive pressures of the 3H:1V geometry obtained by the different methods and configurations (FEA).

Overall independently of the setup variation, the stress distribution in the berm is always significantly lower in the FEA. At the top of the berm, a slight peak might be observed which has the inclination of the Kp obtained by the NAVFAC charts as was mentioned in both cases. Also in the MCW method, the pressures in the berm are getting unrealistically high towards the base of the berm, probably partly because of the geometry being restricted, with the assumption of planar slip surface, not allowing the slip surface to pass below the toe of the berm. This problem is addressed in the Wallap software which for this cases also considers the slip surface below the ground level with two block mechanism. In the case of the node at the excavation level, the slip surface is horizontal. This point is located at the excavated level when transitioning from the berm to the ground and where the water table is set. This offset or drop is more pronounced when the soil-wall friction is increased and is very slight when no friction of the wall is assumed.

6. Conclusions & Recommendations

6.1 Conclusions

It is a common practice to use soil berms as a support of the embedded walls offering the additional resistance and the displacements control. However there not so many methods nor the agreement on to which method should be used. Two main approaches were carried out the FEA and the limit equilibrium MCW method. Finite element analysis performed by the PLAXIS software for two different geometries 2H:1V and 3H:1V and the variations with the different values of the soil and wall stiffness as well as initial horizontal stresses. The MCW was carried out for the same two geometries in order to allow the comparison of the results. Both geometries were set to close to the failure conditions for the greater mobilization of the passive resistance and consequently closer results of the MCW and FEA, as the limit equilibrium methods are close to upper bound solutions which occur at near failure situations.

The main conclusions are:

a) The MCW method tends to give the values of the effective stresses much greater than FEA analysis, especially inside the berm.

b) The MCW give a great singularity point at the excavated level, which tends to increase for the greater values of the soil-wall friction.

c) The pressures obtained by the MCW method are close to once obtained by using the chart presented in Lam (1991) for the wall retained soils with inclined backfills, however similar chart in NAVFAC 7.02 (1986) give greater values.

d) There is a presence of the unrealistic spike when using the MCW method with suctions.

e) Variation of the initial horizontal stresses by altering the K_o coefficient affect very slightly the pressure distribution inside the berm. But greatly affects the earth pressures below the excavated level.

f) The wall and soil stiffnesses have a very small effect on the earth pressure distribution but have a greater effect on the force distribution along the wall and great effect on the wall displacements.

g) The close to failure conditions assumed in the MCW approach may not be feasible as the displacements needed to achieve that conditions are considerably high.

h) The REF method even though it gives conservative values of stress when compared to the other limit equilibrium methods, when compared to the FEA analysis it is not conservative.

6.2 Recommendations for future work

The work completed in this thesis has provided a comparison of existing procedures for the evaluation of the restraint provided by earth berms supporting embedded retaining walls, a number of interesting features have been identified and of particular concern is the apparently unsafe estimation of passive restraint from simpler methods in comparison to finite element analysis.

In order to address these concerns, the following future studies are suggested:

a) The use of alternative analytical methods and slip surface mechanisms (e.g. log-spiral) to understand how the predicted passive restraint provided by the berm varies, i.e. identify the critical slip surface configuration more precisely, especially below the berm.

b) Evaluation of the same berm effects for different methods but based on undrained soil response in the berm materials, and a deeper examination of the impact of short-term construction induced suctions and long-term effects when the berm is above the groundwater table.

c) Comparison and modification of the methods discussed in this thesis on the basis of experimental data.

REFERENCES

Daly M P, Powrie, W (2001). Undrained analysis of earth berms as temporary supports for embedded retaining walls, Proc. of the Institution of Civil Engineers - Geotechnical Engineering 149(4): 237-248

Easton M R, Darley P (1999). Case history studies of soil berms used as temporary support to embedded retaining walls (TRL Report 380), Transport Research Laboratory, Crowthorn, Berks, UK.

Fleming K, Weltman A, Randolph M, Elson K (2009). Piling Engineering, 3rd Ed., Taylor & Francis, Abingdon, Oxon, UK.

Gaba A R, Simpson B, Powrie W, Beadman D R (2003). Embedded retaining walls - guidance for economic design (CIRIA C580), Construction Industry Research and Information Association, London, UK.

Gourvenec S M, Powrie W (2000). Three-dimensional finite element analyses of embedded retaining walls supported by discontinuous earth berms, Canadian Geotechnical Journal 37(5): 1062-1077.

Lam T (1991). Computation of passive earth pressure by a simplified method of slices, Geotechnical Engineering J., 22(1): 43-57

NAVFAC 7.02 (1986). Foundations and Earth Structures, Naval Facilities Engineering Command, Washington, USA.

Padfield C J, Mair R J (1984). Design of retaining walls embedded in stiff clay (CIRIA Report 104), Construction Industry Research and Information Association, London, UK.

Shiau J S, Augarde C E, Lyamin A V, Sloan S W (2008). Finite element analysis of passive earth resistance in cohesionless soils, Soils & Foundations, 48(6): 843-850

Simpson B, Powrie W (2001). Embedded retaining walls: theory, practice and understanding, In Proceedings of the 15th Intl. Conf. on Soil Mechanics and Geotechnical Engineering, 2505-2524.

Smethurst J A, Powrie W (2008). Effective-stress analysis of berm-supported retaining walls, Proc. of the Institution of Civil Engineers - Geotechnical Engineering 161(1): 39-48

WALLAP (2012). WALLAP V6.0 User Manual, Geosolve Ltd, http://www.geosolve.co.uk/wallap1.htm

APPENDIX A – MCW SPREADSHEET IMPLEMENTATION

1. Introduction

This appendix explains the calculations and assumptions required for the application of the automated Multiple Coulomb Wedge (MCW) method which was implemented using the Excel software with builtin solver tool and VBA code.

The MCW method is the limit equilibrium method which uses the Coulomb wedges defined by the critical slip surface at each node in order to calculate the value of the critical earth impulse at each node. The pressure is given as the product of the difference of the earth impulses of the two adjacent nodes divided by the distance between them.

2. Parameter and values

2.1. Input parameters

a) Problem geometry

The following geometric terms **Table.A.1** are used in the calculation of the passive or active pressures in the MCW method (see **Figure 58**):

Table.A 1. – Geometric terms

Parameter	Symbol	Units
Berm height above the excavated level	h_{berm}	m
Width of the top of the berm	b	m
Angle of the slope of the berm to horizontal	α	°
Wall height above the excavated level	f	m
Wall embedment below the excavated level	d	m
Pivot point (depth from the top of the wall that corresponds to rotation point of the wall)	Zp	m
Distance between the excavated level and the water table behind the wall (negative when the water table is below the excavated level)	i	m
Distance between the excavated level and the water table in front of the wall (negative when the water table is below the excavated level)	j	m

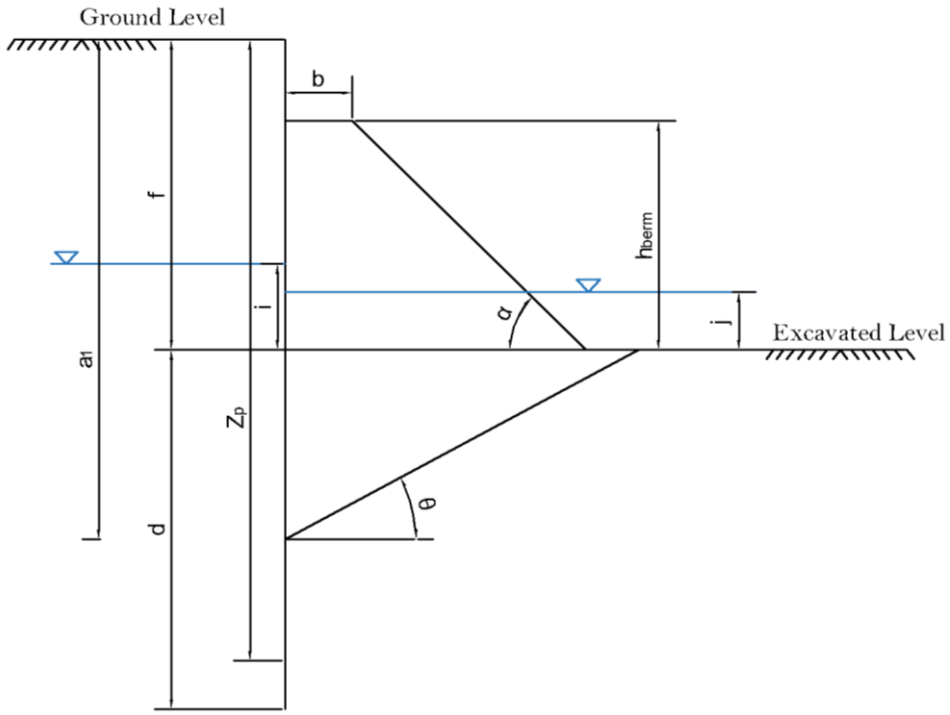

Figure 58 - Schematic representation of the berm geometry.

b) Soil parameters

ϕ'(°) – angle of shearing resistance of soil

δ/ϕ' – ratio of wall friction angle to soil shearing resistance

c' – apparent cohesion of soil

c'_w –adhesion at soil/wall interface

ϒ – unit weight of soil (20kN/m^3)

$ϒ_w$ – unit weight of water (9,81kN/m^3)

c) Other input parameters

θ (°) – angle of the slip surface (value can be set manually as a starting point for posterior iterations)

Suctions – parameter that enables to the pore water pressure gradient above the water table to be adjusted. ("0" – no suctions, "1" – the gradient is equal to the gradient below the water table)

M – mobilization factor applied to tg(ϕ')

a_1 (m) – height of the wedge (counted from the top)

h* (m) – height increment between successive wedges

2.2. Calculated parameters

Wedge nº - number of the wedge for which calculations are made

Moment (kNm/m) – moment generated by the wedge due to the passive or active impulse (depending when above or below the pivot point)

Pressure (kPa/m) – pressure exerted by the wedge (Passive or active, depending when above or below the pivot point)

F (kN/m) – force exerted by the wedge (Passive or active, depending on the wedge)

N' (kN/m) – normal Force acting on the slip surface (without water impulse)

U_r (kN/m) – water Impulse acting on the slip surface

U_w (kN/m) – water Impulse acting between wall and the wedge

W (kN/m) – weight of the wedge

l (m) – length of the slip surface

l* (m) – length of the slip surface below the water table (relevant when the slip surface extends above the water table)

c'*l (kN/m) – resultant force due to a soil cohesion

c_w*a_1 (kN/m) – resultant force due to the wall cohesion

θ (°) – angle of the slip surface from horizontal

θ_{min} (°) – angle from horizontal of a line extending from the toe of the berm to current wedge; potential slip surfaces sloping below the line defined by this angle are not valid (relevant for the calculation of the slip surface while inside the berm)

θ* (rad) – angle that slopes to the toe of the berm when the node is below the ground level (used for the calculation of active wedges)

ϕ'_d(°) – Angle of shearing resistance of the soil with a factor of safety applied

δ_p (°) – wall friction angle on the passive side of the wall

u_1* (kPa/m) – pore water pressure at the end of the slip surface without "suction factor" applied

u_2* (kPa/m) – pore water pressure at the beginning of the slip surface without "suction factor" applied

u_1 (kPa/m) – pore water pressure at the end of the slip surface with "suction factor" applied

u_2 (kPa/m) – pore water pressure at the beginning of the slip surface with "suction factor" applied

u_3 (kPa/m) – pore water pressure at the top of the berm with "suction factor applied"

u_{pgr} (kPa/m) – gradient of pore water pressure on the passive side of the wall

u_{agr} (kPa/m) – gradient of pore water pressure on the active side of the wall

x_1 – horizontal distance between the node and the intersection of the slip surface with the line l_1 (which will be defined in the next section)

x_2 – horizontal distance between the node and the intersection of the slip surface with the line l_2 (which will be defined in the next section)

x_3 – horizontal distance between the node and the intersection of the slip surface with the line l_3 (which will be defined in the next section)

A_{trap} (m^2) – area of the trapezium for the auxiliary calculation (which will be defined in the next section)

A_{triang} (m^2) – area of the triangle for the auxiliary calculation (which will be defined in the next section)

A (m^2) – total area of the wedge

A_{berm} (m^2) – total area of the berm

α (rad) – angle of the slope of the berm in radians

Total moment table:

Stabilizing – total stabilizing moment, produced by the passive earth pressures

Destabilizing – total destabilizing moment, produced by the active earth pressures

Water Impulse Stab – total stabilizing moment, produced by the water impulses

Water Impulse Destab – total destabilizing moment, produced by water suctions (if present) and by water Impulses respectively

Factor of Safety – ratio between total sum of the stabilizing over destabilizing moments

Coulomb table:

K_a – horizontal active earth pressure coefficient on the back of the wall calculated using Coulomb's method

K_p – horizontal passive earth pressure coefficient on the back of the wall calculated using Coulomb's method

δ_a (rad) – wall friction angle on the active side of the wall

I_a – Active Impulse behind the wall calculated using Coulomb's method

I_p – Passive Impulse behind the wall calculated using Coulomb's method

PWP table (pore water pressures)

u_{pgr} (kPa/m) – gradient of pore water pressure on the passive side of the wall

u_{agr} (kPa/m) – gradient of pore water pressure on the active side of the wall

u_f – pore water pressure at the bottom of the wall

3. Calculation

3.1. Calculation of the earth passive impulse F and the normal force N'

Assuming the forces that are acting on the wedge, as shown in the **Figure 59**:

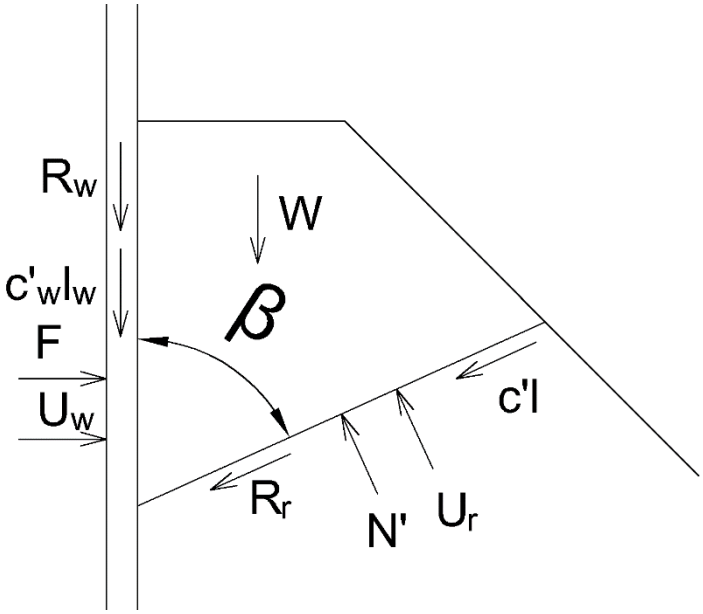

Figure 59 - Forces actuating on the wedge.

In order to calculate F and N' sum of the resultant vertical and horizontal forces were used.

Since the forces that are acting on the passive and on active wedge are the same, but some of them have the opposite direction, for the next demonstration, some of the ± signs are marked "red". Where the sign on the bottom is for the active wedge.

For the following equations:

$$\beta = 90^\circ - \theta$$

For the horizontal:

$$\sum F_h = 0 \leftrightarrow F + U_w \mp c'l \times sin\beta \mp R_r \times sin\beta - N'cos\beta - U_r \times cos\beta \leftrightarrow F$$
$$= (N' + U_r)cos\beta - U_w \pm (c'l + R_r)sin\beta$$

Assuming that:

$$R_r = N'tan\varphi'$$

Then the previous equation can be expressed as:

$$F = \pm(N'tan\varphi' + c'l)sin\beta + (N' + U_r)cos\beta - U_w$$

For the vertical:

$$\sum F = 0 \leftrightarrow W \pm R_w \pm c'_w l_w - (N' + U_r)sin\beta \pm (R_r + c'l)cos\beta = 0$$

Assuming that:

$$R_w = Ftan\delta = \pm(N'tan\varphi' + c'l)sin\beta tan\delta + (N' + U_r)cos\beta tan\delta - U_w \times tan\delta$$

Then previous equation can be expressed as:

$$\begin{aligned} &N'sin\beta \mp N'tan\varphi'cos\beta \mp N'tan\varphi'sin\beta tan\delta - N'cos\beta tan\delta \\ &= W \pm c'_w l_w \pm c'l \times cos\beta - U_r \times sin\beta \pm c'l \times sin\beta tan\delta + U_r \times cos\beta tan\delta - U_w \\ &\times tan\delta \leftrightarrow N' \\ &= \frac{\pm c'l(cos\beta + sin\beta tan\delta) + U_r(cos\beta tan\delta - sin\beta) + W - U_w \times tan\delta \pm c'_w l_w}{sin\beta \mp tan\varphi'cos\beta \mp tan\varphi'sin\beta tan\delta - cos\beta tan\delta} \end{aligned}$$

So the final equations that are used are:

$$N' = \frac{\pm c'l(cos\beta + sin\beta tan\delta) + U_r(cos\beta tan\delta - sin\beta) + W - U_w \times tan\delta \pm c'_w l_w}{sin\beta \mp tan\varphi'cos\beta \mp tan\varphi'sin\beta tan\delta - cos\beta tan\delta}$$

$$F = \pm(N'tan\varphi' + c'l)sin\beta + (N' + U_r)cos\beta - U_w$$

For the calculation of these forces, besides the soil characteristics and angle of the slip surface, the following parameters must be determined: l, U_w, U_r, W. These will be derived in the next section.

3.2. Calculation of the weight, the area of the wedge, of the slip surface line and definition of the lines

For the calculation of the weight of the wedge, the corresponding area must be calculated. The weight of the wedge is given by the next expression:

$$W = \gamma \times A$$

Where γ is an input parameter and A needs to be calculated.

Assuming "a_1" is a distance from the top of the berm until the node point, "h_{berm}" is a height of the berm, "b" is a width of the top of the berm, "α" is the angle between horizontal line and the slope of the berm, "θ" is the angle between horizontal line and the slip surface.

Two general situations were set in a spreadsheet as nested functions for calculation of the area of the wedge. (see **Figure 60**)

1) When $a_1 <= h_{berm}$, in other words, when the slip surface of the wedge slopes from a point above or at the excavation level or from the ground level.
2) When $a_1 > h_{berm}$ and the slip surface slopes from the point which is situated below the excavation level.

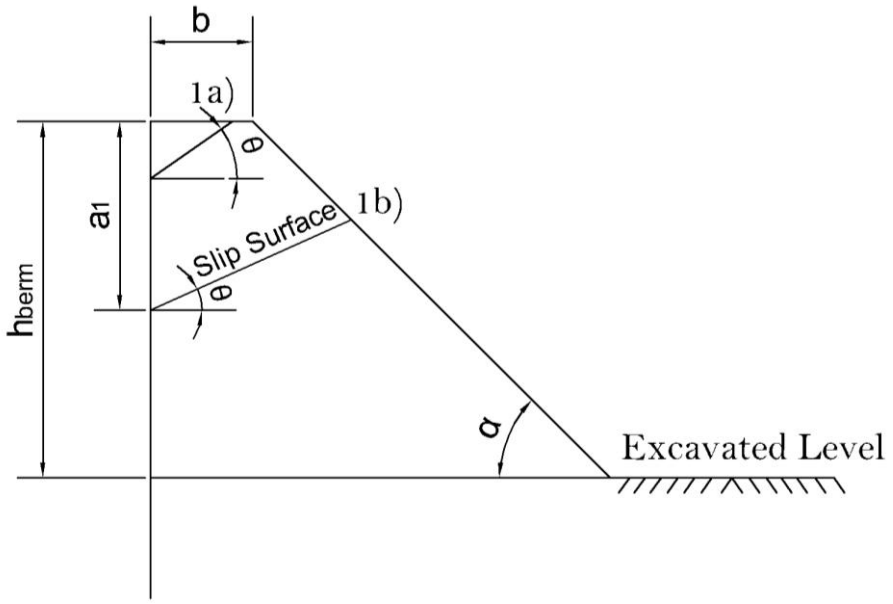

Figure 60 - Slip surfaces inside the berm

For the first case two situations were assumed:

1a) when the slip surface intersects the bench at the top of the berm (in trapezium like type of the berms)

1b) when the slip surface intersects the soil sloping from the top of the berm.

In order to distinguish the two situations, two variables were defined that will dictate whether the situation is of type 1a) or 1b) will apply.

Those variables are x_1 and x_2 which define the horizontal distance between the point on the wall from which the slip surface projects to intersect a line of the top of the berm or the sloping surface of the berm respectively (**Figure 61**). Assuming three lines that would limit the area of the wedge(not counting the wall) with the reference origin in the node point, that can be defined by simple equations like y=mx+c(where m and c are constants).The first line l_1 is the line passing through the top of the berm that has an equation:

$$l_1 = y = a_1$$

The second line is the line defining the slip surface y=x*tg(θ) and the third line l_2 that defines the slope of the berm as illustrated in Fig. A.4. Slope line assumes positive values of α and always has a negative inclination of m. Therefore:

$$m = -tg(\alpha)\ and\ for\ x = 0 \rightarrow y = a_1 + btg(\alpha) = c \rightarrow l_2 = y = a_1 + btg(\alpha) - xtg(\alpha)$$

To determine the x_1 next equation needs to be solved:

$$xtg(\theta) = a_1 \rightarrow x_1 = \frac{a_1}{tg(\theta)}$$

Which is the intersection of the slip surface line with the berm line.

With regard to $x_{2,\,the}$ equation is:

$$a_1 + btg(\alpha) - xtg(\alpha) = xtg(\theta) \rightarrow x_2 = \frac{a_1 + btg(\alpha)}{tg(\theta) + tg(\alpha)}$$

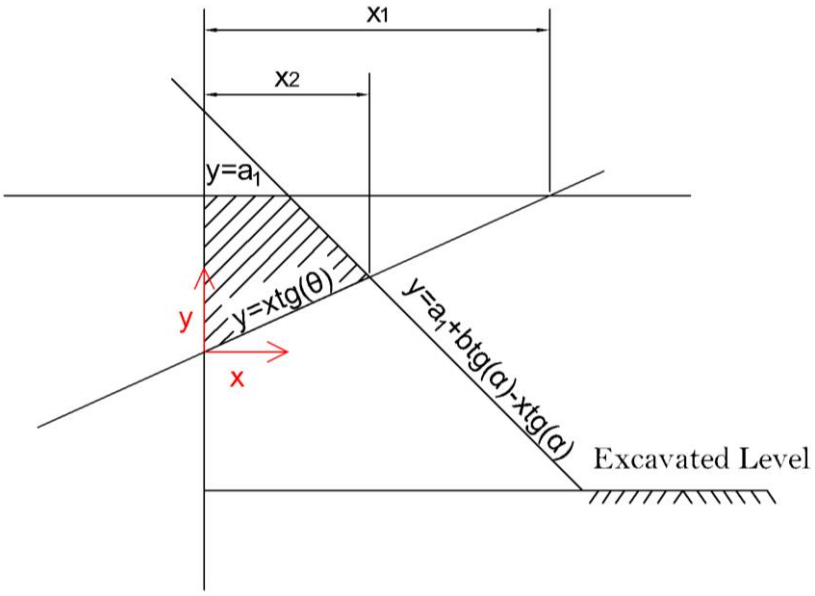

Figure 61 - Line definition.

Area calculation:

Depending on whether $x_1 <= x_2$ or opposite the obtained situation will be a) or b) respectively. For the first situation, the area is given as:

$$A = \frac{x_1 \times a_1}{2}$$

For the second situation:

$$A = A_{triangle} + A_{trapezium}$$

$$A_{triangle} = \frac{(x_2 - b) * (a_1 - btg(\theta))}{2}$$

$$A_{trapezium} = (\frac{2a_1 - btg(\theta)}{2}) \times b$$

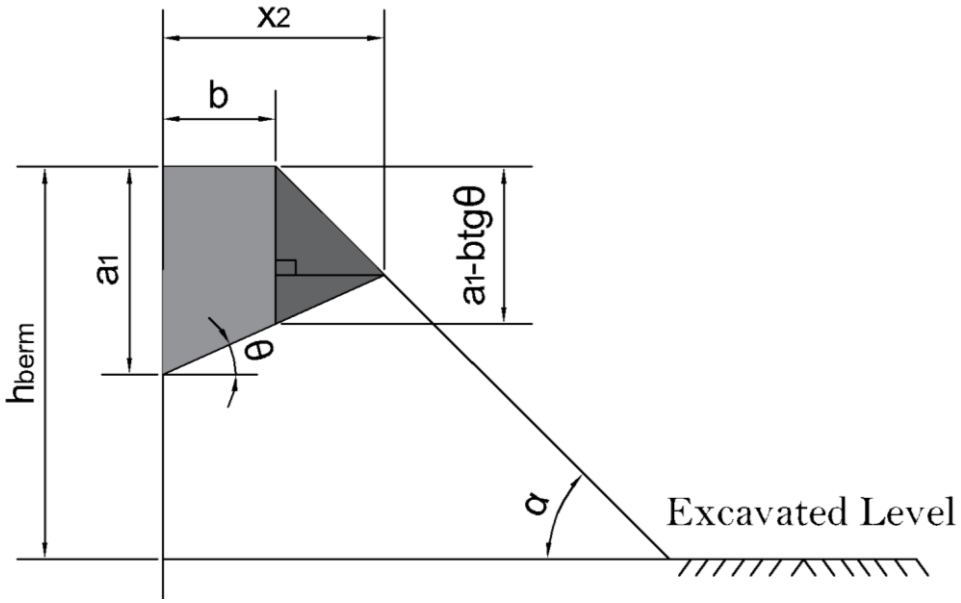

Figure 62 - Area of the wedge inside the berm.

For the second case, two situations were assumed as well:

2a) When the slip surface intersects the ground level

2b) When the slip surface intersects the slope of the berm

Similarly to the previous case to distinguish two situations lines were used and variables x_2 and x_3,

Where x_2 is the same as in the previous case and x_3 is the horizontal distance between the wall and a point of intersection of slip surface and the ground level. The equation for the ground level line is:

$$l_3 = y = a_1 - h_{berm}$$

Accordingly to determine x_3 next equation needs to be solved:

$$xtg\theta = a_1 - h_{berm} \gg x_3 = x = \frac{a_1 - h_{berm}}{tg\theta}$$

For the situation a) condition $x_2 >= x_3$ needs to be verified and the area is given as:

$$A = A_{berm} + A_{wedge\ triangle}$$

$$A_{berm} = \left(\frac{2b + \frac{h_{berm}}{tg\alpha}}{2} \right) \times h_{berm}$$

$$A_{wedge\ triangle} = \frac{x_3 \times (a_1 - h_{berm})}{2}$$

As shown in **Figure 63**

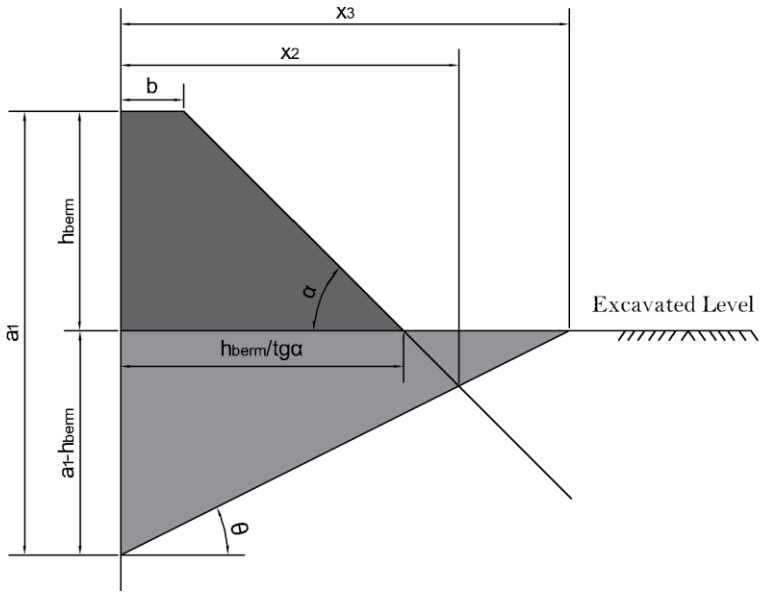

Figure 63 - Area of the wedge inside the ground.

For the second situation condition is $x_2<x_3$ respectively. And the area is given in the same way as in the 1b)

The next Excel's nested "IF" function was used in order to distinguish two situations with two cases each:

$$IF\left(\mathrm{a}_1 > h_{berm}; IF\left(AND(x_3 > x_2; \theta \neq 0); \frac{(\mathrm{a}_1 - h_{berm}) \times x_3}{2} + A_{berm}; A_{trap} + A_{triangle}\right); IF\left(AND(x_1 \leq x_2; x_1 \geq 0; x_2 \geq 0; \theta > 0); \frac{x_2 \times \mathrm{a}_1}{2}; A_{trap} + A_{triang}\right)\right)$$

For the calculation of the active impulses another variable was introduced θ^* which is the angle that slopes form the node towards the toe of the berm below the excavated level. Which is calculated by the following equation:

$$\theta^* = arctg\left(\frac{\left(b + \frac{h_{berm}}{tg\alpha}\right)}{a_1 - h_{berm}}\right)$$

Definition of this angle allows evaluating on which side of the toe of the berm the active slip line passes. As represented in the **Figure 64** there are three different situations with different ways to calculate areas.

The third situation is separated from the other two by the slip surfaces that has the angle of θ^*, so if $\theta < \theta^*$, then the area of the berm is:

$$A = A_{berm} + \frac{(a_1 - h_{berm})^2}{2tg\theta}$$

In the other two situations if $x_1 < x_2$ than the area is given as:

$$A = \frac{a_{1\times} x_1}{2}$$

Otherwise, the area is given as:

$$A = A_{trap} + A_{triangle}$$

This results in the following nested function:

$$A = IF(\theta < \theta^*;\ A = A_{berm} + \frac{(a_1 - h_{berm})^2}{2tg\theta}; IF(x_1 < x_2; A = \frac{a_{1\times} x_1}{2}; A = A_{trap} + A_{triangle}))$$

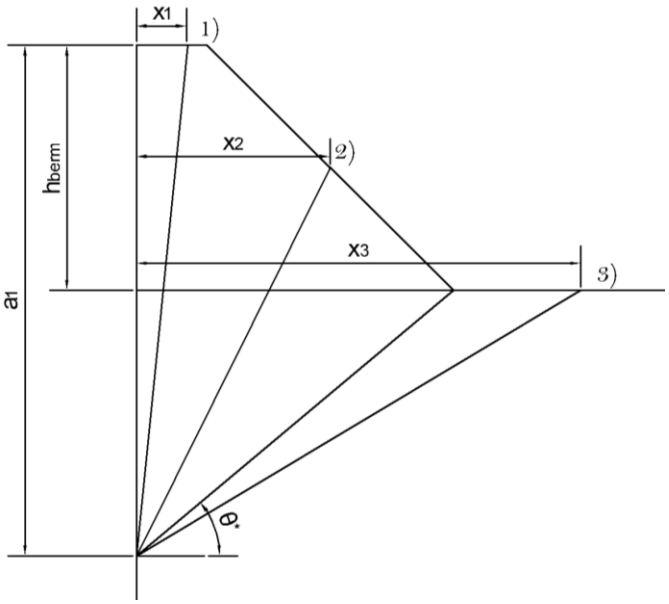

Figure 64 - Lines x_1, x_2 and x_3.

3.3. Pore water pressures and water impulses calculations

3.3.1. Definition of steady state seepage

To define the water pressure linear steady-state seepage was assumed. This assumes that a reservoir of water is available in the soil, that the wall is impermeable, and that the soil has homogeneous permeability characteristics."(CIRIA Report 104)

Assuming that i and j are positive when the water table is above the ground level. Then as can be observed in the figure below, the head difference between A and B is (f+i-j).Which is dissipated uniformly along the flow path (2d+f+i+j) which runs down the back of the wall and up the front. The pore water pressure distribution calculated on the basis of this simplification is less than hydrostatic pressure behind the wall and greater in front. The schematic representation of the general situation is presented in the **Figure 65**.

The head at the given distance "x" below the water table on the back of the wall is given as:

$$H_x = H - \Delta H \times x$$

Then the Head at the bottom of the wall is given as:

$$H_f = f + d + i - \frac{(f + i - j)(f + d + i)}{f + 2d + i + j} = \frac{(f + d + i)(f + 2d + i + j) - (f + i - j)(f + d + i)}{f + 2d + i + j}$$
$$= \frac{(f + d + i)(f + 2d + i + j - f - i + j)}{f + 2d + i + j} = \frac{2(f + d + i)(d + i)}{f + 2d + i + j}$$

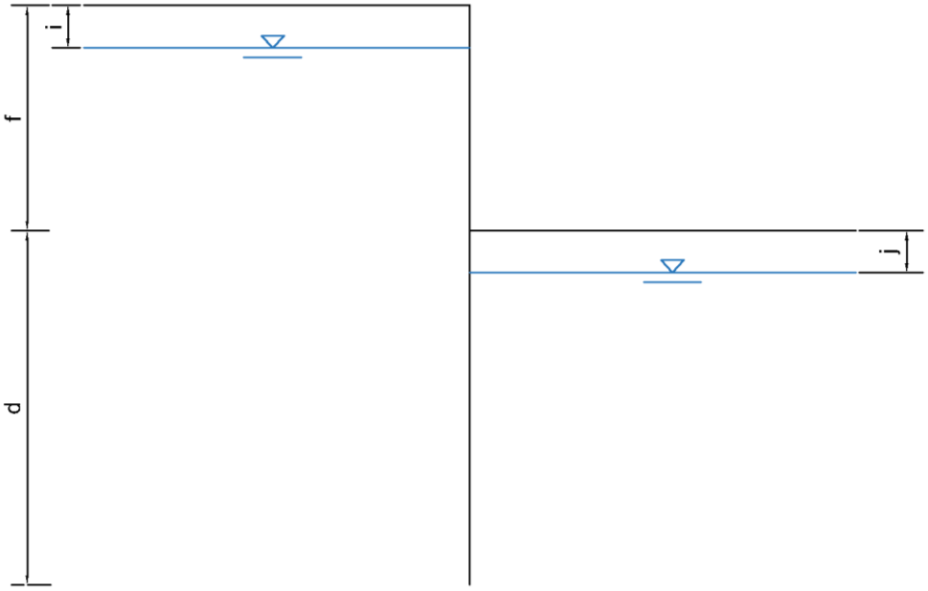

Figure 65 - Schematic representation of the parameters of the water table.

Taking into account that:

$$H = \frac{p}{\gamma} + z + \frac{u^2}{2g}$$

And that square of the velocity is approximately zero and z at the bottom is zero as well:

$$u_f = p = \frac{2(f + d + i)(d + i)}{f + 2d + i + j}\gamma_w$$

3.3.2. Pore water pressure

Assuming u_2* and u_1* are the pore water pressures on the wall at the node point and on the surface where the slip surface ends respectively. And u_3* is a pore water pressure on top of the berm. Assuming suctions above the water table level with the gradient equal to the one below the water table.u_1, u_2 and u_3 are the pore water pressures in the aforementioned locations with the suction parameter applied.

Similarly to calculations of areas, u_1* will depend on whether the node is situated above or below the excavated level and in which line does slip surface ends l_1, l_2 or l_3. For the cases where the node point is situated below the excavated level, three situations are assumed a), b) and c) as illustrated in **Figure 66**.

In the situation a) the slip surface intersects the top of the berm (which may happen with the shorter, but wider berms as presented in the figure A.9) in that case u_1^* is given as:

$$u_1^* = (-h_{berm} + j) \times u_{pgr}$$

In the situation b) the slip surface intersects berm slope and u_1^* is given as:

$$u_1^* = (a_1 - h_{berm} - x_2 tg\theta + j) \times u_{pgr}$$

In the situation c) when slip surface intersects with the excavated level is

$$u_1^* = j \times u_{pgr}$$

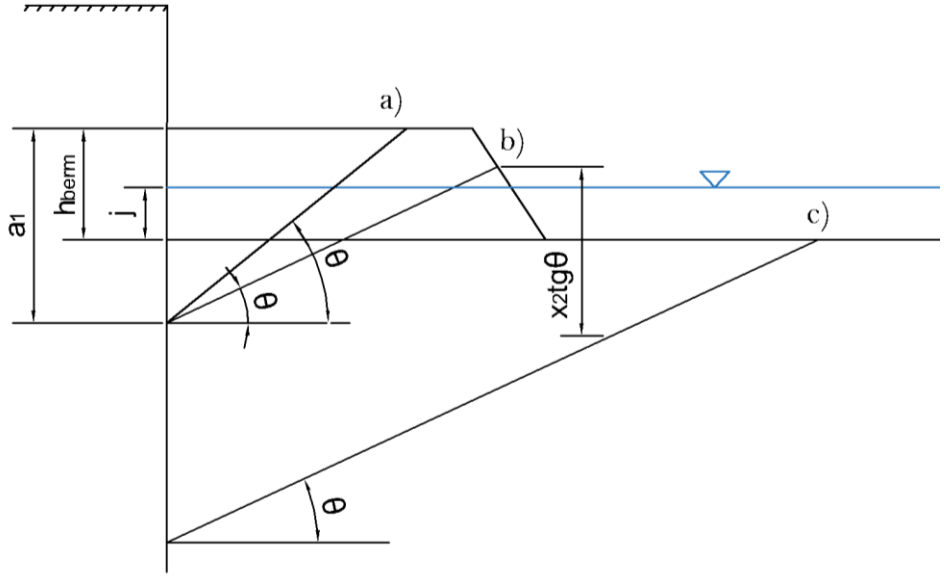

Figure 66 - Three different situations of the slip surface.

Regarding the cases when the node is inside the berm two situations are given as well.

When slip surface intersects top of the berm:

$$u_1^* = (-h_{berm} + j) \times u_{pgr}$$

When the slip surface intersects slope of the berm:

$$u_1^* = (a_1 - h_{berm} - x_2 tg\theta + j) \times u_{pgr}$$

This results in the next nested function:

$$u_1^* = IF(a_1 > h_{berm}; IF(x_2 > x_3; IF(x1 < x2; (-h_{berm} + j) * u_{pgr}; (a_1 - h_{berm} - x_2 tg\theta + j) * u_{pgr}); j * u_{pgr}); IF(x_1 \leq x_2; (-h_{berm} + j) * u_{pgr}; (a_1 - h_{berm} - x_2 tg\theta + j) * u_{pgr}))$$

For the active wedge, however, u_1^* can be calculated as:

$$u_1{}^* = IF(\theta < \theta^*; j \times u_{pgr}; IF(x_1 < x_2; (-h_{berm} + j) \times u_{pgr}; a_1 - h_{berm} - x_2 tg\theta + j) \times u_{pgr}$$

On the other hand, u_2* can be always defined as:

$$u_2{}^* = (a_1 - h_{berm} + j) \times u_{pgr}$$

Note: When the point from which the slip surface slopes is above the ground level a_1-hberm has negative values which will result in suctions and opposite when that point is below the ground level.

Regarding the pressure at the top of the berm u_3^* is always given as:

$$u_3{}^* = (-h_{berm} + j) * u_{pgr}$$

Note: in the spreadsheet u_3^* is not represented, the final value u_3 with the suction factor applied is only presented, which is explained in the next section.

3.3.3. Suction factor

This factor allows to alter the suctions above the water table level by adjusting the gradient of water pressures above the water table. The gradient above the water table will be multiplied by this factor. For example, if the factor equals to 0.7, then the gradient of the water pressures above the water table level will correspond to 70% of the gradient below the water table, if the factor equals to zero then no suction is assumed in the calculations.

This was done by multiplying u_1*, u_2* and u_3* by this factor in scenarios where pore water pressure is negative, using simple nested functions

$$u_1 = IF(u_1{}^* < 0; u_1 = u_1{}^* \times suctions; u_1 = u_1{}^*)$$

$$u_2 = IF(u_2{}^* < 0; u_2 = u_2{}^* \times suctions; u_2 = u_2{}^*)$$

$$u_3 = IF(u_3{}^* < 0; u_3 = u_3{}^* \times suctions; u_3 = u_3{}^*)$$

3.3.4 Water Impulses

The water impulse U_w on the side of the wall is a resultant force produced by the water pressures along the side of the wall, where the key values are u_2 and u_3. u_3 – assumes negative values or zero and u_2 can assume any value. Taking that into account the water impulse can be calculated either as a trapezium pressure distribution (when u_2 is negative) along the length a_1 or sum of the resultant forces from the two triangular pressure distribution with the opposite sign, where the length of the surface associated with pressure u_2 and u_3 are given by the next expression:

$$L_{u_2} = a_1 - h_{berm} + j$$

$$L_{u_3} = h_{berm} - j$$

Then the water Impulse can be expressed by the next nested function:

$$U_w = IF\left(u_2 < 0; U_w = \frac{(u_2 + u_3)}{2} \times a_1; U_w = u_2 \times \frac{a_1 - h_{berm} + j}{2} + u_3 \times \frac{h_{berm} - j}{2}\right)$$

For the water Impulse acting on the slip surface, U_r new parameter must be calculated. l*- which is the length of the slip surface emerged in the water. Two situations and one condition are assumed in this case, the condition is when the angle of slip surface is zero the value of l*=l, the two situations are when the node point is below or above the ground level. As shown in the **Figure 67**. It is expressed by the next nested function:

$$l^* = IF(\theta \neq 0; IF\left(a_1 > h_{berm}; l^* = \frac{a_1 - h_{berm} + j}{sin\theta}; l^* = \frac{j - h_{berm} - a_1}{sin\theta}\right); l)$$

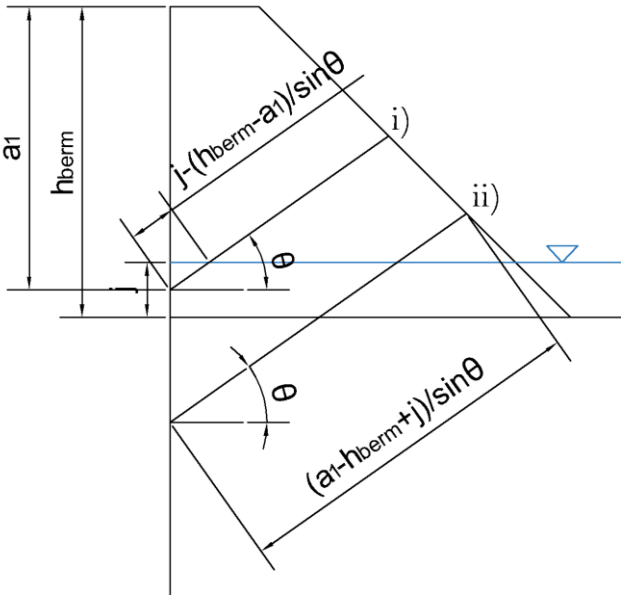

Figure 67 - Slip surfaces for the different l* calculation.

For the calculation of U_r two situations are assumed as well as for the calculation of the U_w.

When l* has a negative value or value that is greater than l, that means that slip surface is either situated above the water table or completely emerged respectively. Then for this cases u_1 and u_2 have the same sign and the resultant force is given as the trapezium pressure distribution over the whole slip surface, otherwise, it is given as a sum of two triangular pressure distribution over the length l* and l-l*. This results in the next nested function:

$$U_r = IF(OR(l^* < 0; l^* \geq l); U_r = \frac{u_1 + u_2}{2} \times l; U_r = \frac{u_2 \times l^*}{2} + \frac{u_1 \times (l - l^*)}{2})$$

3.4. Calculating the angle of the critical slip surface (or critical angle)

3.4.1 Calculation procedure and methods

The critical angle "θ" is the angle that maximizes or minimizes the active or the passive earth pressure respectively. In order to determine the respective angle, the solver add-in was used.

By default, there are three algorithms available LP Simplex, GRG-nonlinear, and Evolutionary. For this problem, GRG-nonlinear and Evolutionary algorithms were used owing to the fact that the functions that are used to estimate the value of F (I_P) are nonlinear and irregular. GRG-nonlinear searches for the local optimal value using a gradient to find the optimal solution, with central or forward derivatives. Taking that into account and the fact that the function is not continuous due to the use of nested functions for some situations GRG-nonlinear cannot be used by itself. Because if the function has more than one minimum (maximum) it may not converge to the absolute optimal value, but to the local optimal value which depends on and is closest to the starting value of "θ". **Figure 68** serves as an example of where and how it can happen, by showing the variation of the earth pressure values with the angle of the critical slip surface for a given depth.

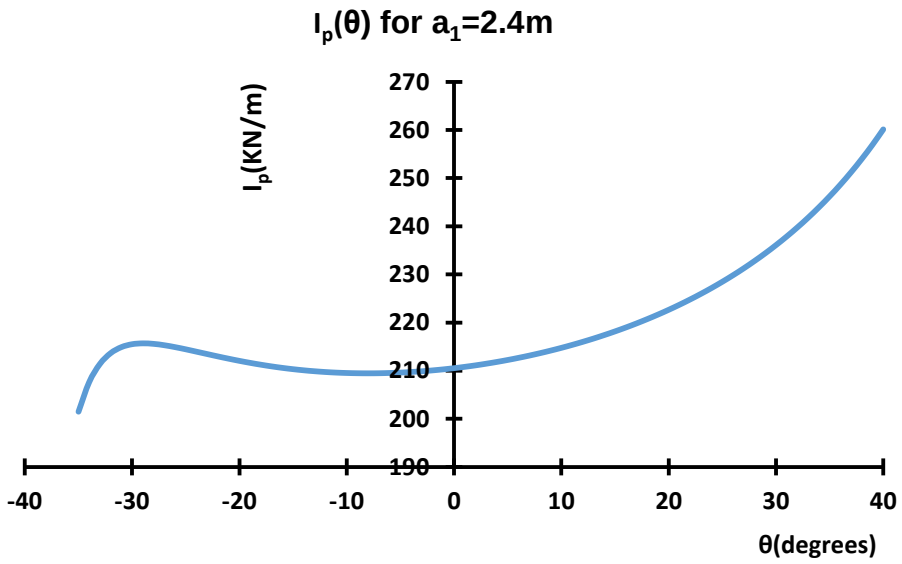

Figure 68 - Critical angle θ against I_p chart for the depth of 2.4 m.

For example, if the starting value for the "θ" is somewhere in between -25° and 40° resultant value of "θ" shall be at around -10° which is a local minimum. But in reality, there is another slip surface which is more critical, the one that is associated with the angle of approximately -36°. For that type of situations, the Evolutionary algorithm is to be used or at least should be used first. The Evolutionary method uses directly the decision variables and problem functions. The advantages of this method are:

1) Randomness – it relies on a random sample of candidate values (population)

2) Population – where most classical optimization methods maintain a single best solution found so far, an evolutionary algorithm maintains a population of candidate solutions only one of these is “best”, but the other members of the population are “sample points” in other regions of the search space where a better solution may be later found. That way it won’t be trapped in the local optimum.

Drawbacks: this algorithm finds better solutions in comparison to other presently known solutions. So it won’t find the optimal solution. And it will only stop if time, iteration or a candidate solution value limit is achieved. Another drawback of the Evolutionary is a time that it takes to calculate the solution especially if there are many wedges (nodes) to consider.

Taking this into account the most precise procedure to estimate the optimal value would be to run first Evolutionary which will guarantee that the found solution is situated close to the absolute optimal solution. And afterward, run GRG-nonlinear to direct the previous solution towards the absolute optimal value.

Next set of restrictions for GRG-nonlinear and Evolutionary methods was applied, for passive Impulses:

$$\theta \geq \theta_{min}$$

$$\theta \leq 60^{\circ}$$

Where θ_{min} is either the angle that slopes from the node towards the toe of the berm for the situations when the node is situated insde the berm or is set to the approximate value of 0.1°. To note that the situation when the node is at the excavated level the angle is forced to 0° which results in the horizontal slip surface. Altogether this restriction guarantees that the slip surface won’t go below the excavated level when inside the berm and that the angle of the slip surface when below the excavated level is greater than 0° evading horizontal or below the horizontal lines. The value of 60° for the maximum angle was set as the value that reduces the number of unrealistic values for θ. This condition is resulted in the next nested function:

$$\theta_{min} = DEGREES(IF\left(a_1 \leq h_{berm}; IF\left(a_1 \neq h_{berm}; -arctg\left(\frac{(h_{berm} - a_1)}{\left(\frac{h_{berm}}{tg\alpha}\right) + b}\right); 0\right); 0.002\right))$$

Note: the value of 0.002 is the value that when transformed to the degrees is approximately 0.1°. The DEGREES function transforms the values of radians to the degrees

The objective of the methods is to set the value of $F(I_p)$ to a minimum by changing the value of θ.

For the calculation of the active impulse, on the contrary, the objective is to maximize the value of $F(I_a)$, and for that, the following conditions are applied.

$$\theta \geq 30^{\circ}$$

$$\theta \leq 80^{\circ}$$

As was already mentioned before in order to make solver run automatically it was necessary to write a programming code in the built-in the VBA that may be found at the end of the current section. There are four buttons in the spreadsheet called: GRGPassive, EvolutionaryPassive, GRGActive and EvoulutionaryActive each of which corresponds to the respective solver method and to the respective impulse that is being calculated.

In order to use the solver buttons the input referencing numbers of the wedges must be introduced as shown in the example of the **Table A. 2** below:

Table.A 2 – Solver input menu.

Solver Configuration			
	Solver method	from	to
Passive	Evolutionary wedges (i)	1	40
	GRG-nonlinear wedges (i)	1	40
Active	Evolutionary wedges (i)	41	45
	GRG-nonlinear wedges (i)	41	45

The numbers in the table are the number of the wedges from which the solver will start a calculation and on which will end respectively. Each method has its own set of referencing numbers for active and passive wedges.

3.4.2. Comments regarding the solver use

The important things to mention would be the fact that although the automatized spreadsheet can estimate the values of the critical angle, it is still necessary to check the results and see if there are some values that do not make sense and that need to be corrected “by hand”. This usually concerns the situation when the pressure value is negative or when the resultant pressure diagram is too heterogeneous, with the exception of some of the “spikes” that are explained in the MCW section of the thesis. This may happen because the solver could not converge to the optimal value, this may be solved by trying to change the values by hand and run the solver GRGnonlinear afterwards, or by using the Evolutionary method, but as was already mentioned before the downside of it is that it is slower, especially for the situations when the wall friction is included. In this situation, it can slow down to the degree that it does not justify to use the method or on some occasions it might even stop.In those cases in order to find a solution the manual alteration of the value of the angle of the slip surface in conjuncture with the GRG-nonlinear method may be used. By running the GRG-nonlinear first and then altering the values of θ in the singularity points and running the GRG-non linear again.

3.4.3. Macros for the solver

Following are the VBA codes for each of the four aforementioned buttons:

For the GRGPassive:

```
Sub GRGNonlinearPassive()
Dim i As Long
 For i = (2 + Cells(51, 20)) To (2 + Cells(51, 21))
  Dim a As Long
    SolverReset
    SolverOptions MaxTime:=180, Iterations:=9999, Precision:=0.1, _
       Convergence:=0.1, StepThru:=False, Scaling:=True, AssumeNonNeg:=False, _
       Derivatives:=1
          SolverOk SetCell:=Cells(7, i), MaxMinVal:=2, ValueOf:=0, ByChange:=Cells(21,
i), Engine:= _
       1, EngineDesc:="GRG Nonlinear"
    SolverAdd CellRef:=Cells(21, i), Relation:=1, formulaText:="60"
    SolverOk SetCell:=Cells(7, i), MaxMinVal:=2, ValueOf:=0, ByChange:=Cells(21, i),
Engine:= _
       1, EngineDesc:="GRG Nonlinear"
    SolverAdd CellRef:=Cells(21, i), Relation:=3, formulaText:=Cells(23, i)
    SolverOk SetCell:=Cells(7, i), MaxMinVal:=2, ValueOf:=0, ByChange:=Cells(21, i),
Engine:= _
       1, EngineDesc:="GRG Nonlinear"
    SolverDelete CellRef:=Cells(21, i), Relation:=3, formulaText:=Cells(23, i)
    SolverAdd CellRef:=Cells(21, i), Relation:=3, formulaText:=Cells(23, i)
    SolverOk SetCell:=Cells(7, i), MaxMinVal:=2, ValueOf:=0, ByChange:=Cells(21, i),
Engine:= _
       1, EngineDesc:="GRG Nonlinear"
    SolverOk SetCell:=Cells(7, i), MaxMinVal:=2, ValueOf:=0, ByChange:=Cells(21, i),
Engine:= _
       1, EngineDesc:="GRG Nonlinear"
    SolverSolve userfinish:=True
    SolverFinish KeepFinal:=1
Next i
End Sub
```

For the EvolutionaryPassive:

```
Sub Evolutionary2Passive()
' Evolutionary2 Macro
Dim i As Long
 For i = (2 + Cells(50, 20)) To (2 + Cells(50, 21))
 Dim a As Long
'(2+Cells(50,20)) To (2+Cells(50,21))
'For i = 3 To 118
```

```
   SolverReset
   SolverOptions MaxTime:=120, Iterations:=99, Precision:=0.1, _
      Convergence:=0.1, StepThru:=False, Scaling:=True, AssumeNonNeg:=False, _
      Derivatives:=1
   SolverOptions PopulationSize:=20, RandomSeed:=0, MutationRate:=0.075,
Multistart _
      :=False, RequireBounds:=True, MaxSubproblems:=0, MaxIntegerSols:=0, _
      IntTolerance:=0.1, SolveWithout:=False, MaxTimeNoImp:=30
   SolverOk SetCell:=Cells(7, i), MaxMinVal:=2, ValueOf:=0, ByChange:=Cells(21, i),
Engine:= _
      3, EngineDesc:="Evolutionary"
   SolverAdd CellRef:=Cells(21, i), Relation:=1, formulaText:="60"
   SolverOk SetCell:=Cells(7, i), MaxMinVal:=2, ValueOf:=0, ByChange:=Cells(21, i),
Engine:= _
      3, EngineDesc:="Evolutionary"
   SolverAdd CellRef:=Cells(21, i), Relation:=3, formulaText:=Cells(23, i)
   SolverOk SetCell:=Cells(7, i), MaxMinVal:=2, ValueOf:=0, ByChange:=Cells(21, i),
Engine:= _
      3, EngineDesc:="Evolutionary"
   SolverDelete CellRef:=Cells(21, i), Relation:=3, formulaText:=Cells(23, i)
   SolverAdd CellRef:=Cells(21, i), Relation:=3, formulaText:=Cells(23, i)
   SolverOk SetCell:=Cells(7, i), MaxMinVal:=2, ValueOf:=0, ByChange:=Cells(21, i),
Engine:= _
      3, EngineDesc:="Evolutionary"
   SolverOk SetCell:=Cells(7, i), MaxMinVal:=2, ValueOf:=0, ByChange:=Cells(21, i),
Engine:= _
      3, EngineDesc:="Evolutionary"
   SolverSolve userfinish:=True
   SolverFinish KeepFinal:=1
Next i
End Sub
```

For the GRGActive:

```
Sub GRGNonlinearActive()
  Dim i As Long
 For i = (2 + Cells(53, 20)) To (2 + Cells(53, 21))
  SolverReset
  SolverOptions AssumeNonNeg:=False
   SolverOk SetCell:=Cells(7, i), MaxMinVal:=1, ValueOf:=0, ByChange:=Cells(21, i),
Engine:= _
      1, EngineDesc:="GRG Nonlinear"
   SolverAdd CellRef:=Cells(21, i), Relation:=1, formulaText:="80"
   SolverOk SetCell:=Cells(7, i), MaxMinVal:=1, ValueOf:=0, ByChange:=Cells(21, i),
Engine:= _
      1, EngineDesc:="GRG Nonlinear"
   SolverAdd CellRef:=Cells(21, i), Relation:=3, formulaText:="30"
```

```
   SolverOk SetCell:=Cells(7, i), MaxMinVal:=1, ValueOf:=0, ByChange:=Cells(21, i),
Engine:= _
        1, EngineDesc:="GRG Nonlinear"
   SolverOk SetCell:=Cells(7, i), MaxMinVal:=1, ValueOf:=0, ByChange:=Cells(21, i),
Engine:= _
        1, EngineDesc:="GRG Nonlinear"
   SolverSolve userfinish:=True
SolverFinish KeepFinal:=1
 Next i
End Sub
```

For the EvolutionaryActive

```
Sub EvolutionaryActive()
  Dim i As Long
  For i = (2 + Cells(52, 20)) To (2 + Cells(52, 21))
   SolverReset
    SolverOptions MaxTime:=180, Iterations:=1000, Precision:=0.000001, _
        Convergence:=0.1, StepThru:=False, Scaling:=True, AssumeNonNeg:=False, _
        Derivatives:=1
    SolverOptions PopulationSize:=20, RandomSeed:=0, MutationRate:=0.075,
Multistart _
        :=False, RequireBounds:=True, MaxSubproblems:=0, MaxIntegerSols:=0, _
        IntTolerance:=0.1, SolveWithout:=False, MaxTimeNoImp:=30
    SolverOk SetCell:=Cells(7, i), MaxMinVal:=1, ValueOf:=0, ByChange:=Cells(21, i),
Engine:= _
        3, EngineDesc:="Evolutionary"
    SolverAdd CellRef:=Cells(21, i), Relation:=1, formulaText:="80"
    SolverOk SetCell:=Cells(7, i), MaxMinVal:=1, ValueOf:=0, ByChange:=Cells(21, i),
Engine:= _
        3, EngineDesc:="Evolutionary"
    SolverAdd CellRef:=Cells(21, i), Relation:=3, formulaText:="30"
    SolverOk SetCell:=Cells(7, i), MaxMinVal:=1, ValueOf:=0, ByChange:=Cells(21, i),
Engine:= _
        3, EngineDesc:="Evolutionary"
    SolverDelete CellRef:=Cells(21, i), Relation:=3, formulaText:="30"
    SolverAdd CellRef:=Cells(21, i), Relation:=3, formulaText:="30"
    SolverOk SetCell:=Cells(7, i), MaxMinVal:=1, ValueOf:=0, ByChange:=Cells(21, i),
Engine:= _
        3, EngineDesc:="Evolutionary"
    SolverOk SetCell:=Cells(7, i), MaxMinVal:=1, ValueOf:=0, ByChange:=Cells(21, i),
Engine:= _
        3, EngineDesc:="Evolutionary"
    SolverSolve userfinish:=True
    SolverFinish KeepFinal:=1
Next i
End Sub
```

3.5. Other calculations

This section discusses the rest of the calculations in the spreadsheet. These calculations regard the back of the wall which is evaluating the active pwp using the steady state seepage that was previously mentioned and the passive and active earth impulses. Another calculation that was made is the total moments that contribute to the stabilization and destabilization of the whole soil-wall system.

3.5.1. Earth impulses in the back of the wall and PWP

For the back of the wall, Coulomb's equation was used In order to estimate the coefficients for the passive K_p and active K_a earth impulses respectively. The configuration in the back of the wall is the simple wall with a level ground surface which can be adequately estimated using Coulomb's equation. Coulomb's equation was used rather than the Rankine equation due to the presence of the soil-wall friction.

Example of this calculation is presented in the **Table.A 3** below extracted from the spreadsheet

Table.A 3 – Earth Impulses back of the wall.

Earth Impulses back of the wall	
Coulomb's Method:	
Ka	0.25
Kp	8.95
Ia (kN/m)	252
Ip (kN/m)	1039

The PWP was calculated with the same method as was described in the previous sections, but now the gradient of the water pressure is lower due to the increased length of the flow path.

The other table is the table with the total moments represented an example in the **Table.A 4** below:

Table.A 4 – Total moments and factor of safety.

Total moment	**front of the wall**	**behind wall**
Stabilizing	4426	516
Destabilizing	195	842
Water Impulse Stab	241	
Water Impulse Destab	0.00	1745
Moment Factor	2.00	

The total stabilizing or destabilizing moment in front of the wall is the sum of the moment contribution of each passive or active wedge respectively. The total stabilizing or destabilizing moments in the back of the wall is the moments generated by the aforementioned earth impulses. The destabilizing moment in front of the wall that is produced by the water impulse is due to the presence of the suctions if allowed.

The last parameter is the Moment Factor which is the ratio between the sum of the stabilizing moments over the sum of the destabilizing moments.

Note: all of the moments are calculated with the relation to the point of the wall at the user-defined depth Z_p.